Integrative and Scalable Pipeline for Multi-omic Characterization of Biological Tissues

by

Seo Woo Choi

M.S. Chemical Engineering Practice, Massachusetts Institute of Technology, 2019
B.S. Chemical Engineering, University of Illinois at Urbana-Champaign, 2017

Submitted to the Department of Chemical Engineering
in partial fulfillment of the requirement for the degree of

Doctor of Philosophy in Chemical Engineering

at the

MASSACHUSETTS INSTITUTE OF TECHNOLOGY

February 2024

Author……..
Department of Chemical Engineering
Nov 14, 2023

Certified by……...
Kwanghun Chung
Associate Professor of Chemical Engineering
Thesis Supervisor

Accepted by …….
Hadley D. Sikes
Willard Henry Dow Professor of Chemical Engineering
Chairman, Committee for Graduate Students

Integrative and Scalable Pipeline for Multi-omic Characterization of Biological Tissues

by

Seo Woo Choi

Submitted to the Department of Chemical Engineering
on Nov 14, 2023, in partial fulfillment of the
requirement for the degree of
Doctor of Philosophy in Chemical Engineering

Abstract

Study of mammalian organs is essential to understand functions and dysfunctions at the state of health and disease. Specifically, comprehensive characterization of the mammalian brain is crucial to understand brain physiology and neurological diseases. Depending on the goal of the study, various brain models, such as those involving mice, postmortem humans, and three-dimensional (3D) organoids derived from human induced pluripotent stem cells (hiPSCs), can be utilized. Regardless of the models used, a large-scale, unbiased study of the brain is yet to be achieved due to the vast complexity and high interconnectedness of the cells in the brain.

For the unbiased and holistic approaches toward the elucidation of brain structures and molecular profiles, we need to achieve effective retention of biomolecular information throughout the entire volume of tissue. The elucidation of the connections, molecular profiles, and structures within these models is performed with the help of highly specific molecular probes. Revealing the identities of thousands of molecules with intact spatial context, however, is challenging as repeated exposure to molecular probe attachment conditions damages the biomolecular integrity.

To address this challenge, we developed a method to rapidly and effectively preserve biomolecular information inside the large-scale biological tissues for holistic and three-dimensional characterization. This technology, termed EPIC-SHIELD, takes a novel approach for formaldehyde fixation to achieve rapid, homogenous preservation of biomolecules across the tissue volume, which is then complemented with a carefully adjusted polyepoxy crosslinking (SHIELD) that forms stable tissue-gel hybrid for long-term stabilization of biomolecules with minimal chemical damage. To improve the scalability of informational acquisition and processing, we developed a pipeline that involves light-sheet microscopy and nuclei-based co-registration. We achieved multi-omic and multiplexed characterization of thick mouse brain tissues using our pipeline that enabled cell type analysis and ontogeny studies. Furthermore, effective preservation by EPIC-SHIELD allowed successful characterization of fresh frozen human brain samples that provided invaluable opportunity to study postmortem tissues at health and disease. As a

demonstration, we compared the molecular compositions and spatial distributions of various cell types and pathological traits in control and Alzheimer's disease samples. Lastly, we applied our EPIC-SHIELD technology for unbiased characterization of hiPSC-derived cerebral organoids co-cultured with microglia. Using our technologies, we envision that we can be a step closer to fully understand the mechanisms behind the brain physiology.

Thesis Supervisor: Kwanghun Chung
Title: Associate Professor of Chemical Engineering

Acknowledgments

First of all, I am truly grateful for all the support and opportunity provided by my PI, Professor Kwanghun Chung (KC) and the Department of Chemical Engineering at MIT. I have learned a great deal from KC, who taught me from scratch how to design experiments, interpret and present datasets, and be a leader in a project or in a team. His exceptional mind in thinking outside the box led me to become a scientist and an engineer who can come up with new ideas and approaches different from the conventional ones.

Also, I would like to express my sincere gratitude towards my thesis committee members: Professor Hadley Sikes, Professor Jacqueline Lees, and Professor Beth Stevens. I am honored to have you in my committee. Throughout my doctoral studies, your valuable comments and advice have helped me greatly in shaping my thesis. In addition to being my thesis committee members, your career advice and support have been tremendously helpful in my PhD training.

I would like to acknowledge the past and the current Chung lab members for all the help. In every step of my path as a graduate student, I learned that collaborative work is crucial for research. MIT is a hub to which brilliant and smart scholars all around the world gather, and share their knowledge and expertise. I learned from post-docs, research scientists, collaborators, and colleagues around me, and they were always willing to help me in achieving my goal.

Outside the work, I would like to thank my tennis friends: Jaeyeon, Taehoon, Soonhyoung, Jaewoo, Hojoon, Matt, Jinsoo, Hyunji, Soyoung, Joonhyuk. Without you all, this Cambridge life would have been so boring and uneventful. Thank you all for all the memories and fun.

To my girlfriend, Woo Mi, I thank you for being the one whom I can always go to talk and gain emotional support. Through our relationship, I found home and happiness which gave me the motivation and driving force to complete my thesis successfully. Despite the long distance we have, she was always there to listen and give practical and emotional support I needed. I am thrilled to see what awaits in our future.

This journey would not have been possible without the support of my family. My mom (Kyung Eun), dad (Jae Ho), and my older brother (Hyuk Joo) always supported me and listened to all my complaints and chitchats throughout my PhD. Knowing that you all are there for me was the ultimate support I had during my hardship.

Table of Contents

List of Figures

List of Tables

Chapter 1 – Introduction

The materials from this chapter are adapted from:

Seo Woo Choi†, Webster Guan†, Kwanghun Chung. Basic principles of hydrogel-based tissue transformation technologies and their applications. *Cell*, 2021; 184(16): 4115-4136.

Seo Woo Choi†, Chuanxi Zhao, Xinyi Gu, Jose Vargas-Asencio, Juhyuk Park, Yuxuan Tian, Lee Kamentsky, Nicholas B. Evans, Minyoung E. Kim, Kit-Yi Yam, Nicholas Townsend Haas, Clover Su-Arcaro, Caitlin S. Latimer, Aimee M. Schantz, C. Dirk Keene, and Kwanghun Chung, Effective preservation of biomolecules in large-scale non-perfusable tissues for spatial multi-omic analysis. *Submitted*, 2023.

†Indicates first authorship

1.1 Interrogation of the brain

Mammalian brain is a system which involves complex, yet highly organized structures[1]. Study of the composition and connections of brain cells provides insights to brain function and dysfunction. Therefore, it is crucial to map out molecular and structural profiles of cells in the mammalian brains with high spatial resolution. Yet, owing to the complexity and high interconnectedness of the brain cells, elucidation of full structures and molecular details of the cells within the brain remains an unmet goal in the fields of neuroscience, medicine, and biology.

Depending on the goal of a study, various brain models have been introduced which possess advantages and disadvantages over others, and these models can yield a great synergy when complemented to each other. One of the methods is using an animal model, in which the mammalian brains are studied using mice, rats, and non-human primates[2]. Combined with the

genetic tools, the animal models have become powerful means to study conserved molecular characteristics and functional aspects of the brain, which can further be combined with *in vivo* behavioral studies[3]. However, interspecies difference that omits human-specific neural development mechanism limits the use of animal models in various translational studies[2]. Another method is using postmortem human brain samples. The study of postmortem tissues allows direct observation into human brain architecture which can be linked to the behavioral or pathological traits of donors, resulting in high translational potential. However, limited availability and varying quality of human tissues, combined with ethical and biohazard issues, restrict their widespread use in many laboratories. An alternative model to postmortem tissues is the stem cell derived cerebral organoids and spheroids. Stem cells have been widely used to study human diseases. Recently, the advent of organoids, which are three-dimensional, self-assembled neural structures that recapitulate the early organogenesis of the human brain, has established an effective way to study neurodevelopmental and neurodegenerative diseases with *in vitro* settings[4,5]. However, due to the differentiation protocol that skews cell identities towards a certain germ layer, stem cell models often lack cell types from other germ layers. Furthermore, culture conditions and the batch-to-batch variability stand as major problems in reproducing results.

Irrespective of the specific model we select for brain research, we need to rely on molecular probes and tools to extract the biological information. Recently, various molecular tools have been developed to probe the human brain[6–9]. These methods are pioneering works for the study of the human brain samples; yet, the study has been limited to the single-omic characterization performed on single-cell thickness. Thus, an effective method that can preserve multi-omic information in a volumetric sample is required for an unbiased interrogation of brain tissues.

1.2 Tissue fixation and hydrogel-based tissue transformation technologies

Mammalian organs consist of a vast array of highly specialized cells that are closely connected to one another. To gain a thorough understanding of how these organs function and to elucidate underlying causes in case of dysfunction, it is essential to visualize cells at multiple levels, ranging from the smallest nanoscopic details of biomolecular components to the larger, organ-scale connections between cells. Furthermore, various molecular profiles including transcriptome analysis, proteome analysis, and mapping of cellular connections (connectome, projectome), will uncover unique biomolecular characteristics that enable collaborative and synergistic research efforts. Recent advancements in technologies like single-cell sequencing, tissue processing, and imaging have revolutionized our ability to gather detailed information about the characteristics of individual cells and their spatial relationships within organs. These breakthroughs have enabled researchers to identify new types of cells and uncover their functions[10–12]. To extend our understanding of the complexity of biological systems within their spatial context, ongoing large-scale initiatives, such as the Human Cell Atlas Initiative, Human Biomolecular Atlas Program, and Brain Initiative Cell Census Network, are working towards creating comprehensive reference atlases of all human cell types[13–15]. Nevertheless, exploring the remarkable intricacies of biological systems still necessitates the development of new technologies and innovative approaches.

Classical histology has traditionally served as the primary method for investigating biological tissues. Various chemical and mechanical techniques have been proposed to simultaneously preserve and extract structural and molecular details from the intact tissue samples.

One of the most frequently used methods involves using aldehyde-mediated chemical fixation in combination with mechanical tissue sectioning.

Aldehyde fixation effectively minimizes biomolecular degradation within the tissues. When aldehydes encounter biomolecules, they undergo crosslinking reaction to chemically tether biomolecules, which helps maintain the structural integrity of the tissue while deactivating proteins, including enzymes, that can break down biomolecules. After the fixation, the tissues are often mechanically sectioned into thin slices, typically ranging from 10 to 200 μm in thickness. In more advanced technologies, like array tomography, fixed tissues are embedded in a plastic resin. Such additional stability provided by the resin allows for the generation of ultrathin sections, typically measuring between 100 to 200 nm. Subsequently, high-resolution imaging is performed, followed by precise 3D reconstruction of the tissue's structure[16]. While the sectioning exposes biomolecules within cells to molecular probes and monochromatic light, mechanical disruption of cellular compartments is labor-intensive, and often leads to the loss of valuable information, such as the intricate connectivity of neural network. These limitations have driven the need for a more scalable approach capable of efficiently processing intact, large-scale tissues.

In the last decade, innovative optical tissue clearing techniques and hydrogel-based tissue transformation methods have emerged as novel approaches for investigating the molecular and structural details of various biological systems. These techniques modify the physical and chemical properties of tissues, such as making them optically transparent, enhancing molecular permeability, altering tissue size, and adjusting mechanical properties, all while preserving the native spatial information of biomolecules. These tissue-gel hybrids, coupled with innovative chemical and optical tools[17], provide unprecedented level of access to the rich three-dimensional information present in intact tissues.

For instance, researchers have been improving tissue transparency since the early 1900s, which led to the development of advanced tissue clearing methods in recent years[18]. These methods enable 3D imaging at cellular resolution in intact biological systems, ranging from plants and invertebrates to mice, primates, and human organs[19,20,29,30,21–28]. When combined with genetic labeling techniques, biomolecular probes, and state-of-the-art microscopy technologies, tissue clearing has revolutionized the fields of mapping neuronal circuits[20,23–25,28,31–34], studying neural activity[29,34], and characterizing cellular phenotypes[20,30–35].

The invention of hydrogel-based tissue transformation methods has stimulated significant changes in how we can manipulate the physical and chemical properties of biological tissues, reaching far beyond optical clearing. A major challenge in volumetric tissue analysis is the presence of lipids in tissues, which can impede the penetration of molecular probes and light. Hydrogel-tissue hybrid successfully addressed this challenge by allowing the efficient removal of lipids (delipidation) within intact tissues while preserving the spatial relationships between cells and molecules. Moreover, hydrogel-based techniques have opened up possibilities for altering tissue properties through the use of various chemical modifiers and synthetic hydrogels. For example, tissue-gel hybrids can be rendered resistant to heat and chemicals[20,32,33], adjustable in size[35–37], and elastic[38]. These unique characteristics of tissue-gels enable multi-scale imaging, ranging from the nanoscale to the macroscale, of multi-omic features in intact biological tissues such as transcriptomics, proteomics, and anatomical features like projectomics and connectomics. For example, these techniques have made it possible to analyze nanoscale synaptic structures[35–37,39,40], study the molecular profiles of individual cells[20,30,32,33,36,40–43], and explore intercellular connectivity within tissues[32,33]. Thus, hydrogel-based tissue transformation presents a great potential for accelerating and facilitating interdisciplinary research efforts.

1.3 SHIELD

SHIELD (Stabilization under Harsh conditions via Intramolecular Epoxide Linkages to prevent Degradation) is an innovative hydrogel-based tissue transformation technology introduced by Park and colleagues in 2019. It is designed to preserve biological tissues through a process involving both intra- and intermolecular crosslinking facilitated by multi-arm polyepoxide molecules[33]. SHIELD is a versatile method that effectively preserves both the transcriptomic and proteomic information. In SHIELD, the epoxy group in five-arm epoxy molecule named polyglycerol-3-polyglycidyl ether (P3PE) undergoes a ring-opening reaction to react with primary amines in the nucleic acids and proteins (**Figure 1-1**).

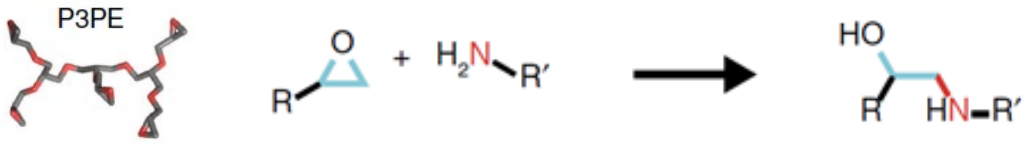

Figure 1-1. Basic mechanism of SHIELD (P3PE)[33]

The presence of multiple epoxide groups within a single P3PE molecule is a key feature, as it allows the formation of both intra- and inter-molecular crosslinks. These crosslinks anchor biomolecules such as nucleic acids and proteins within the tissue, which allows preservation of their spatial distribution and enhances the overall mechanical stability of the tissue. This unique property of P3PE is particularly advantageous when it comes to preserving fluorescent proteins (FPs). The structural integrity of FPs plays a crucial role in fluorescence excitation and emission processes. By preserving the molecular structure of FPs through the intra- and inter-molecular crosslinking facilitated by P3PE, SHIELD ensures the fluorescence-based imaging and analysis within biological tissues.

1.4 Molecular probes for biomolecular detection

In light-based tissue characterization, fluorophores are attached to molecular probes that are specific and selective towards the biomolecular target of interest. Broadly, we use peptide or protein specific antibodies produced in animals to extract proteomic information, and complementary oligonucleotide to obtain transcriptomic information within biological samples. The former, known as immunofluorescence (IF) in general or immunohistochemistry (IHC) if used for tissues, is a technique that relies on the interaction between antigens and antibodies to detect specific protein targets within biological tissues. A wide range of antibodies, typically generated by injecting proteins or peptides of interest into animals, is used[44]. Fluorescence *in situ* hybridization (FISH), on the other hand, is a technique that harnesses the complementary base pairing of DNA or RNA transcripts to locate specific nucleic acids of interest within biological tissues[45].

The detection of molecular probes is achieved through the fluorophore labeling. However, signal amplification is often necessary as the copy number of biomolecular targets may be limited, which hinders efficient detection and analysis. For IHC, secondary antibodies conjugated with fluorophores bind to the multiple sites on the primary antibodies, thereby amplifying the signals[44]. For FISH, hybridization chain reaction (HCR) is used, which is an enzyme-free method employed to amplify signals[46]. HCR makes use of metastable DNA hairpins that can self-assemble into polymers when they bind to initiator molecules. This technique is particularly useful when the signal is weak, either due to a low copy number of the target or the short length of the target transcripts. HCR amplification enhances the signal-to-noise ratio (SNR) by attaching a series of

alternating hairpins, each with a fluorophore. **Figure 1-2** provides an illustration of the mechanisms behind these molecular characterization techniques.

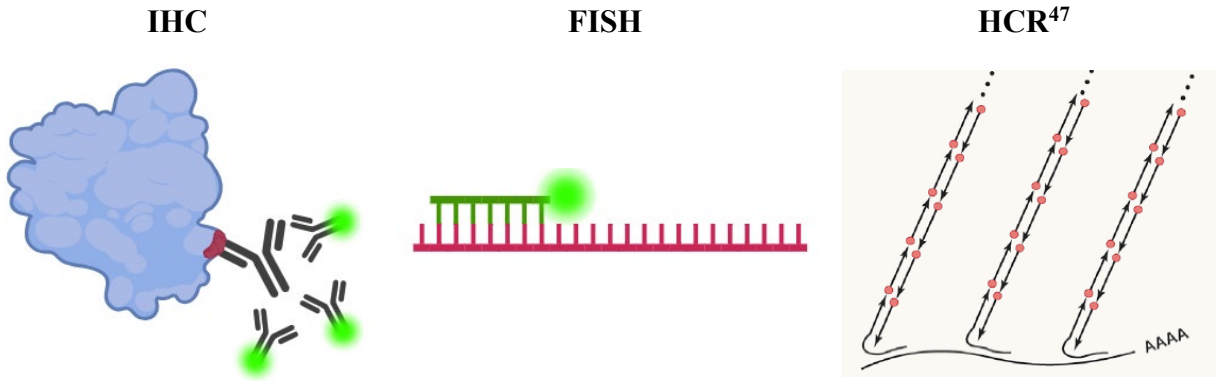

Figure 1-2. Illustrations for IHC, FISH, and HCR[i]

[i] The illustrations were generated using biorender.com

1.5 Multiplexing

Light-based tissue characterization techniques encounter a significant problem due to the use of fluorophores, known as spectral overlap, when visualizing multiple targets simultaneously. For example, **Figure 1-3** shows excitation and emission profiles of common fluorophores. As depicted in the figure, it becomes impossible to excite individual fluorophores separately when their excitation spectra overlap, and separating signals becomes exceedingly challenging when their emission spectra overlap. Consequently, the maximum number of biomolecular targets that can be simultaneously examined in a single round of molecular probe staining is limited to 3 to 5, depending on the specific fluorophores used.

To increase the number of biomolecular targets we can visualize, we employ a technique known as multiplexing, which consists of two primary approaches: barcoding and multi-round schemes. The barcoding method involves converting each fluorophore signal into a code, exponentially increasing the number of distinguishable targets. For example, in 2015, Chen and colleagues reported a method called multiplexed, error-robust FISH (MERFISH)[48]. In this method, the presence of a signal is represented as a binary signal (1), while the absence of a signal is denoted as (0), allowing for a binary code that can expand multiplexing capacity exponentially. The advantage of this approach lies in its ability to identify a vast number of targets. However, due to the high magnification imaging and computational process required for image registration, the thickness of tissues is limited to a single-cell-thick layer (approximately 10 μm), which leads to a loss of volumetric context such as cellular connectivity. On the other end of the multiplexing scheme, we have multi-round technique, in which the tissues are labeled, imaged, and de-labeled so that the number of targets increase linearly. This linear multiplexing capacity, however, caps

the practical number of identifiable targets at less than a hundred. Nevertheless, when combined with volumetric staining methods, multi-round schemes can be applied to tissues at the scale of organs, ranging from millimeters to centimeters. It is important to note that effective biomolecular preservation is crucial in multiplexing schemes, as repeated tissue interrogation can inevitably lead to the loss of biomolecular information.

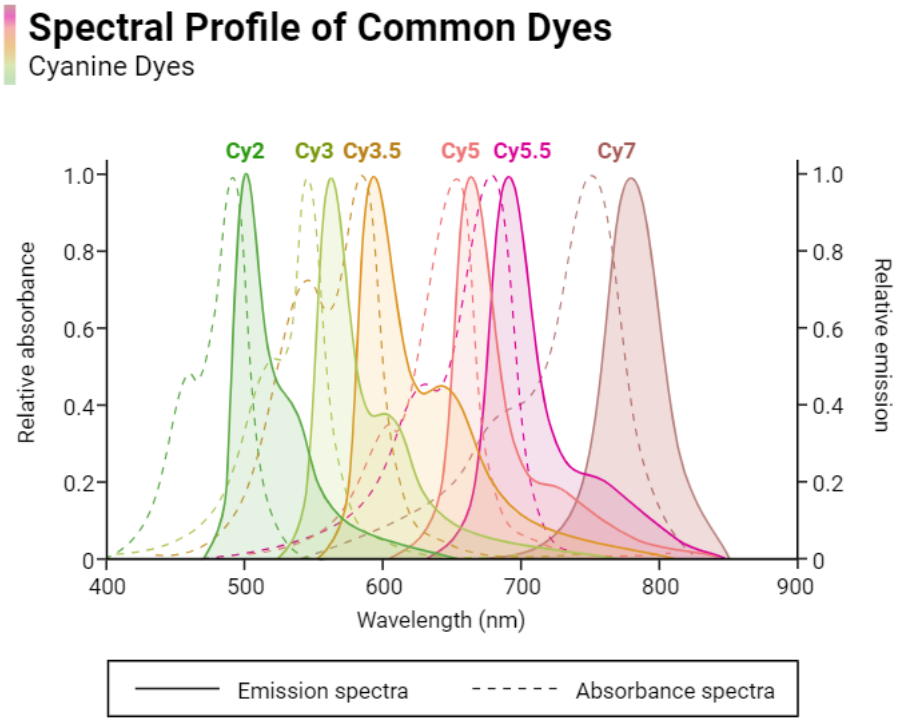

Figure 1-3. Illustration of spectral overlap of Cy dyes[ii]

[ii] The illustrations were generated using biorender.com

1.6 Spatial transcriptomics

Analyzing the various cell types and their gene expressions with spatial context is essential for gaining insights into the relationships between the structure and function of biological systems. Recent progresses in *in situ* transcriptomics technologies allowed the mapping of gene expression profiles with higher precision and multiplexing capabilities. For example, single-molecule fluorescence *in situ* hybridization (smFISH) allows the mapping of individual RNA molecules at single-cell resolution within their spatial information intact[49,50]. Spatial, spectral, and sequential barcoding techniques applied in smFISH have allowed the identification of multiple RNA species within individual cells[51,52]. One of these barcoding methods, MERFISH, has significantly expanded the number of RNA species that can be identified within single cells, with the ability to detect up to 1,000 RNA species[48]. Coupled with single-cell RNA sequencing technology, MERFISH was utilized in identifying as many as 70 distinct neuronal populations in the hypothalamic preoptic region of mouse brain[53].

Many of these techniques, however, have primarily been demonstrated on monolayer cell cultures or on thin tissue slices. Hydrogel-based tissue transformation technologies present a novel opportunity to expand the applicability of these technologies to organ-scale intact tissues. Covalently attaching mRNA to a hydrogel mesh has proven to be an effective method for preserving mRNA integrity. The CLARITY technique was one of the pioneers in successfully preserving mRNA within tissue-gel hybrids and demonstrated its compatibility with *in situ* hybridization techniques using mouse brains[20,30]. Over time, hydrogel chemistry has been further refined to optimize RNA preservation. For example, Sylwestrak and colleagues introduced a method that involves crosslinking RNA transcripts to the hydrogel mesh using 1-Ethyl-3-3-

dimethyl-aminopropyl carbodiimide (EDC)[41]. This approach enhanced the preservation of various types of RNA molecules, including messenger RNA (mRNA), non-coding RNA, and microRNAs. With EDC-CLARITY, the researchers were able to successfully conduct hybridization-based 3D visualization of RNA transcripts in tissues that are millimeters thick. Another significant development was reported from Park and colleagues, who demonstrated that the SHIELD technique can effectively and uniformly preserve mRNAs in large-scale tissues[33]. Furthermore, Chen and colleagues performed multiple rounds of *in situ* hybridization on an expandable tissue-gel hybrid, demonstrating that the external hydrogel mesh can preserve the integrity of mRNA transcripts during repeated data acquisition[54]. These various techniques collectively show the effectiveness of preserving RNA transcripts within tissue-gel hybrid.

Synthetic tissue-gel platforms significantly enhance the detection of labeled RNA molecules via altering physical and optical properties of the tissues. The main challenges in RNA detection via fluorophores are optical crowding and autofluorescence both of which can reduce the signal-to-noise ratio (SNR) and increase error rates, resulting in false-positive and false-negative signals. To address these challenges, a combination of ExFISH and MERFISH, referred to as MERFISH-ExM, has been developed. MERFISH-ExM physically de-crowds FISH signals by expanding tissue samples, allowing for the detection of RNA species with high densities[43,54]. In addition to the physical expansion, hydrogel-based methods offer reduction in autofluorescence through delipidation and optical homogenization. For example, SeqFISH incorporated PACT-delipidation for low autofluorescence and employed HCR amplification of smFISH signals to visualize mRNA signals in 0.5-mm-thick tissue sections[55]. The use of hydrogel-based clearing for enhanced SNR was also reported in the visualization of bacterial rRNA and in combination with MERFISH[56,57]. Of note, SeqFISH+ demonstrated a multiplexing capacity up to 10,000 genes on

tissues embedded in hydrogels[58]. These examples illustrate that hydrogel-based tissue techniques can be combined with novel *in situ* transcriptomics approaches to advance beyond limitation in various fields.

Another approach involves the sequencing of mRNA *in situ*. For instance, *in situ* sequencing and fluorescent *in situ* RNA sequencing (FISSEQ) are methods that generate complementary DNA (cDNA) amplicons that are sequenced by consecutive rounds of hybridization and imaging[59,60]. Furthermore, spatially resolved transcript amplicon readout mapping (STARmap) utilized hydrogel to anchor cDNA nanoballs (amplicon) that contain amine-modified nucleotides functionalized with acrylic acid N-hydroxysuccinimide ester[61]. Following delipidation and protein removal, the transcriptional information enclosed within the hydrogel-DNA amplicons was extracted through *in situ* sequencing. Using STARmap, 160 to 1,020 genes were identified within the mouse brain cortex. As shown in these examples, hydrogel-based tissue transformation technologies are orthogonal to the spatial transcriptomics technologies, allowing a synergistic and scalable approach towards the targeted and untargeted analysis of transcriptomic information in large-scale tissues.

1.7 Microglia

In the brain, microglia are specialized glial cells dedicated to immune functions within the central nervous system (CNS). Microglia make up approximately 5-10% of the total brain cell population and belong to the myeloid lineage, similar to macrophages. Microglia serve various defensive roles, including phagocytosis of foreign or dead cell debris and the secretion of cytotoxic substances that can induce cell death[62]. Additionally, they play crucial roles in the early development of the brain by engaging in synaptic pruning, a process that refines neural connections. Microglia actively interact with other cell types in the CNS, such as astrocytes and neurons[63]. These interactions are mediated by various cytokines and growth factors produced by microglia, which contribute to the maintenance of brain homeostasis.

Given their diverse roles in both health and disease, it is essential to understand microglial behavior and their gene expression profiles. For instance, changes in microglial morphology, transitioning between amoeboid and ramified shapes, are indicative of their activation states and are accompanied by alterations in their transcriptional profiles. Notably, microglial morphology undergoes continuous changes from an amoeboid to a ramified shape during brain development, though the reasons for these alterations remain unclear. Therefore, there is a need for precise classification and quantification of microglia with high spatial and temporal resolution to unravel their roles in the CNS.

1.8 hiPSC-derived cerebral organoids with microglia

The human brain is composed of a wide variety of cells, each with its distinct gene expression profiles. Investigating these cells, in both healthy and diseased states, presents various opportunities for research with practical applications. However, the limited availability of human brain tissue for study has led researchers to rely on animal models to explore brain functions and disorders, which suffer from limited translational capacities due to the interspecies differences. To address these challenges, cerebral organoids generated from stem cells have opened up new avenues for examining brain development and diseases. Cerebral organoids are three-dimensional neural structures that self-assemble and closely resemble the human brain cytoarchitecture. Cerebral organoids offer an effective means for developmental and pathological studies and hold great potential for patient-specific drug screening. These 3D neural structures can be generated using both human embryonic stem cells (hESCs) and human induced pluripotent stem cells (hiPSCs) in a relatively short period[4,5].

Despite their novelty and self-assembled 3D structures, cerebral organoids possess limitations. One notable limitation is that they lack a crucial cell type known as microglia. Recent advances have led to the development of protocols for differentiating microglia from cerebral organoids. In one such approach, microglia can develop naturally from cerebral organoids, originating from a small population of mesodermal-lineage cells during undirected differentiation[64]. However, the incorporation and differentiation of microglia within organoids tend to be limited, with incorporated microglia typically unable to be retained for more than a couple of months within the organoids. Therefore, new approaches for extended survival of

microglia are necessary to better recapitulate the human brain physiology and disease in an *in vitro* setting.

1.9 Thesis aims

Aim 1 – Development of an effective method to preserve biomolecular information in various brain models

Expanding upon the recent hydrogel-based tissue preservation technology, SHIELD, my emphasis will be on preserving both transcriptomic and proteomic information[33]. Many existing tissue transformation technologies have been designed to preserve a single-omic profile, resulting in a restricted view of volumetric tissues. Through the development of EPIC-SHIELD (**E**xtended **P**reservation of molecules in **I**ntact **C**leared tissue using SHIELD), my goal is to achieve effective preservation of multi-omic information in large-scale tissues. This approach will offer flexibility in tissue characterization and stability for scalable and multiplexed analyses.

Aim 2 – Multi-omic characterization of mouse models with high scalability and multiplexity

Given the limited availability of human brain tissue, mouse models have become one of the most widely used models for researching brain function and physiology. The mouse brain shares several molecular similarities to the human brain, and the advent of advanced genetic tools has enabled the creation of humanized mouse models, which significantly improved the translational potential. However, the main challenge in studying the mouse brain lies in the scalability of existing omics technologies, which often face limitations in terms of either volumetric scale or multiplexing capacity. In this chapter, my objective is to present an integrative, scalable pipeline for processing large-scale tissues, including molecular preservation, labeling, imaging, and data integration and quantification.

Aim 3 – Multi-omic characterization of postmortem human brain tissues

While various animal models serve as valuable tools for investigating human brain physiology, the direct examination of postmortem human brain tissue offers unparalleled advantages over these approaches. Nevertheless, the experimental use of human brain tissue has been constrained by factors such as limited availability and inconsistent tissue quality. As a result, the direct analysis of the human brain has primarily been confined to thin tissue sections and to proteomic studies. In this chapter, I aim to provide a scalable approach that addresses the specific challenges associated with studying the human brain, including biomolecular degradation, the presence of auto-fluorescent lipofuscin, and high lipid content.

Aim 4 – Development of human brain model using human induced pluripotent stem cells

While the use of animal models and the examination of postmortem human brain tissues have advanced our understanding of human brain physiology, there has been a need for functional, live human brain structures. Additionally, due to differences in brain size and developmental trajectories between mice and humans, various neurodevelopmental diseases could not be effectively studied. To address these challenges, human induced pluripotent stem cell (hiPSC)-derived cerebral organoids have emerged as an ideal model for recapitulating early human brain organogenesis, offering a platform for the study of human brain physiology and neurodevelopmental disorders. Despite their advantages of being derived from human cells and having 3D structures, current forebrain cerebral organoids primarily consist of neuroectodermal lineage cells, lacking important cell types like microglia, which are the resident immune cells in the brain that play crucial role in maintaining homeostasis and during the disease progression. To address these limitations, my goal is to create a hiPSC-derived organoid model with microglia

incorporated. Moreover, by modifying the co-culture conditions, I aim to prolong the survival of microglia within the organoid, potentially enabling the maturation of microglia towards a state resembling primary microglia.

Chapter 2 – Development of an effective method to preserve biomolecular information in various brain models

The materials from this chapter are adapted from:

Seo Woo Choi†, Chuanxi Zhao, Xinyi Gu, Jose Vargas-Asencio, Juhyuk Park, Yuxuan Tian, Lee Kamentsky, Nicholas B. Evans, Minyoung E. Kim, Kit-Yi Yam, Nicholas Townsend Haas, Clover Su-Arcaro, Caitlin S. Latimer, Aimee M. Schantz, C. Dirk Keene, and Kwanghun Chung, Effective preservation of biomolecules in large-scale non-perfusable tissues for spatial multi-omic analysis. *Submitted*, 2023.

†Indicates first authorship

2.1 Introduction

Comprehensive molecular examination of intact biological tissues has been a major challenge in biology, leading to various technological breakthroughs and innovations aimed to stabilize and capture biomolecular information within biological tissues[17,20,21,29,32–34,65]. Most early efforts focused on proteomic characterization[9,17,20,21,29,32–34,65], due to the relatively higher abundance and stability of proteins compared to mRNAs[66].

The advent of single-cell sequencing technologies[67], highlighted the potential of RNA profiling to determine cell types/states, function or dysfunction among others[10,12]. To overcome the intrinsic loss of crucial spatial information in single-cell based technologies, novel spatial RNA profiling methods have been developed, such as *in situ* hybridization methods[48,49,51,54,58], *in situ*

sequencing methods[59–61,68], and spatial reconstruction methods[69,70]. Collectively, these methods have demonstrated the potential to achieve transcriptomic characterization while maintaining spatial information. However, the labile nature of mRNA transcripts, their lower abundance compared to proteins, and the prolonged tissue processing required for volumetric tissue processing and imaging of thick tissues, have prevented scaling up towards volumetric analysis as seen in the field of proteomics[9,17,20,21,29,32–34,65]. Therefore, transcriptomic and/or multi-omics analysis of thick tissues, particularly human clinical samples, remains an unmet goal in biology and requires new approaches that enable robust preservation of mRNAs in thick optically cleared tissues.

There are two main mechanisms causing loss of transcriptomic information: (1) physical leakage of mRNAs away from its original location and (2) chemical damage of mRNAs. Physical leakage of mRNAs can occur when cell membranes are compromised due to cell death and/or damages associated with tissue processing procedures (e.g., tissue sectioning[6,71], freeze-thaw cycles, and membrane permeabilization/removal) (**Figure 2-1 a**). Once membranes are disrupted, mRNAs that are not permanently bound to intra-cellular mesh structures can diffuse out, resulting in loss of information. Leakage of mRNAs can continue to occur during and even after chemical fixation of tissue samples if the degree of fixation is not sufficient to form a stable intra-cellular mesh that can chemically tether mRNAs[32,33,72]. Chemical tissue fixation, though necessary, is another mechanism that causes loss of transcriptomic information as the fixation reaction inevitably leads to modification of chemical properties of mRNA molecules. Such modification can interfere with mRNA-probe binding reactions required for many transcriptomic assays.

To address these challenges, we introduce EPIC-SHIELD, a two-step tissue preservation strategy for maximal preservation of biomolecular information within thick tissues. First, we

demonstrate how alkaline conditions can accelerate formaldehyde-based fixation of tissues, preventing the loss of biomolecular information and significantly enhancing its capture. Then, to achieve robust stabilization of biomolecules with minimal chemical damage, a carefully adjusted complementary polyepoxy-based crosslinking (SHIELD[33]), was implemented to create a stable tissue-gel mesh where biomolecules are covalently tethered (**Figure 2-1 b**). Using computational models and experimental validations, we demonstrate that fixation under alkaline conditions greatly improves transcriptomic preservation in large-scale, non-perfusable biological tissues. Combined with a polyepoxy treatment, EPIC-SHIELD technology enables multiple rounds of FISH and IHC in thick tissues, increasing the amount of data that can be collected per tissue sample.

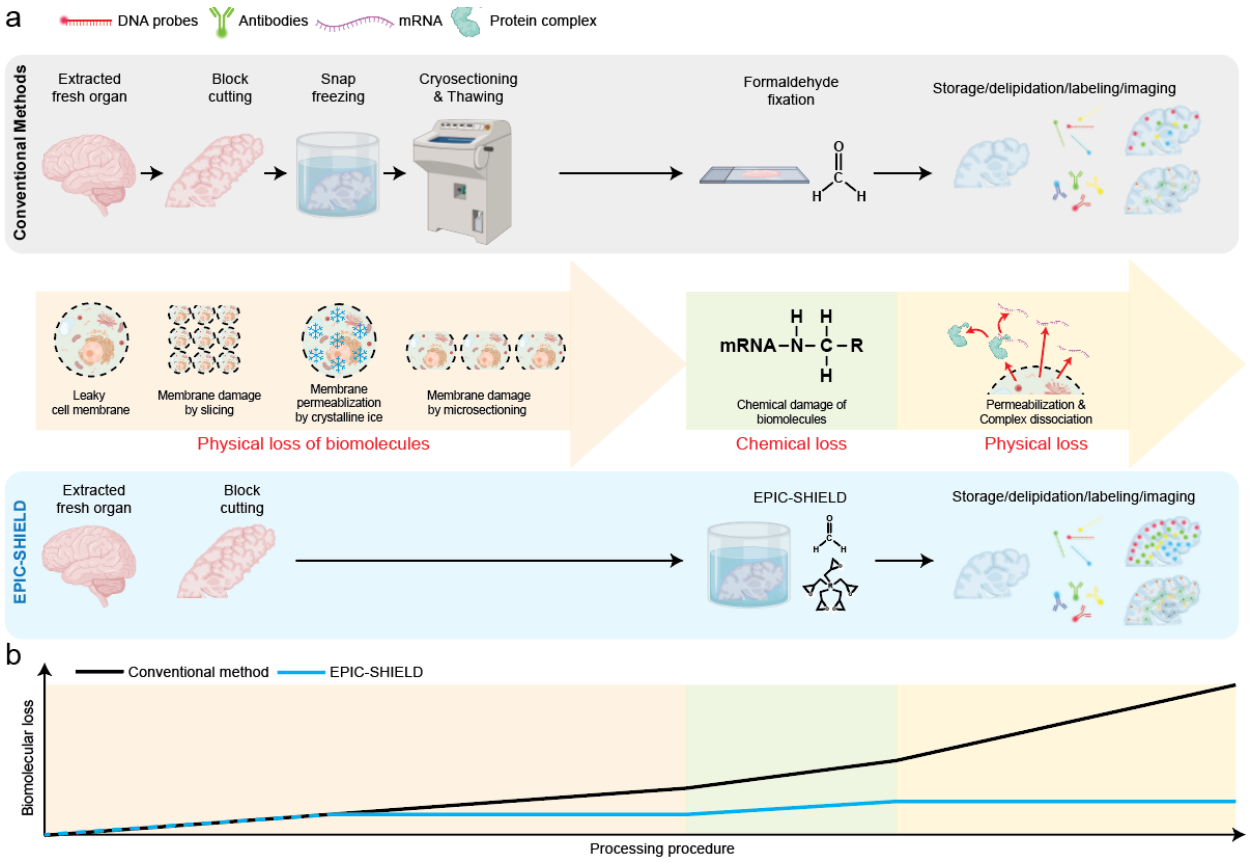

Figure 2-1. Minimized biomolecular loss by EPIC-SHIELD

(**a**) Schematic representation of improved preservation by EPIC-SHIELD through prevention of physical and chemical biomolecular loss at multiple stages of tissue processing. (**b**) Projected progression of biomolecular loss between conventional methods and EPIC-SHIELD across the tissue processing stages shown in (a).

2.2 Experimental Methods

2.1.1 COMSOL modeling of PFA reaction with biomolecules

COMSOL modeling was performed using COMSOL 6.1 (Comsol, Inc., Burlington, MA, USA). Finite element method was used to solve for the diffusion-reaction kinetics. For the simulation of methylene glycol and formaldehyde diffusion into the tissue, a rectangular geometry with 5-mm width and 2-mm height was used. A Dirichlet boundary condition was set at x=0 for methylene glycol / formaldehyde solution to mimic fixative diffusion into the tissue. Both methylene glycol / formaldehyde and uncharged / charged amine pairs were set at equilibrium while allowing uncharged amine and monomeric formaldehyde molecules to react in the tissue volume. To simulate the second, irreversible reaction of methylol with amides, an arbitrary concentration of amides was used, with a 10-fold slower reaction rate coefficient. For 1~30-day simulations, a spherical geometry was chosen with a diameter of 5 mm. In order to minimize the numerical noise due to the step change in amine concentration, an adaptive mesh setting was applied on the edge of the tissue by adding boundary layers. Below are the values for the COMSOL simulation (**Table 1**).

Table 1. Table of COMSOL simulation parameters

Simulation parameters	Value
Initial total concentration of CH_2OH_2/CHOH	1333 mol/m^3
Initial concentration of CH_2OH_2	1332.6 mol/m^3
Initial concentration of CHOH	0.40255 mol/m^3
Initial concentration of amide	49.624 mol/m^3
Initial total concentration of amines at pH7.4[32]	49.624 mol/m^3
Initial concentration of uncharged amine (lysine) at pH7.4	0.03676 mol/m^3
Initial concentration of uncharged amine (lysine) at pH10	11.308 mol/m^3
Initial concentration of charged amine (lysine) at pH7.4	49.587 mol/m^3
Initial concentration of charged amine (lysine) at pH10	38.316 mol/m^3
Diffusivity of CH_2OH_2/CHOH[73,74]	4.6296e-9 m^2/s
Forward reaction rate coefficient of CHOH and uncharged amine[75]	1.7e-7 m^3/(s·mol)
Reverse reaction rate coefficient of methylol[75]	0.23e-4 s^{-1}
Forward reaction rate coefficient of methylol and amide*	1.7e-8 m^3/(s·mol)
Equilibrium constant, formaldehyde ($\frac{[CH_2OH_2]}{[CHOH]}$)[76]	3311.4
Equilibrium constant, amine ($\frac{[NH_3^+]}{[NH_2]}$) at pH7.4	1349
Equilibrium constant, amine ($\frac{[NH_3^+]}{[NH_2]}$) at pH10	3.3884
pH	7.4 or 10
pKa of Lysine side chain	10.53

2.1.2 C^{13} NMR analysis on 4% PFA

The ^{13}C NMR measurements of formaldehyde were conducted using Bruker Avance Neo spectrometer operating at 400.17 MHz (Bruker Biospin AG, Rheinstetten, Germany). The spectra of 4% (w/v) PFA at pH 7.4 and pH 10 were measured using inverse gated 1H-decoupling pulse sequence, with 32 scans and a relaxation delay of 5s. The pH of 4% (w/v) paraformaldehyde (15714-S; Electron Microscopy Sciences) was adjusted by diluting 10x PBS, and by adding 50 mM sodium carbonate and 50 mM sodium bicarbonate for pH 7.4 and pH 10, respectively.

2.1.3 Mouse brain drop-fixation

Adult C57BL/6J mice (6-8 weeks) were housed in a 12-hour light/dark cycle with food and water provided *ad libitum*. All animal experimental protocols were conducted with the approval of the MIT Institutional Animal Care and Use Committee and the Division of Comparative Medicine. All work with animals adhered to federal and institutional regulations regarding the use of animals for research purposes. Mice were transcardially perfused with solution containing ice-cold 1x PBS. The brains were extracted and drop-fixed in 4% (w/v) paraformaldehyde (PFA) at pH 7.4 (1x PBS) and pH 10 (50 mM sodium carbonate + 50 mM sodium bicarbonate) for 8 hours at 4°C. After washing the brains overnight with PBSN (1x PBS + 0.02 w/v% NaN_3; S2002; Millipore Sigma) at 4°C, the brains were sectioned into 200-µm-thick slices using vibratome (VT1200S, Leica Biosystems). The slices were kept in PBSN.

2.1.4 mRNA preservation characterization and quantification

For FISH experiments, various anti-sense oligo probes were designed. For mouse and human probes, we followed the steps previously published by Kishi et al. (2019)[77]. Briefly,

antisense probes of 36-41nt were designed using OligoMiner[78] with GC% of 45-60% and melting temperature of <80°C. We appended the probes with 'TT' or 'ATAT' spacer to attach bc42 sequences. All of the probes were ordered in 100-200 μM concentration by IDT (Coralville, IA) and diluted for the experiments. For amplification, we used custom hairpin probe sets conjugated with SeTau-488, Seta-555, and SeTau-647 (SETA BioMedicals) or commercially available hairpin probe sets with Alexa Fluor (Molecular Instruments Inc.). Mean fluorescence was quantified using ImageJ software. Briefly, the background subtraction was performed on the original image using the rolling ball algorithm. Then cells were segmented using Gaussian Blur and watershed algorithm. For the mouse brain tissues, the mean signal intensity was measured for each segmented cell, and multiple values in segmented area were averaged to obtain a single mean fluorescence intensity for the image. Mean fluorescence intensity values from multiple slices were used for statistical analysis. For the human brain tissues, the mean signal intensity was measured for each segmented cell, and multiple values in segmented area were used for statistical analysis.

2.1.5 YFP retention test

Thy1::YFP H-line mouse brains were PFA-fixed, sliced and SHIELD-treated (1-8 w/v%) by previously stated protocols. After extensive washing with PBSN, each coronal slice was imaged before and after the heat treatment (1xPBS at 70°C for 24 hours). Mean fluorescence was quantified using ImageJ software at the same region. Imaging was performed using Leica confocal microscope using 20x 0.5 NA objective.

2.1.6 Thawing and characterization of fresh frozen human brain tissue

4-mm-thick fresh frozen human brain slabs were obtained from the University of Washington BioRepository and Integrated Neuropathology (BRaIN) lab. Tissues were obtained

with appropriate informed consent from the donor where appropriate and the legal next of kin. Fresh frozen human brain tissues (temporal lobe) were dissected at -80°C and then immersion-fixed in 4% (w/v) PFA at pH 7.4 or pH 10 for 24 hours at 4°C. The tissues were washed with PBSN overnight at 4°C. PFA-fixed human brain tissues were sectioned into slices using vibratome.

2.3 Results and Discussion

2.3.1 COMSOL modeling of paraformaldehyde diffusion and reaction

To minimize the physical leakage of mRNAs, we hypothesized that rapid tissue fixation, performed before any significant mechanical tissue damage occurs, is essential. In conventional methods, steps such as snap freezing, subsequent thin-sectioning, and thawing can disrupt cell membranes, leading to the physical leakage of mRNAs[79] (**Figure 2-1 a, b**). Avoiding these processes prior to chemical fixation may greatly improve mRNA preservation. However, this approach necessitates the fixation of thick unsliced tissue blocks, requiring rapid delivery of fixatives into thick tissues, which has been historically considered a major challenge in fixing non-perfusable tissues. Formaldehyde, a monomeric form of paraformaldehyde or PFA, is the most commonly used chemical fixative which can penetrate thick tissues rapidly due to its small size (MW: ~30Da). Furthermore, the majority (>99.9%) of molecules in formaldehyde solution exists in the form of methylene glycol, an unreactive hydrated form that readily diffuses into the tissue without depletion[47] (**Figure 2-2 a, b**). Simulation of the diffusion-reaction of a 4% formaldehyde solution in a 10-mm-thick tissue slab under traditional fixation conditions (PBS-buffered, ~pH 7.4) showed that methylene glycol molecules can disperse rapidly throughout the entire tissue volume and reach the core of the thick tissue slab in less than an hour (**Figure 2-2 c**). This result indicates that formaldehyde penetration is not the limiting factor in processing thick samples.

2.3.2 COMSOL modeling of paraformaldehyde diffusion and reaction under the traditional fixation conditions

Rapid penetration of methylene glycol molecules does not guarantee rapid tissue fixation, as only the carbonyl formaldehyde (<0.1%) can react with non-charged amines in biomolecules. Based on simulations, biomolecular fixation can take up to days or weeks, as the concentration of both reactants is very low under the traditional fixation conditions (**Figure 2-2 d, e, Methods, Supplementary Note 1**). The slow fixation in traditional methods could cause substantial physical leakage and loss of mRNAs if prolonged sample processing steps are required prior to the transcriptomic assays.

2.3.3 Approaches to increase formaldehyde reaction

To achieve rapid and uniform fixation of thick tissues, we set out to develop conditions that could increase the rate of the formaldehyde fixation reaction without slowing the rate of fixative penetration. The fixation reaction involves a nucleophilic attack of the nitrogen lone pair from the uncharged amine of biomolecules on the carbon atom of formaldehyde[80] (**Figure 2-2 a**). Increasing the concentration of the uncharged amines in the tissues by increasing the pH has the potential to accelerate the fixation reaction rate. Employing alkaline pH conditions (pH 10) leads to approximately 23% of the lysine side chain amines (pKa=10.5) being uncharged, compared to <0.1% at neutral pH, resulting in a substantial increase in reactant concentration and, consequently, an increased rate of fixation (**Supplementary Note 1**).

2.3.4 C^{13} NMR analysis of formaldehyde at different pH

To confirm that an alkaline buffer (pH 10) does not affect the rate of fixative penetration, we evaluated the composition of the formaldehyde solution, as a pH-induced shift in the formaldehyde-methylene glycol equilibrium could lead to depletion and reduce penetration efficacy. ^{13}C NMR analysis on PBS-buffered 4% PFA (pH 7.4) and carbonate-bicarbonate-buffered 4% PFA (pH 10) revealed no significant changes in the composition of the formaldehyde solution[81] (**Figure 2-2 b**), indicating that the equilibrium remains unaffected and the rate of fixative penetration is not compromised.

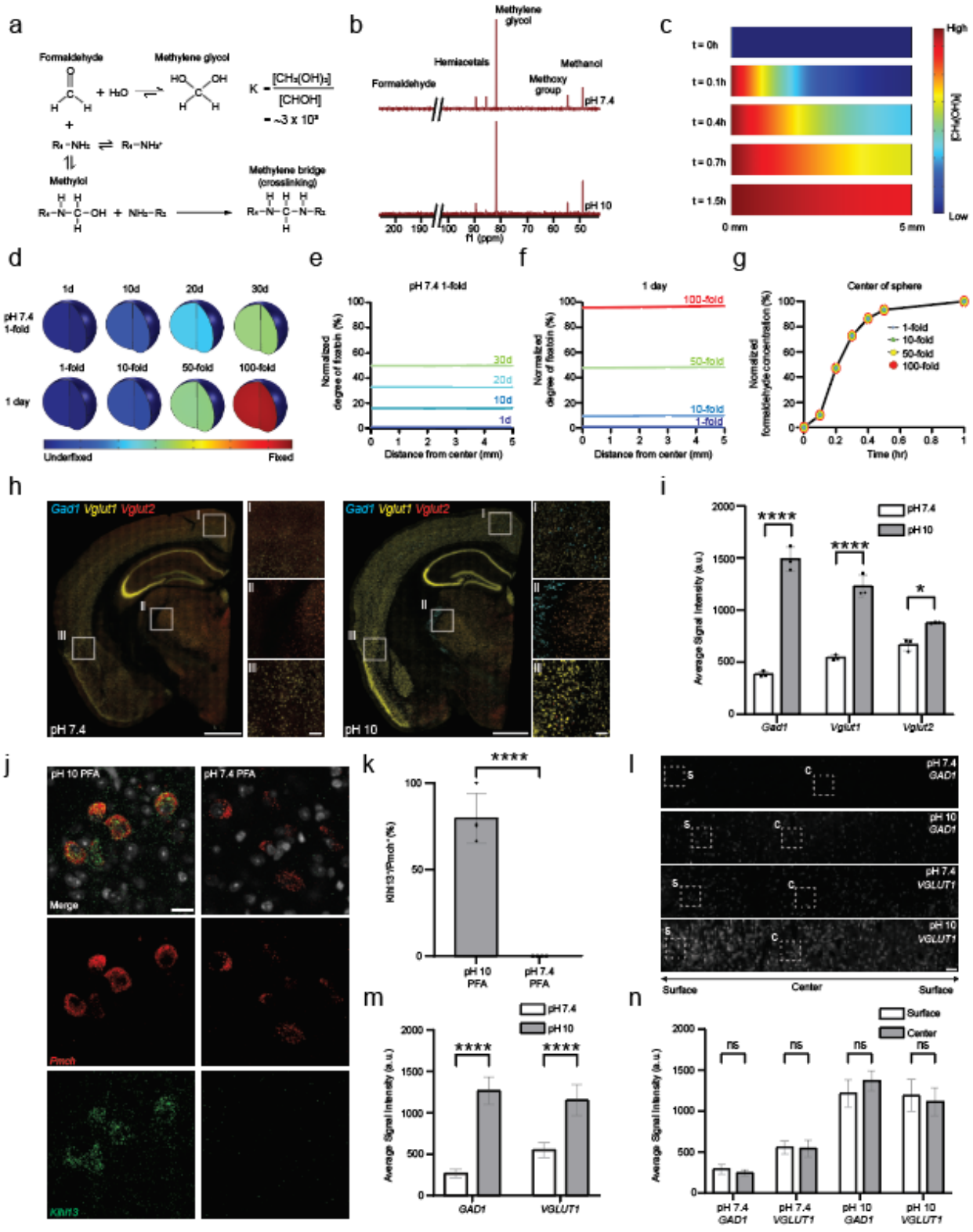

Figure 2-2. Accelerated PFA fixation in EPIC-SHIELD

(**a**) Chemical reaction steps involved in formaldehyde fixation of biomolecules, and the chemical equilibrium between methylene glycol and formaldehyde. (**b**) ^{13}C NMR spectra of 4% formaldehyde solution at pH 7.4 (PBS-buffered) and pH 10 (carbonate/bicarbonate-buffered). (**c**) Simulated diffusion dynamics of methylene glycol molecules through a 10-mm-thick slab. Color bar indicates the concentration. (**d-f**) Model-based fixation dynamics for formaldehyde across varying (**d**) time (top) and deprotonated amine concentrations (bottom). Color bar indicates the degree of relative fixation. (**e**) Normalized degree of fixation vs distance from tissue center at different time point at pH 7.4. (**f**) Normalized degree of fixation after 1-day fixation vs distance from tissue center with different starting deprotonated amine concentrations. (**g**) Normalized formaldehyde concentration at the center of sphere over time. (**h**) Confocal microscopy images of FISH-stained *Gad1*, *Vglut1*, and *Vglut2* transcripts in a 200 μm mouse brain slices from intact mouse brains fixed for 8 hours at pH 7.4 (left) and pH 10 (right). Scale bars, 1 mm (whole slice image) and 100 μm (insets). (**i**) Average signal intensity for *Gad1*, *Vglut1*, and *Vglut2* FISH signals from images in (h). n=3 tissue samples. (**j**) Confocal microscopy images of FISH-stained *Pmch* and *Klhl13* transcripts in a 200 μm mouse brain slices from intact mouse brains fixed with pH 10 (left) and pH 7.4 (right). Scale bar, 20 μm. (**k**) Percentage values of *Pmch*-positive cells that co-express *Klhl13*. n=4 tissue samples. (**l**) Cross-sectional views of *GAD1* and *VGLUT1* FISH signals in 200 μm slices from 4-mm-thick human brain tissues processed with 4% PFA at pH 7.4 and pH 10. Scale bar, 100 μm. (**m**) Average signal intensity for *GAD1* and *VGLUT1* FISH signals from images in (j). n=1 tissue sample. (**n**) Average signal intensity for *GAD1* and *VGLUT1* FISH signals at the surface and at the center of images in (j). n=1 tissue sample. Mean ± s.e.m. for all bar graphs. For i, m, n: One-way ANOVA, Tukey's multiple comparison test, *P≤0.05, **P≤0.01, ****P≤0.0001. For k: Unpaired t-test, ns P>0.05.

2.3.5 COMSOL modeling of paraformaldehyde diffusion and reaction inside the tissue with varying initial reactant concentration

To evaluate the dynamics of fixative penetration and resulting fixation profile under alkaline pH conditions, we conducted simulations of a 24-hour formaldehyde fixation using a sphere of 5-mm radius mimicking an intact mouse brain across a wide range of fixation reaction rates (1-, 10-, 50-, 100-fold) (**Figure 2-2 d bottom**). The simulations showed no noticeable changes in the rate of fixative penetration and in the uniformity of fixation across the tested range of fixation reaction rates (**Figure 2-2 f, g**, **Figure 2-3**). Consistently, these models demonstrated that the degree and the rate of fixation throughout the thick tissue volume can be improved by increasing the concentration of non-charged amines in the tissue. These findings collectively suggest that alkaline pH conditions could enable uniform and rapid fixation of non-perfusable thick tissues by enhancing the rate of fixation.

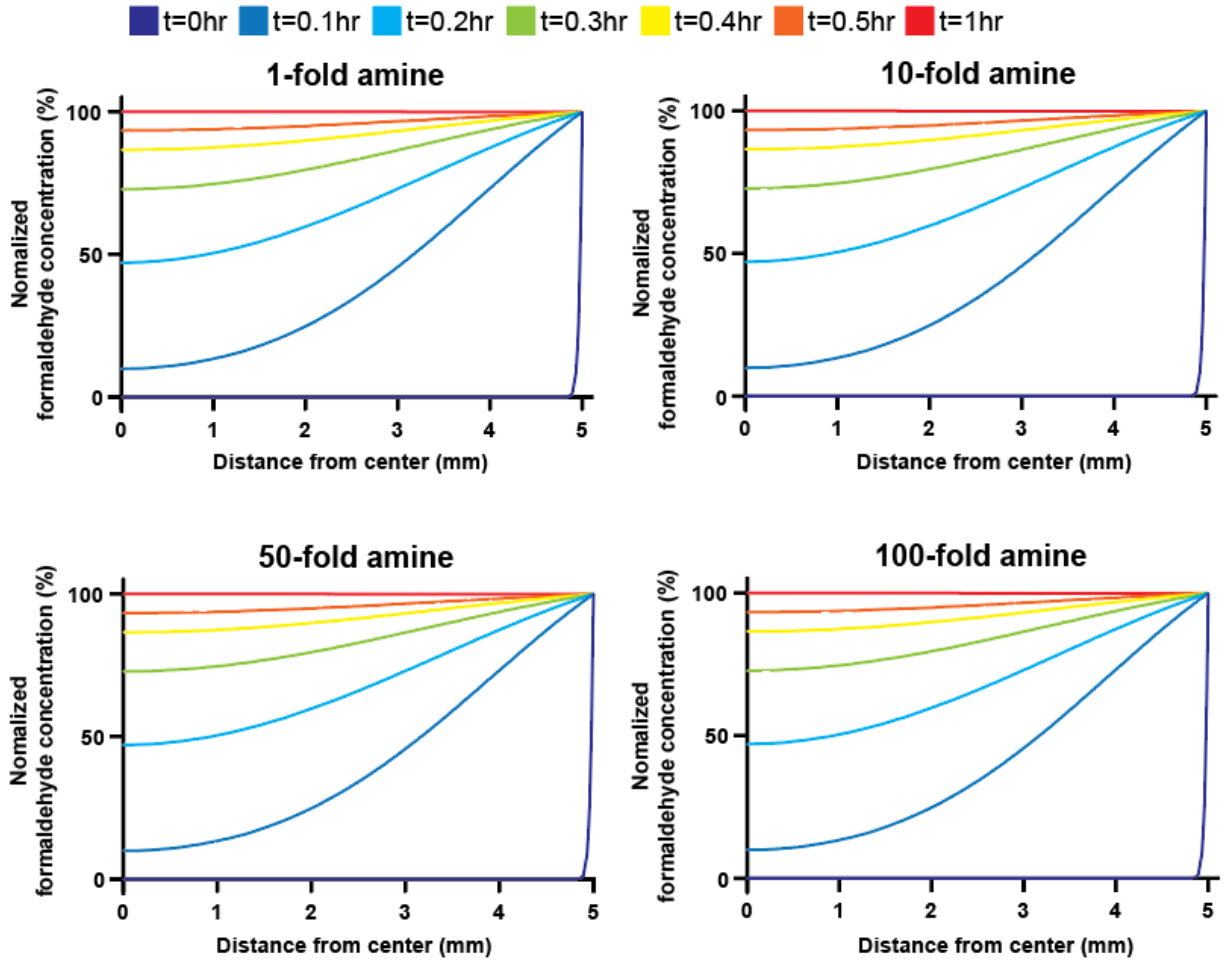

Figure 2-3. COMSOL simulated formaldehyde concentration profiles

Normalized formaldehyde concentration against the distance from the center of sphere at t=0, 0.1, 0.2, 0.3, 0.4, 0.5, and 1 hour. Each graph is from a simulation result of different starting amine concentration.

2.3.6 Fresh mouse brain drop-fixation

To experimentally validate our modeling results, we performed formaldehyde-fixation of freshly extracted mouse brains at pH 7.4 and pH 10. The mouse brains were subjected to transcardial perfusion with ice-cold PBS before extraction and subsequently drop-fixed in 4% PFA under either conventional (pH 7.4) or alkaline conditions (pH 10) at 4°C for 8 hours. Following the fixation, we sliced the mouse brains into thin sections (200 μm) and performed fluorescence *in situ* hybridization (FISH) staining and imaging of mRNAs corresponding to excitatory (*Vglut1*, *Vglut2*) and inhibitory (*Gad1*) neuronal markers. Consistent with our simulation, the FISH signals from the pH 10 alkaline condition exhibited substantially increased brightness compared to the conventional treatment (**Figure 2-2 h, i**), indicating greatly enhanced preservation of mRNAs. Notably, robust FISH signals for *Gad1* were observed in the areas near the cortex (Ctx) and caudoputamen (CP) under alkaline conditions, whereas no detectable signal was found under neutral pH (**Figure 2-2 h, insets**).

Furthermore, we tested whether alkaline fixation conditions cause over-fixation. Due to the unique nature of formaldehyde fixation chemistry, we hypothesized that the probabilistic reaction would allow rapid but sparse fixation of biomolecules even at elevated reactivity. To validate our hypothesis, we perfused mice with 4% PFA at pH 7.4 and pH 10. We performed FISH using common neuronal markers (*Cnr1*, *Drd1*, *Drd2*, *Gad1*, *Gad2*, *Npy*, *Pdyn*, *Penk*, *Th*, *Vglut1*, *Vglut2*, and *Vip*), and the signal quantification did not show significant difference in the intensities between two conditions (**Figure 2-4**).

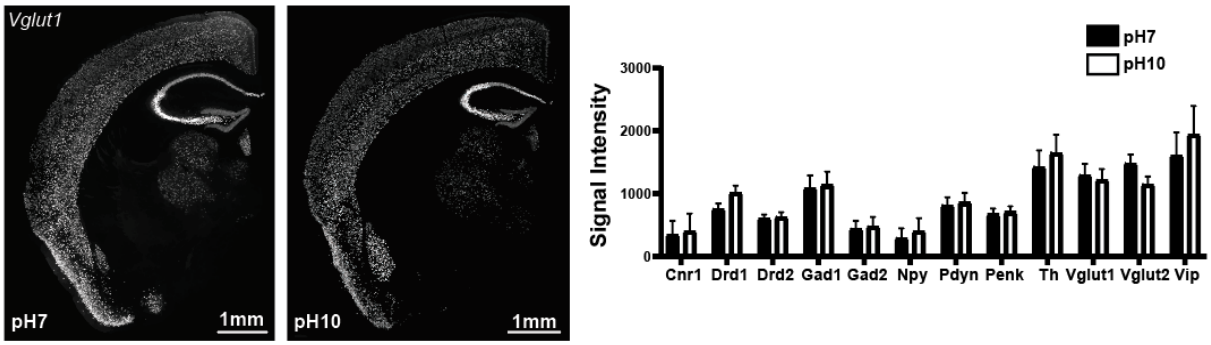

Figure 2-4. Over-fixation test on mouse brain using 12 different FISH markers

2.3.7 Improved sensitivity for low-expressed genes through accelerated fixation

Next, we tested whether accelerated fixation can improve the sensitivity for low-expressed genes. We perfused mouse brains with either conventional (pH 7.4) or alkaline (pH 10) 4% PFA solutions, followed by FISH staining of *Pmch* and *Klhl13* transcripts, which are known to be co-expressed in mouse brain hypothalamus[82]. Among $Pmch^{+}$ neurons detected, 23/31 (74.2%) showed co-localization for tissues fixed with 4% PFA at pH 10, while none, 0/47 (0%), showed co-localization for tissues fixed with 4% PFA at pH 7.4 (**Figure 2-2 j, k**). This result indicates that accelerated fixation by PFA at high pH increases the capture of low-expressed genes, thereby improving the sensitivity.

2.3.8 Thawing of fresh frozen human brain tissues

Next, we evaluated the effects of accelerated fixation on minimizing biomolecular loss in non-perfusable human tissues, where snap freezing and thawing can alter membrane stability, leading to loss of mRNAs if the subsequent tissue fixation process is slow and incomplete. We thawed and fixed 4-mm-thick fresh-frozen human brain samples at 4°C for 24 hours in either conventional (pH 7.4) or alkaline (pH 10) 4% PFA solutions, followed by FISH staining and

imaging of mRNAs corresponding to *VGLUT1* and *GAD1* (**Figure 2-2 l**). Consistent with the results obtained on mouse brain samples, alkaline fixation resulted in significantly brighter signals for both markers (4.77-fold higher for *GAD1*, 2.10-fold higher for *VGLUT1*) indicating that the accelerated fixation significantly improves the preservation of mRNAs in fresh-frozen human tissues (**Figure 2-2 l, m**). No statistically significant differences were observed in the average FISH signal intensities across the tissue depth, further supporting that accelerated fixation does not compromise the uniformity of fixation even for thick, highly myelinated human samples (**Figure 2-2 n**).

2.3.9 Loss of biomolecular integrity over time with PFA-fixed tissues

Having achieved accelerated and uniform fixation of biomolecules using alkaline conditions, we next tested if the preserved mRNAs remain stable long term, which is crucial for volumetric tissue processing, imaging, and multiplex/multi-omic evaluation of thick tissues. We measured FISH signals for *Vglut1* in PFA-fixed wild type (WT, C57BL/6J) mouse brain slices after 2, 4, 8, and 28 days of storage in PBSN (1xPBS + 0.02% (w/v) NaN_3) at 4°C. The FISH signal decayed by 49.4% after 8 days (**Figure 2-5 a, b**). After 28 days (4 weeks) of storage at 4°C, the 4% PFA-fixed samples showed no detectable signals (**Figure 2-5 a**), indicating that physical leakage of mRNAs can slowly occur even after PFA-fixation.

2.3.10 Prevention of post-chemical fixation loss via SHIELD optimization

We hypothesized that intra- and inter-cellular matrix formed by low-degree PFA crosslinking slowly dissociates overtime, causing release and leakage of initially bound mRNAs[72]. Additional crosslinking using multi-functional fixatives could enhance the stability of the fixed cellular matrix, preventing long-term mRNA loss. We previously demonstrated the effectiveness

of a polyepoxy fixation strategy, termed SHIELD, for biomolecular preservation and stabilization, primarily in the context of mouse brain proteome and FP signal[33]. However, mRNA preservation remains a challenge with SHIELD as mRNAs, with their low stability and copy number[66], are more sensitive to the degree of fixation compared to proteins. Therefore, it is crucial to identify optimal polyepoxide fixation conditions that minimize chemical damage while maximizing physical retention of mRNAs (**Figure 2-5 c**).

To determine the ideal conditions for mRNA preservation, we treated 4% PFA-fixed WT mouse brain tissues with varying concentrations of P3PE (polyglycerol 3-polyglycidyl ether, 0 to 16%, w/v), which is the main chemical of SHIELD treatment. The tissues were then delipidated at 37°C for 24 hours and stained with *Vglut1*-FISH probes (**Figure 2-5 d**). *Vglut1*-FISH signals were substantially lower in tissues fixed with 4% PFA alone (59.6% reduction compared to 1% SHIELD, **Figure 2-5 d, e**). The sample treated with 1% SHIELD exhibited the highest FISH signal. However, as the P3PE concentration exceeded 1%, there was a clear decline in the FISH signal (83.2% signal reduction in 16% SHIELD compared to 1% SHIELD, **Figure 2-5 e**). Based on these findings, we concluded that 1% SHIELD, along with 4% pH 10 PFA treatment offers the best trade-off between maximal preservation of mRNAs and minimal chemical damage among the conditions evaluated.

For transcriptomic/multi-omic imaging of intact tissues, it is essential to preserve mRNA for extended periods due to the lengthy processing time required for thick samples. To determine if this new protocol can effectively prevent long-term physical leakage of mRNAs, we prepared WT mouse brain slices fixed with 4% PFA at alkaline condition (pH 10) followed by 1% SHIELD treatment. After the prolonged storage, *Vglut1* FISH labeling and imaging were performed. Unlike the conventionally-fixed tissues (4% PFA at pH 7.4), which exhibited progressive signal loss after storage at 4°C (**Figure 2-5 a, b**), the slices treated with the new protocol showed near complete

signal preservation after 7 days of storage at room temperature (**Figure 2-5 f, g**). These tissues retained robust FISH signals even after 3 months of storage at 4°C (**Figure 2-5 f**). These results indicate that our new protocol, utilizing pH 10 4% PFA and 1% SHIELD treatment, can effectively prevent long-term physical leakage of mRNAs while minimizing chemical damage. Based on our experimental data and computational analysis, we developed protocols for a wide range of species (mouse, rat, marmoset, macaque, human) and sample types (perfusable, non-perfusable, fresh, frozen, thin sections, **Supplementary Note 2**). We termed these protocols as EPIC-SHIELD (**E**xtended **P**reservation of molecules in **I**ntact **C**leared tissue using SHIELD).

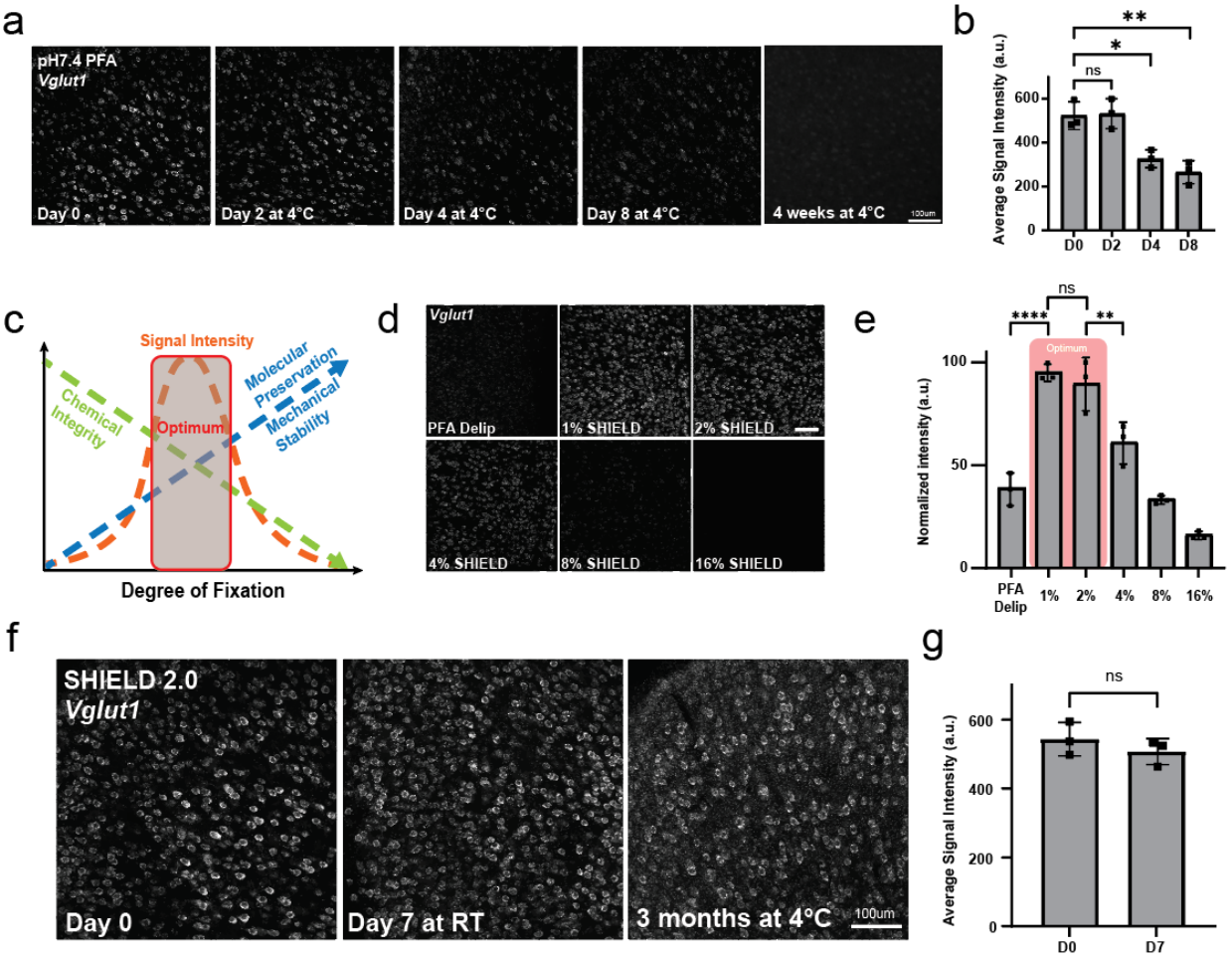

Figure 2-5. Epoxy-based stabilization extends mRNA storage lifetime

(**a**) Confocal microscopy images of Vglut1-FISH signal in 200 µm slices from WT mouse brain tissues fixed using 4% PFA at pH 7.4 and stored in PBSN at 4°C at different time points. Scale bar, 100 µm. (**b**) Average signal intensity for Vglut1-FISH signals from images in (a). n=3 tissue samples. (**c**) Conceptual illustration of optimal range for degree of fixation (**d**) Confocal microscopy images of Vglut1-FISH signals in 200 µm slices from mouse brain treated with increasing SHIELD concentration. Scale bar, 100 µm. (**e**) Normalized signal intensities of Vglut1-FISH from images in (d). n=3 tissue samples. (**f**) Confocal microscopy images of Vglut1-FISH signal in 200 µm, EPIC-SHIELD-treated mouse brain slices stored in PBSN at room temperature (left and middle), and at 4°C for 3 months (right). Scale bar, 100 µm. (**g**) Average signal intensity for Vglut1-FISH signals from images in (f). n=3 tissue samples. Mean ± s.e.m. for all bar graphs. For b, e: One-way ANOVA, Tukey's multiple comparison test, *P≤0.05, **P≤0.01, ****P≤0.0001. For g: Unpaired t-test, ns P>0.05.

2.3.11 Multi-omic preservation capability of EPIC-SHIELD

To validate the multi-omic preservation capacity of EPIC-SHIELD, a wide range of FISH probes and antibodies on both mouse and human brain tissues were tested. We successfully confirmed the compatibility of 78 FISH probes and 465 antibodies for mouse brain tissues, as well as 27 FISH probes and 266 antibodies for human brain tissues (**molecularprobes.org**, **Figure 2-6**, **Figure 2-7**). A full list of markers and antibody validation results are available online (**molecularprobes.org**). To further demonstrate the compatibility of EPIC-SHIELD on other biological systems, such as hiPSC-derived cerebral organoids, we demonstrate transcriptional and proteomic preservation on EPIC-SHIELD treated cerebral organoid slices (**Figure 2-8**, **Figure 2-9**).

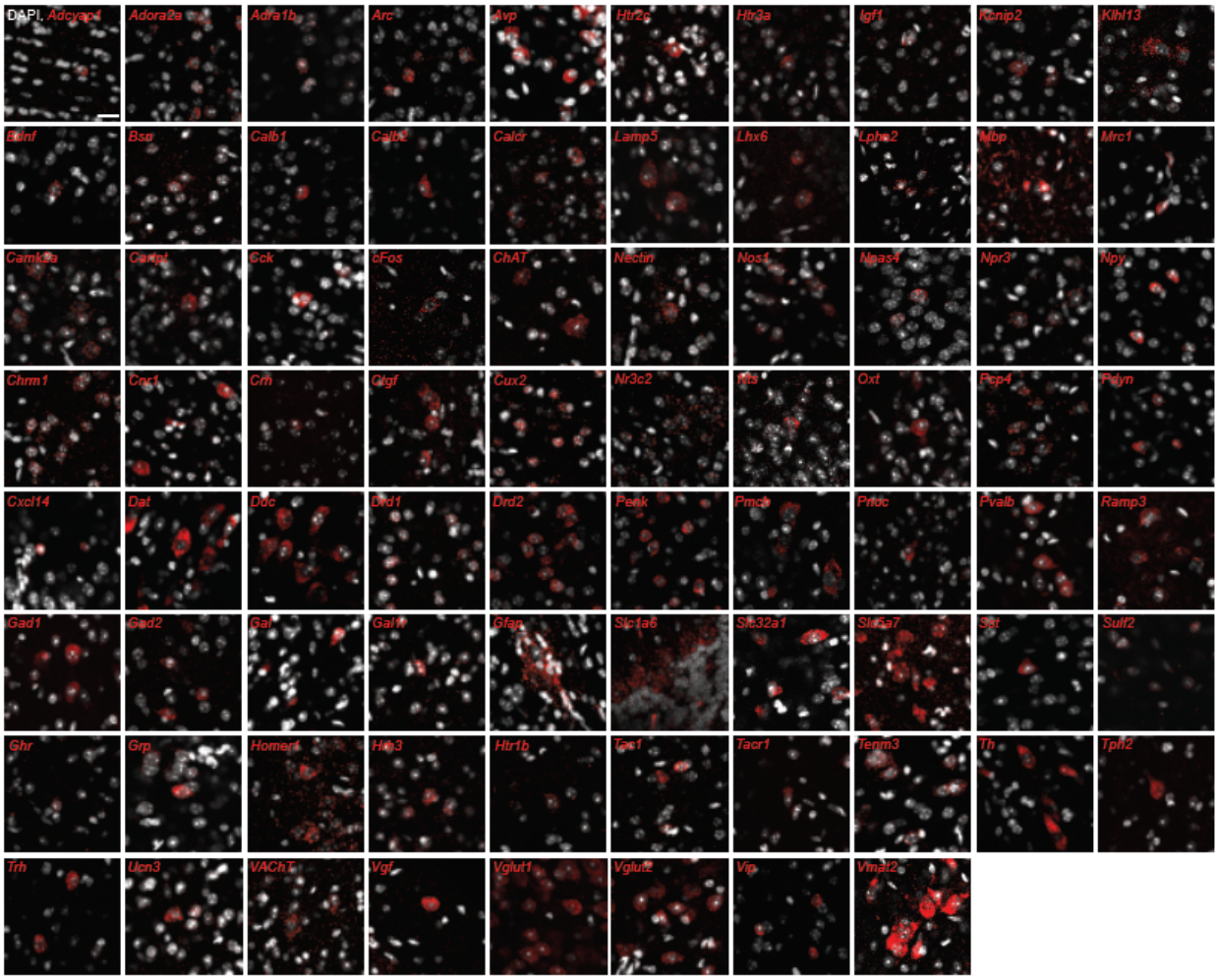

Figure 2-6. EPIC-SHIELD compatible mouse FISH probes

Confocal microscopy images of EPIC-SHIELD compatible mouse FISH probes tested in 200 µm slices derived from various regions of the mouse brain. Scale bar, 20 µm.

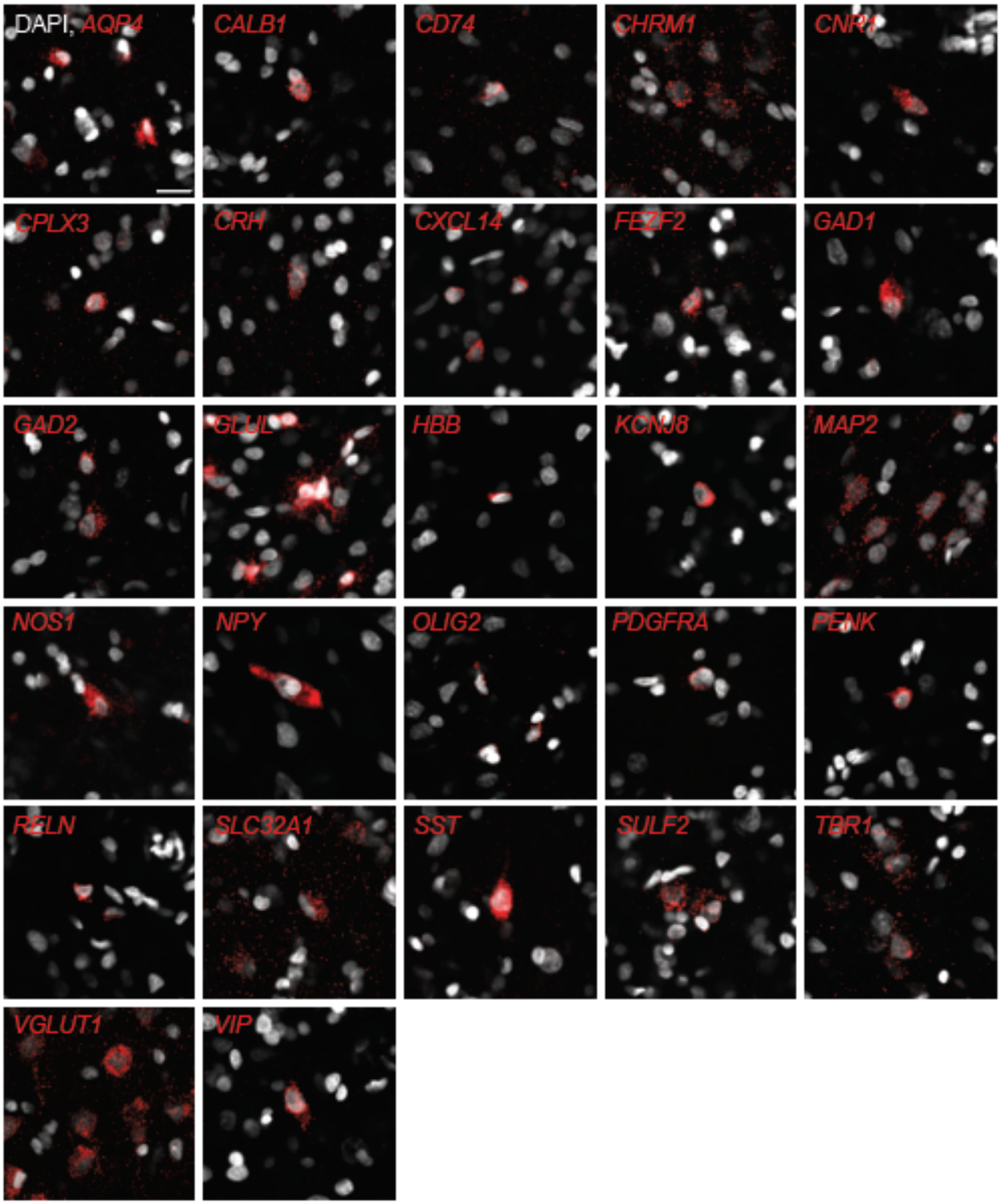

Figure 2-7. EPIC-SHIELD compatible human FISH probes

Confocal microscopy images of EPIC-SHIELD compatible human FISH probes tested in 200 µm slices derived from the human brain cortex. Scale bar, 20 µm.

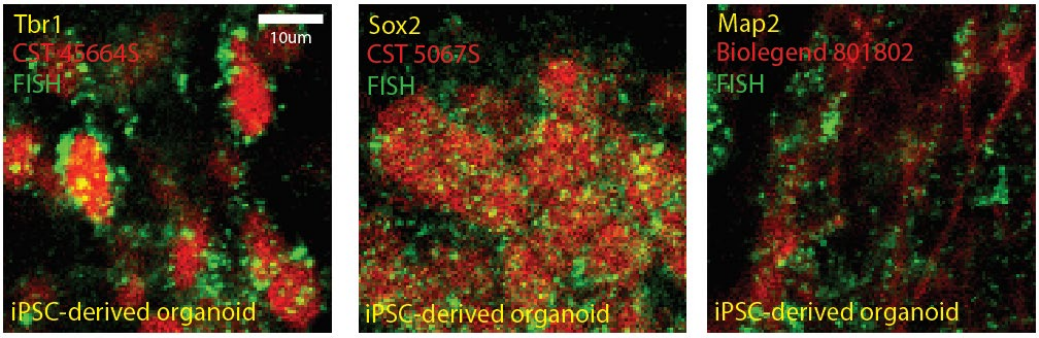

Figure 2-8. EPIC-SHIELD compatible FISH probes tested on cerebral organoid slices

Confocal microscopy images of EPIC-SHIELD compatible human FISH probes tested in 200 µm slices derived from hiPSC-derived cerebral organoid. Scale bar: 10µm

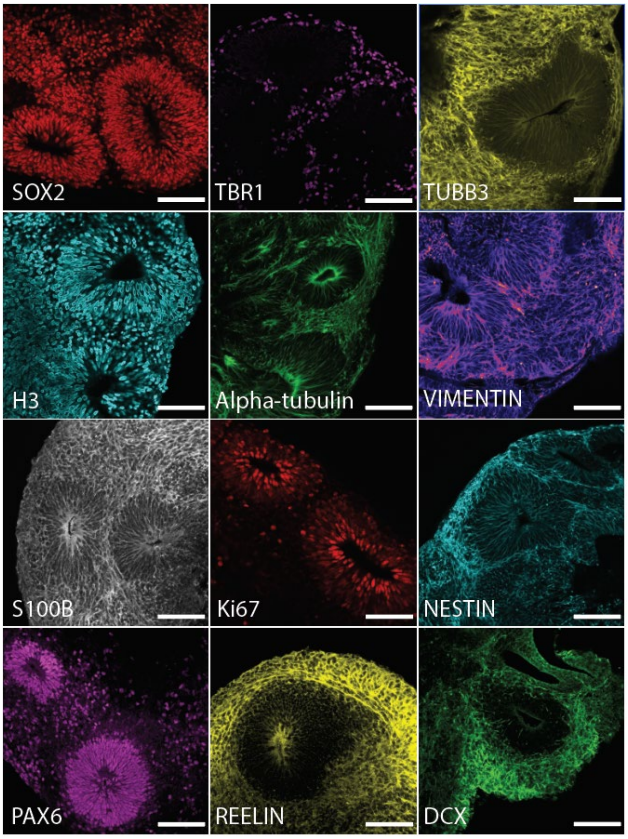

Figure 2-9. EPIC-SHIELD compatible antibodies tested on cerebral organoid slices

Confocal microscopy images of EPIC-SHIELD compatible human antibodies tested in 200 µm slices derived from hiPSC-derived cerebral organoid. Scale bar: 100µm

To determine whether this protocol can also effectively preserve FP signal, we used Thy1-YFP mouse brain tissues. Briefly, 200-μm-thick Thy1-YFP mouse brain coronal slices were initially fixed with conventional 4% PFA, then treated with varying concentrations (0, 1, 2, 4, 8%) of SHIELD solutions and incubated at high temperature (70°C) for 24 hours in 1xPBS. The YFP signal in 1% SHIELD-treated samples was retained at 71 ± 2.6% of the original intensity (**Figure 2-10 a, b**). In contrast, samples treated with PFA alone exhibited near-complete loss of YFP signals (2.3 ± 0.3% retention). Collectively, these results conclusively demonstrate the effectiveness of our EPIC-SHIELD protocol in preserving multi-omic information in large-scale animal and human clinical samples (**Supplementary Note 2**). To test the effect of this mild SHIELD treatment on structural and molecular integrity, we compared mouse brain slices that are SHIELD-treated, with the PFA-fixed ones. After 24hrs of sodium dodecyl sulfate (SDS) treatment at 37°C, PFA-fixed sample showed marked distortion and expansion, while SHIELD-preserved tissues maintained structural integrity (**Figure 2-10 c**).

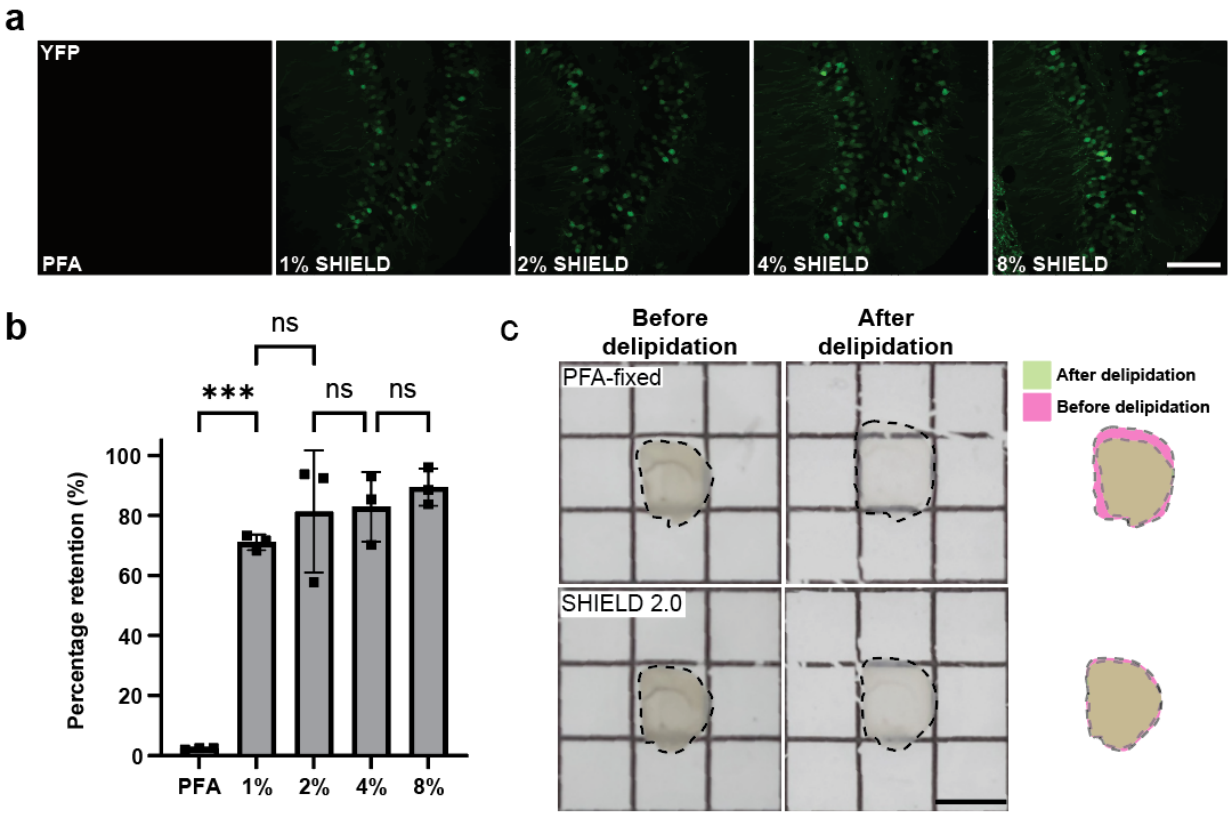

Figure 2-10. Proteomic and structural integrity preserved by mild SHIELD treatment

(**a**) Confocal microscopy images of YFP signals in PFA-fixed and 0-8% SHIELD treated samples following the heat treatment. Scale bar, 100 μm. (**b**) Percentage retention of YFP signals from images in (a). n=3 tissue samples. One-way ANOVA, Tukey's multiple comparison test, ns $P>0.05$, ***$P\leq0.001$. (**c**) Structural deformation comparison between PFA-fixed and EPIC-SHIELD preserved tissues, after 24 hours of delipidation in SDS solution at 37°C. Scale bar, 5 mm

2.4 Conclusion

Preservation of multi-omic information inside the biological tissues is crucial to understand the physiology at health and disease. In this chapter, we introduced EPIC-SHIELD, an effective multi-omic preservation method that was designed to significantly prolong the stability of mRNA information, while simultaneously preserving proteomic information. EPIC-SHIELD is a combination of expediting formaldehyde fixation through adjustments in pH levels, and carefully adjusted SHIELD reaction parameters to minimize the chemical damages. The method is straightforward and does not require any expensive instrumentation, therefore accessible to most laboratories. We believe that the implementation of EPIC-SHIELD treatment on biological samples directly after extraction will significantly improve tissue quality for tissue storage, downstream analysis, and studies. We envision that EPIC-SHIELD will have far-reaching impacts across the broad spectrum of fields including medicine, biology, and engineering. In the following chapters, we will demonstrate how EPIC-SHIELD can synergize with existing brain models to investigate normal brain functions and pathological traits.

Chapter 3 – Multi-omic characterization of mouse models with high scalability and multiplexity

The materials from this chapter are adapted from:

Seo Woo Choi†, Chuanxi Zhao, Xinyi Gu, Jose Vargas-Asencio, Juhyuk Park, Yuxuan Tian, Lee Kamentsky, Nicholas B. Evans, Minyoung E. Kim, Kit-Yi Yam, Nicholas Townsend Haas, Clover Su-Arcaro, Caitlin S. Latimer, Aimee M. Schantz, C. Dirk Keene, and Kwanghun Chung, Effective preservation of biomolecules in large-scale non-perfusable tissues for spatial multi-omic analysis. *Submitted*, 2023.

Minyoung E. Kim†, **Seo Woo Choi**†, Kaoru Saijo, and Kwanghun Chung, MorPheT: a scalable, universal framework for cell morphology phenotyping and mouse fetal brain atlas generation. *In Preparation*.

†Indicates first authorship

3.1 Introduction

A mouse brain model has proven invaluable for studying diseases and biological processes, and scientists have developed various technologies like genetic modification, viral injection, IHC, FISH, and RNA sequencing (RNA-seq) to analyze different aspects of mouse brain biology. However, these methods possess their own strengths and limitations. For instance, RNA-seq can identify hundreds to thousands of genes that are differentially regulated in biological samples, but spatial information is sacrificed during the process. In contrast, *in situ* barcoding techniques like MERFISH and SeqFISH+ can preserve spatial information along with transcriptomic data,

allowing for the analysis of tens of thousands of transcripts per sample[48,58]. Furthermore, some methods, like immuno-SABER and CODEX, extended barcoding concept to proteomics by using oligonucleotide-conjugated antibodies[83,84]. Although these techniques have improved in the multiplexing capacity while preserving spatial information, their volumetric scalability is limited due to the heavy computational burden associated with precise dot-to-dot registration, which requires thinly sliced tissue sections imaged with high-magnification objective. Hence, to complement existing orthogonal technologies effectively and to extract biological information in native spatial context, there is a critical need for a method that offers both high scalability and multiplexity.

In the previous section, we introduced EPIC-SHIELD, which improved the conditions for multifunctional crosslinkers (P3PE) to effectively preserve both transcriptomic and proteomic information[33]. To enhance our ability to comprehensively study mouse models with greater coverage and versatility, this section focuses on characterizing EPIC-SHIELD treated mouse brain tissues. Specifically, we aim to introduce a pipeline that involves (1) a rapid acquisition of volumetric data using oblique selective plane illumination microscopy (oSPIM) at multiple magnifications (4x and 15x), and (2) a full downstream analysis including integration, quantification, and analysis of the multi-round data through nuclei-based co-registration and cell detection.

3.2 Experimental Methods

3.2.1 Reagents and reagent preparation

Paraformaldehyde (PFA) solution preparation

For pH 10 solution, 32% (w/v) PFA solution (15714-S; Electron Microscopy Sciences) was diluted using DI water, sodium carbonate (S7795; Millipore Sigma), and sodium bicarbonate (S5761; Millipore Sigma) to yield final concentration of 4% (w/v) PFA, 50 mM sodium carbonate, 50 mM sodium bicarbonate (pH 10). For pH 7.4 PFA, 32% (w/v) PFA solution was diluted using DI water, and 10x PBS (AM9624; Invitrogen) to yield final concentration of 4% (w/v) PFA in 1xPBS.

SHIELD solution preparation

SHIELD solution preparation was performed as previously reported with adjustments in reaction conditions[33]. The main SHIELD reagent, polyglycerol 3-polyglycidyl ether (P3PE, product name GE38) was provided by CVC Thermoset Specialties of Emerald Performance Materials. P3PE was weighed and dissolved in respective buffer solution by vortex until the solution turned cloudy. The resulting milky solution was centrifuged at 4°C, for 10 min at 7800 rpm, which yielded a clear supernatant and insoluble resin at the bottom. Only the supernatant part was collected for SHIELD processing. Following solutions were prepared for our EPIC-SHIELD protocols, with P3PE dissolved.

EPIC-SHIELD perfusion solution: 50 mM sodium carbonate, 50 mM sodium bicarbonate buffer (pH 10) containing P3PE supernatant and 4% (w/v) PFA, ice-cold

SHIELD-OFF solution: 50 mM sodium carbonate, 50 mM sodium bicarbonate buffer (pH 10) containing P3PE supernatant, 4°C

SHIELD-ON solution: 50 mM sodium carbonate, 50 mM sodium bicarbonate buffer (pH 10) containing P3PE supernatant, room temperature

Clearing solution preparation

Two main clearing (delipidation) solutions were prepared with following detergents: 200 mM Sodium Dodecyl Sulfate (75746; Millipore Sigma) or 280 mM cholic acid sodium salt (J13630A1; Fisher Scientific). Both clearing solutions contained following common chemicals: 150 mM Lithium hydroxide monohydrate (43171; Alfa Aesar), 250 mM Boric acid (B6768; Millipore Sigma), 70 mM sodium sulfite (S0505; Millipore Sigma) in DI water.

Refractive index matching solution

Protos-based RI matching solution, ExProtos (RI ~1.4580), was prepared by dissolving 125 g of iohexol, 5 g of N-methyl-d-glucamine, 3 g of diatrizoic acid in 100 mL DI water. The final RI was adjusted using DI water.

3.2.2 Mouse brain processing

Mice were transcardially perfused with ice-cold 1xPBS, followed by perfusion with 4% (w/v) PFA at desired pH (pH 7.4 or pH 10). The brains were extracted and post-fixed for 24 hours at 4°C using 4% (w/v) PFA. The brains were washed overnight using PBSN at 4°C, and sectioned into slices of desired thickness using vibratome, followed by EPIC-SHIELD treatment.

3.2.3 EPIC-SHIELD processing

The slices were incubated in SHIELD-OFF solution containing 1% (w/v) P3PE for 24 hours with gentle shaking. Then, the slices were moved to an orbital shaker at room temperature to initiate ON step (no solution change). After 24 hours of ON step, the slices were washed with PBSN overnight at room temperature. Delipidation was performed using SDS-based clearing solution at 37°C. Delipidated samples were washed with 0.1% PBSTN (1xPBS + 0.02% (w/v) NaN_3 + 0.1% (v/v) Triton-X; X-100; Millipore Sigma) overnight at 37°C.

3.2.4 Lightsheet microscopy

For a large-scale tissue slab imaging, custom-built Multicolor-Inverted Axially-Swept Lightsheet Fluorescence Microscope (IASLSFM) was used[9]. IASLSFM is equipped with four laser sources (405nm, 488nm, 561nm, and 647nm), whose beam is shaped into a sheet through a cylindrical lens. The illumination and detection objectives were set orthogonally, at a 45-degree angle to the sample surface. For the multi-round imaging and a large-scale human brain imaging, 4x 0.2NA objective was used with a custom dipping cap to acquire long working distance. All synchronized movement of lasers, camera, lens, and the stage were controlled using ASI (Applied Scientific Instrumentation) Tiger controller and a custom-designed LabVIEW software. All acquired images were converted from 45-degree coordinates into conventional XYZ coordinates.

3.2.5 Nuclei-based co-registration

For the nuclei-based co-registration, custom python-based software with GUI was used that aligns the fixed and moving rounds. In brief, the images are roughly aligned manually, followed by matching pair finding from both image volumes, thresholding out matches, and the

calculation of a warping function that translates coordinates from one image to the other. Pair finding, filtering, and warping function calculation steps are repeated until the convergence.

3.2.6 Cell counting and co-positivity analysis

For co-registered multi-round datasets, the visualization and cell spot counting were performed using Imaris 9.0.1 software (Bitplane). For each marker, Imaris software's spot function was used to generate coordinates of positive signals. The accuracy of detection was obtained by comparing with manually generated ground truth data (**Table 3**). For the mouse brain 23-plex dataset, the coordinate of each FISH signal was exported and assigned to the closest DAPI coordinate using MATLAB 2022a (MathWorks).

3.3 Results and Discussion

3.3.1 EPIC-SHIELD pipeline for scalability and multiplexing capacity.

To fully harness the potential of EPIC-SHIELD, it is essential to integrate it into a comprehensive pipeline that encompasses optical, biochemical, and computational methods for the efficient extraction of biomolecular information. Our pipeline has been designed to address three key objectives: 1) ensuring the effective preservation of biomolecules in thick tissues, 2) efficiently extracting information from tissues treated with EPIC-SHIELD while maintaining high scalability, and 3) merging and integrating data to enable multi-omic characterization of biological tissues (**Figure 3-1**).

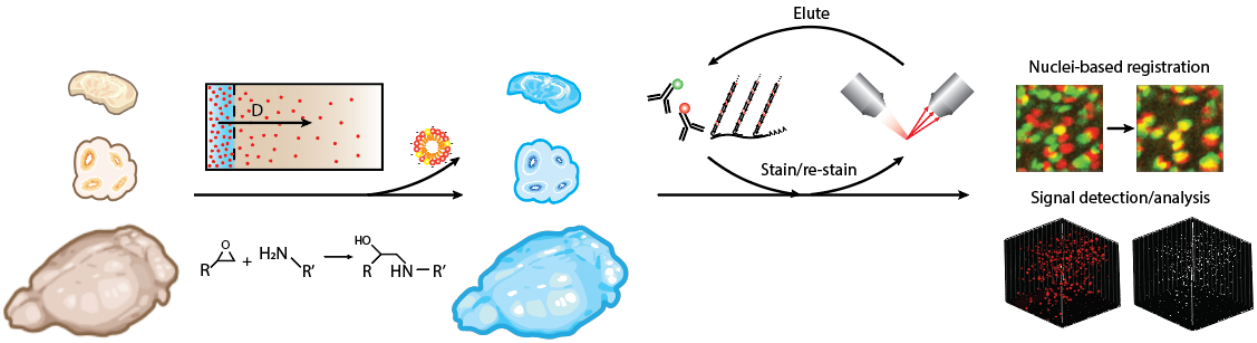

Figure 3-1. Overview of EPIC-SHIELD pipeline for high scalability and multiplexity

3.3.2 Multiple rounds of mouse brain characterizations

EPIC-SHIELD is capable of preserving both transcriptomic and proteomic data effectively, even when harsh delipidation procedures are applied to the samples. Delipidation involves removing lipids from biological tissues, which are the major source of light scattering and can impede deep tissue imaging. Anchoring biomolecules securely during this delipidation process is crucial to prevent molecular loss. When this anchoring process is successful, ensuring effective

preservation, the biological tissues can endure multiple rounds of staining and destaining processes. To assess whether EPIC-SHIELD achieves the desired level of preservation, we initially conducted nine rounds of FISH on 200-μm-thick WT mouse brain tissue that had been treated with EPIC-SHIELD (**Figure 3-2 a**). The results showed robust and intact signals even after multiple rounds of staining, demonstrating the transcriptomic stability provided by EPIC-SHIELD. We then proceeded to assess the preservation of proteomic information. While protein molecules are generally more resilient and stable compared to mRNA molecules, conducting multiple rounds of protein staining presents its own set of challenges. In contrast to the relatively mild destaining process used in FISH multi-round staining, which involves slightly elevated temperatures (~42°C) and a high denaturant content (~90 v/v% formamide), antibody de-staining requires extremely harsh conditions, involving treatment with SDS at 80°C. Such high temperatures can easily damage biological tissues, making effective preservation essential to prevent the loss of information. To evaluate whether EPIC-SHIELD treatment enables biological tissues to withstand these severe conditions, we conducted three rounds of antibody staining on a small section of mouse brain cortex (**Figure 3-2 b**). The results from the multi-round staining demonstrate that EPIC-SHIELD effectively preserves both transcriptomic and proteomic information, enabling the application of harsh conditions to the tissues without loss of information.

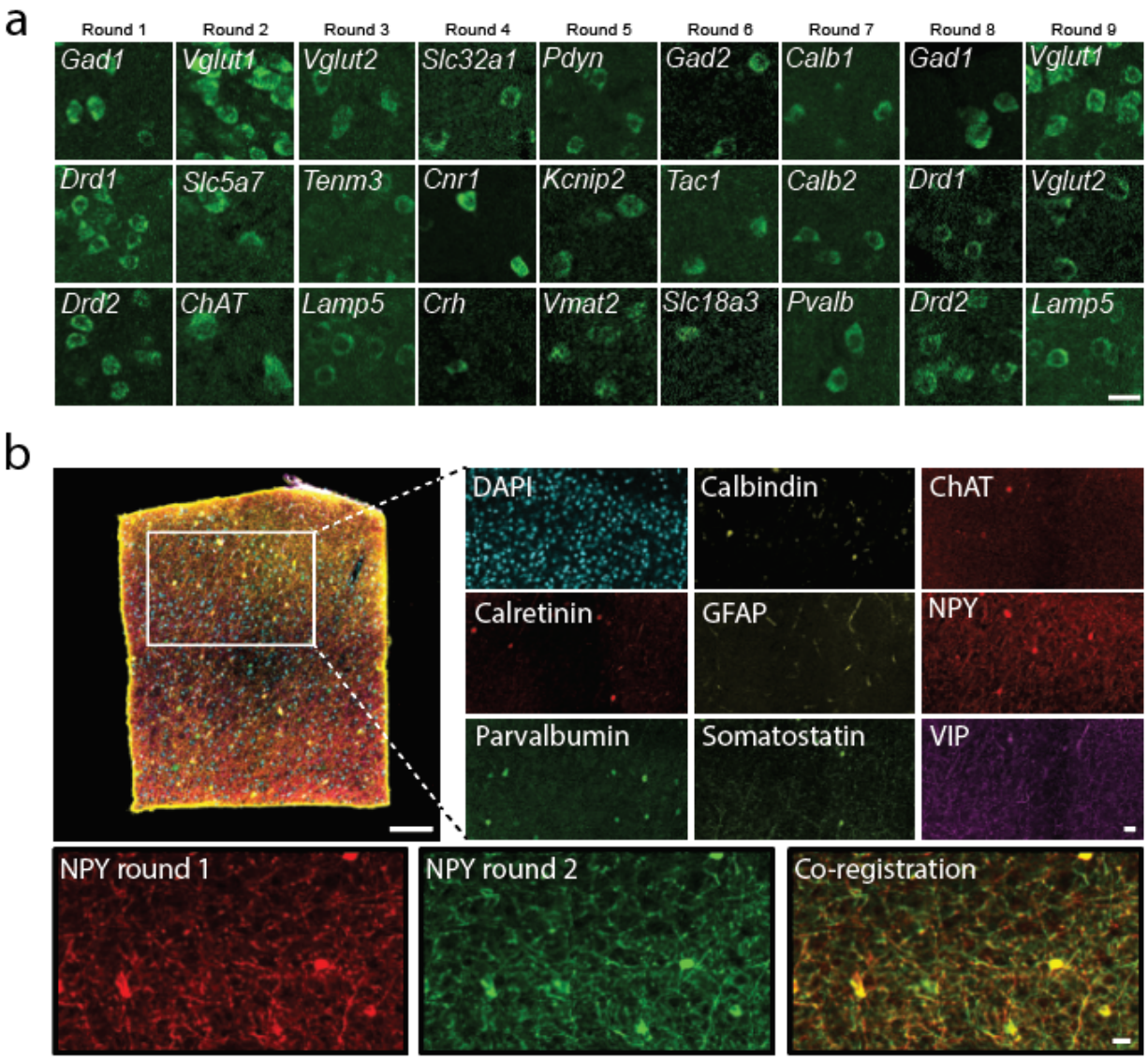

Figure 3-2. Multiple rounds of FISH and IHC on mouse brain

(**a**) Nine rounds of FISH on the same slice of mouse brain treated with EPIC-SHIELD. Scale bar, 20 μm. (**b**) Nuclei-based co-registration on mouse brain cortex, integrating three rounds of IHC. Scale bars, 100 μm (merged), 20 μm (zoomed).

3.3.3 Rapid acquisition of data

To fully leverage the potential of EPIC-SHIELD for comprehensive and unbiased analysis of biological tissues, it is essential to enhance the speed of data acquisition and the ability to analyze larger volumes of tissue. One of the challenges in acquiring volumetric data is ensuring the penetration of probes into the tissue. These issues can be addressed by using DNA probes for FISH and by applying the SWITCH concept to antibodies[32,41]. DNA FISH probes have low molecular weight, which enables them to passively penetrate thick tissues even on the millimeter scale. On the other hand, antibodies are relatively heavy, and it would take prohibitively long time to fully stain thick tissues. However, by quenching the binding reaction and solely allowing diffusion, it is possible to prevent probe depletion and allow the penetration of antibodies deep into the tissues. When combined with the delipidation and optical clearing of tissues using refractive index (RI) matching solutions, these labeling methods will enable the characterization of volumetric tissues.

Another bottleneck lies on the acquisition speed of the data. Confocal microscopes use a point-scanning method, which not only prolongs data acquisition but also increases the risk of photobleaching due to extended exposure to high intensity laser. To address this challenge, we developed a custom oSPIM. oSPIM transforms the light source into a sheet, allowing it to illuminate an entire plane instead of just a point. Consequently, data acquisition time can be significantly reduced, enabling highly scalable data collection. For instance, while it may take overnight to several days to image a 4-channel, 500-μm-thick mouse brain hemi-coronal slice using a confocal microscope (with a 20x objective), oSPIM can accomplish the same task in approximately 2-3 hours (using a 15x objective).

3.3.4 Data integration and quantification

Integrating multiple rounds of data poses another challenge in effectively utilizing our multiplexing technologies. For the maximal use of our technologies, it is crucial to merge datasets in a way that enables the analysis of co-positive cells and the identification of expression profiles at single-cell level. To achieve this, we employed nuclei-based co-registration methods. Previously, we utilized a lectin-based co-registration approach[32]. However, nuclei-based co-registration is preferred particularly for co-positivity analysis as it allows us to precisely extract the exact coordinates of nuclei. Additionally, this approach is applicable to the study of biological systems that lack vascular systems, such as human induced pluripotent stem cell (hiPSC)-derived cerebral organoids. For the proof of concept, we applied nuclei-based co-registration to our previous multi-round data, which involved three rounds of antibody staining on a small section of mouse cortex (**Figure 3-2 b**). Initially, we manually adjusted each DAPI channel to achieve rough alignment. Next, both the fixed and moving profiles were Gaussian blurred to locate nuclei centers. These coordinates were found by identifying centers that have decreasing intensity with increasing distance. Subsequently, we generated a grid on both the fixed and moving images, which acts as a reference point when choosing nuclei centers for warping. The patch of moving nuclei centers was moved in the direction of the highest correlation. After the filtering steps to select only those with good match (within threshold), the entire process was repeated until the whole profile was co-registered within few pixels (**Figure 3-3**). Each round of warping function was merged to calculate the final warping function that could be applied to other non-DAPI channels. As a result of this co-registration process, we successfully combined the datasets with single-cell resolution, as depicted in **Figure 3-2 b**. Remarkably, through nuclei-based co-registration alone, we also achieved the registration of fiber signals within a few pixels (**Figure 3-2 b**).

To quantify the co-registered datasets, we employed the commercially available Imaris software. In brief, we extracted three-dimensional cell coordinates from the co-registered molecular signals along with the coordinates of DAPI-stained nuclei. Next, we calculated the three-dimensional Euclidean distance between the molecular signals and all DAPI signals using custom MATLAB code. We selected the shortest distance, and if the value fell below a certain threshold, the signal was assigned to the corresponding DAPI coordinate. As a result, a binary dataset was generated that represented all co-positivity among the FISH markers.

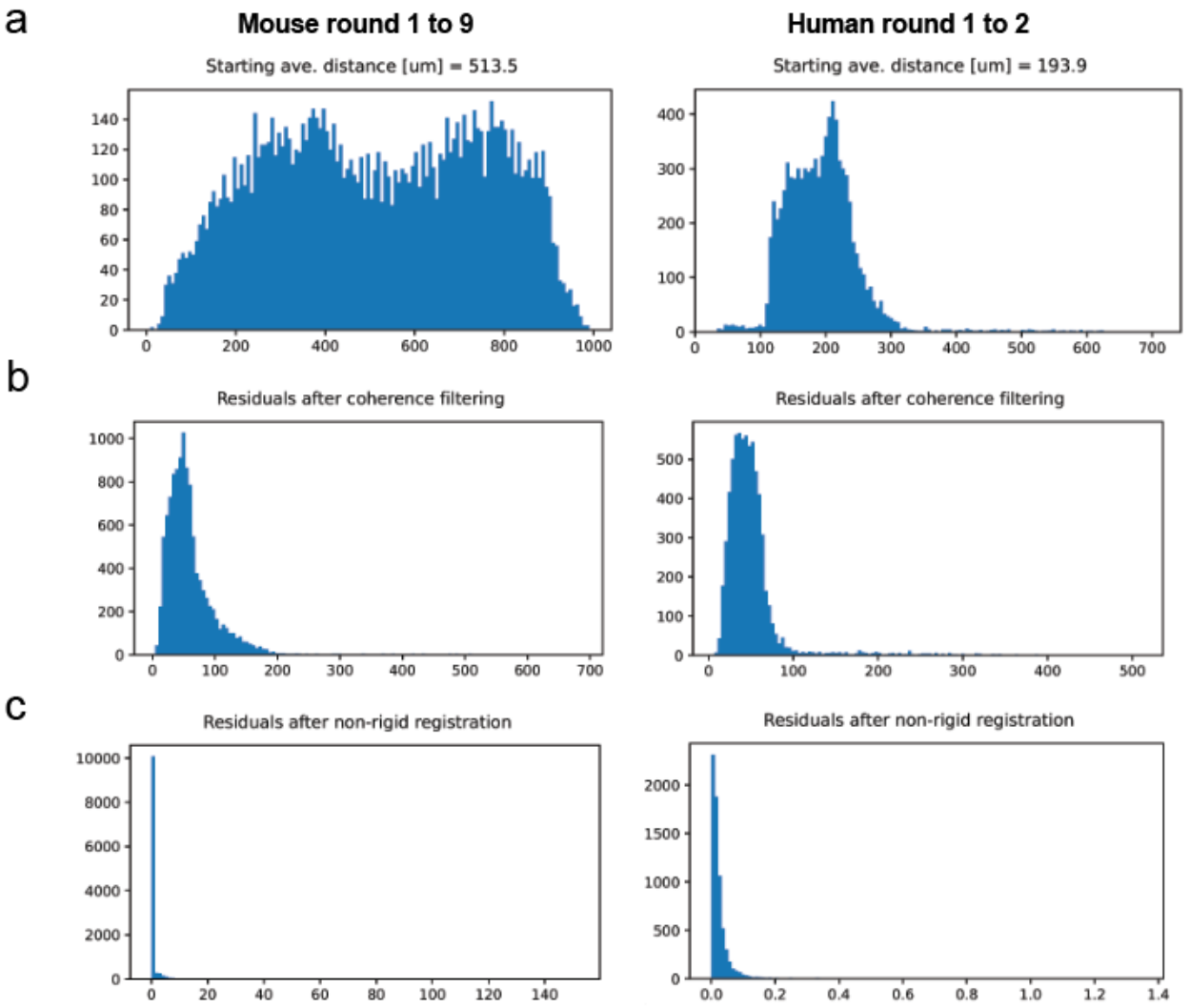

Figure 3-3. The performance of co-registration algorithm on mouse and human datasets

(**a**) Histogram of starting average distance for corresponding nuclei blobs of fixed and moving images (round 1 and 9 for mouse, and round 1 and 2 for human). (**b**) Histogram of residual errors between corresponding nuclei blobs after warping and coherence filtering. (**c**) Histogram of residual distances between corresponding nuclei blobs after the last round of non-rigid registration.

3.3.5 Combining molecular phenotypes with morphological details

To demonstrate the utility of EPIC-SHIELD, we applied our pipeline to study Mononucleotide Repeat Frameshift (MORF) brains. MORF brains are sparsely labeled using a Cre-line, where the labeled neurons can express either FPs or tagged proteins like V5. By combining EPIC-SHIELD with MORF technologies, we can extract both molecular profiles and morphological information from thick tissues at a single-cell level. As a preliminary demonstration, we conducted four rounds of FISH targeting specific genes (*Gad1*, *Gad2*, *Drd2*, *Vmat2*, *Slc32a1*, *Th*, *Dat*, *Vglut1*, *Vglut2*, *Calb1*, *Calb2*, *Ddc*) and a single round of anti-V5 immunostaining on a brain slice from a MORF3/Camk2a-CreER mouse. We then applied nuclei-based co-registration to the data (**Figure 3-4 a**). Upon zooming in on the V5-positive cells, we were able to clearly visualize both the expressional profile and the morphological details of the neurons (**Figure 3-4 b**). Additionally, we utilized various ventral tegmental area (VTA) markers (*Drd2*, *Vmat2*, *Th*, *Dat*, *Ddc*), which displayed the expected co-positivity (**Figure 3-4 c, d**). This combined approach illustrates that EPIC-SHIELD pipeline is a powerful tool for studying the mouse brain through multi-omic preservation.

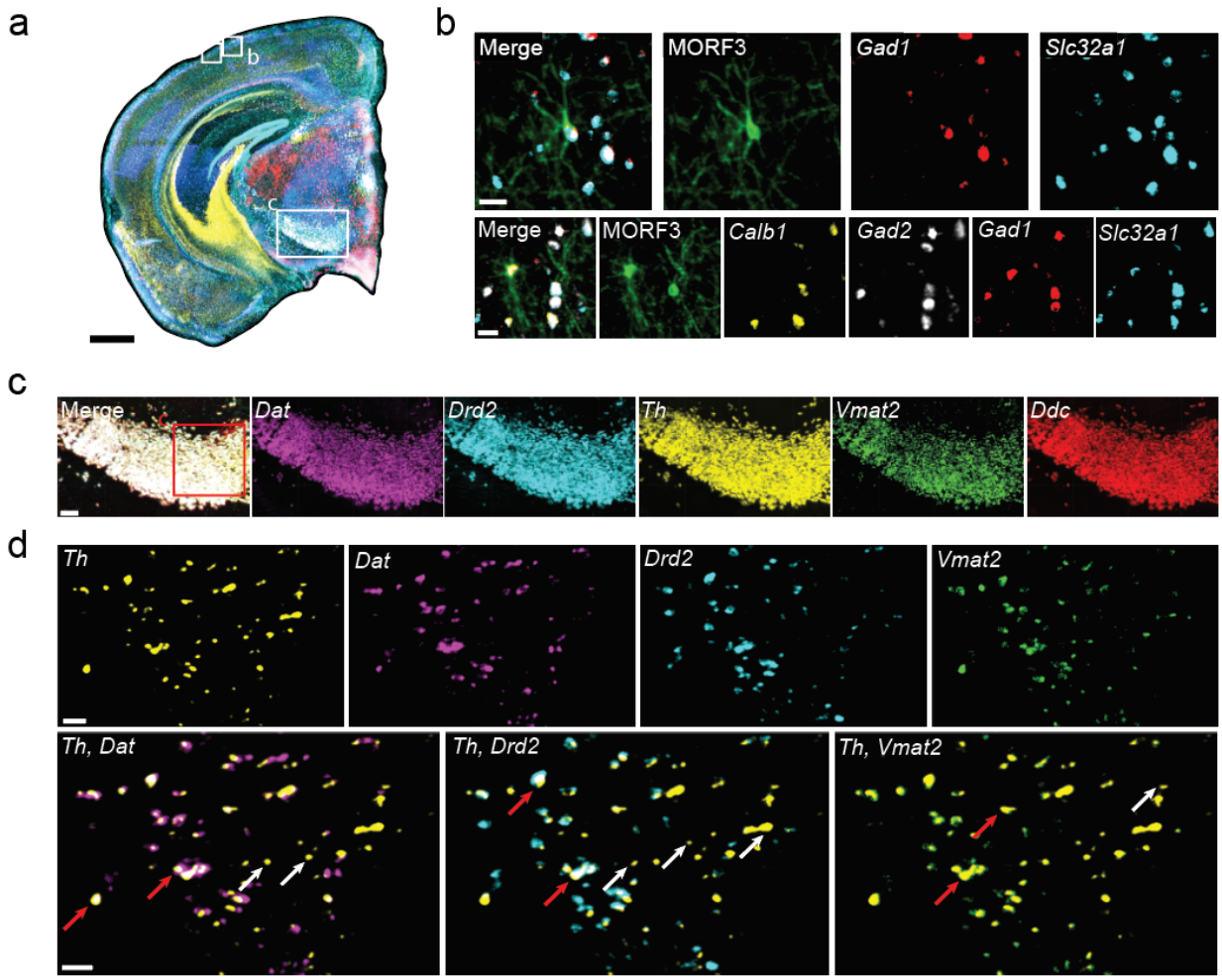

Figure 3-4. Co-registered image of a MORF brain slice

(**a**) Merged image of 12-FISH markers and anti-V5 staining. Scale bar, 800 μm (**b**) Zoomed image of V5-positive cells in the cortex. Scale bar, 30 μm. (**c**) Zoomed image of VTA region. Scale bar, 100 μm. (**d**) Single (white arrow) and double-positive (red arrow) cells. Scale bar, 30 μm.

3.3.6 Multiple rounds of FISH for spatial transcriptomic

To demonstrate how the optimal and long-lasting mRNA preservation in EPIC-SHIELD enables volumetric evaluation and multiplexing, 8 net rounds of imaging were conducted on a 500-µm-thick WT mouse brain coronal slice treated with EPIC-SHIELD (**Table 2**). Leveraging the high-throughput imaging capabilities of the Inverted Axially-Swept Light-Sheet Fluorescence Microscopes (IASLSFM)[9], 8 rounds of imaging were completed within 4-5 hours. We successfully detected transcripts for 23 representative genes across the entire tissue volume while preserving structural and anatomical tissue features for the entire coronal slab (**Figure 3-*5* a**, **Table 2**). Transcripts from genes associated to 14 cortical (*Calb1*, *Cnr1*, *Ctgf*, *Cxcl14*, *Gad1*, *Gad2*, *Mbp*, *Nos1*, *Npy*, *Pdyn*, *Sst*, *Vglut1*, *Vglut2*, *Vip*), 5 striatal (*ChAT*, *Drd1*, *Drd2*, *Penk*, *Tac1*) 4 hypothalamic (*Adcyap1*, *Calb2*, *Th*, *Trh*) regions were captured using this multiplexing strategy (**Figure 3-*5* a** insets). The biomolecular profiles obtained from the multiple rounds of staining were integrated using our previously described nuclei-based co-registration algorithm[9]. Enabling multi-round imaging of thick tissues and high-speed light-sheet imaging resulted in a remarkable increase in the number of cells that can be characterized within intact tissue volumes. Focusing on a sub-volume (0.6 mm x 0.6 mm x 0.6 mm) near the motor cortex, a linear relationship between the number of captured cells and the tissue thickness was observed (28,670 cells in the 500µm-thick whole slab volume compared to 1,093±118 cells in representative 20-µm-thick virtual slice volumes, **Figure 3-*5* b**). To demonstrate the practical utility and scalability of the multiplexing technology, we performed cell type inference using cumulative information from a set of cortical markers (*Vglut1*, *Gad1*, *Gad2*, *Npy*, *Mbp*) known to be associated with major cell types[85–87]. Using a classification scheme based on the combined expression, excitatory and inhibitory neurons, and oligodendrocytes were identified (overall accuracy = 98.3%, **Table 3**). 3D reconstruction of these

data provides an initial view of cellular architecture within thick tissues (**Figure 3-*5* c**). Multiplexed volumetric evaluation also enabled the detection of a rare type of inhibitory long-range projecting neuron (*Vglut1*$^{-}$, *Gad1/2*$^{+}$, *Nos1*$^{+}$, *Npy*$^{+}$, *Sst*$^{+}$, **Figure 3-*5* d**)[88]. Only 8 of these cells were detected across the cortical sub-volume described above. Using virtual 10-µm-thick optical sections, these would have appeared in 6/60 cases, which can be missed in subsampling-based thin-section assays, highlighting the value of thick tissue analysis (**Figure 3-*5* d**).

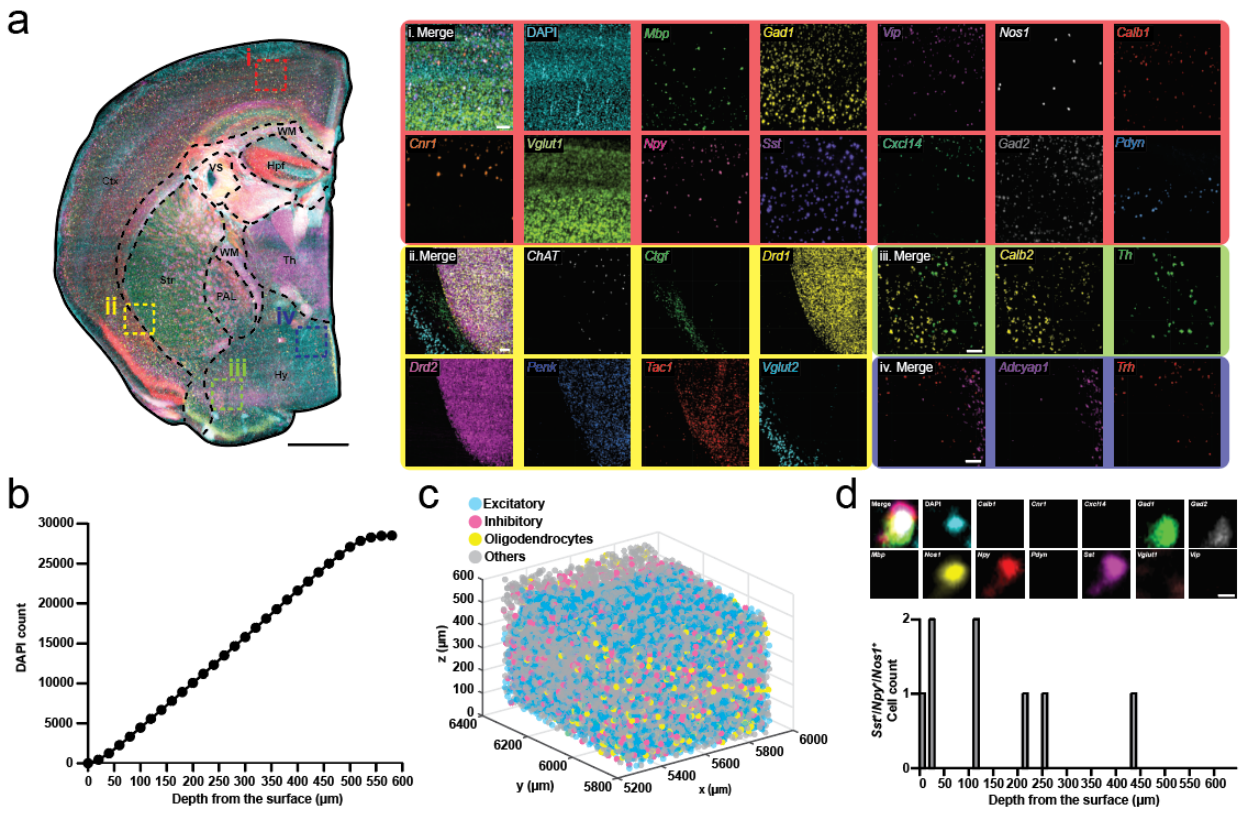

Figure 3-5. Multi-omic characterization of mouse brain, enabled by EPIC-SHIELD

(**a**) Maximum projection image of 23-plex multi-round imaging of a 500-µm-thick mouse brain coronal slice treated with EPIC-SHIELD. Four representative regions of interest are highlighted in color-coded, zoomed in insets: i: cortex ii: striatum, iii: amygdala nucleus, iv: hypothalamus. Scale bars, 1 mm (whole image) and 100 µm (insets) (**b**) Cumulative DAPI counts from consecutive 20 µm optical slices from a 0.6 mm x 0.6 mm x 0.6 mm sub-volume extracted from the cortical region of image in (a). (**c**) 3D reconstruction of cellular architecture of the cortical sub-volume used in (b). (**d**) Representative images of detected *Gad1*$^{+}$/*Gad2*$^{+}$/*Nos1*$^{+}$/*Npy*$^{+}$/*Sst*$^{+}$/*Vglut1*$^{-}$/*Vip*$^{-}$/*Pdyn*$^{-}$/*Mbp*$^{-}$/*Cxcl14*$^{-}$/*Cnr1*$^{-}$/*Calb1*$^{-}$ cells (top) and a histogram of detection events of *Gad1*$^{+}$/*Gad2*$^{+}$/*Nos1*$^{+}$/*Npy*$^{+}$/*Sst*$^{+}$/*Vglut1*$^{-}$/*Vip*$^{-}$/*Pdyn*$^{-}$/*Mbp*$^{-}$/*Cxcl14*$^{-}$/*Cnr1*$^{-}$/*Calb1*$^{-}$ cells in 10-µm-thick optical slices from sub-volume in (c). Scale bar, 10 µm.

Table 2. Multi-round FISH on 500-um-thick mouse brain coronal slice

	488	**561**	**642**
Round 1	*Ctgf*	*Drd1*	*Mbp*
Round 2	*Gad1*	*Calb1*	*Tac1*
Round 3	*Vip*	*Nos1*	*Drd2*
Round 4	*Cnr1*	*Vglut1*	*Vglut2*
Round 5	*Npy*	*Sst*	*Pdyn*
Round 6	*Cxcl14*	*Gad2*	*ChAT*
Round 7	*Arc*	*Th*	*Calb2*
Round 8	*Trh*	*Penk*	-
Round 9	-	*Adcyap1*	-

Table 3. FISH/DAPI detection accuracy (%), mouse

	Gad1	***Gad2***	***Vglut1***	***Mbp***	***Npy***	**DAPI**	**Overall**
Accuracy	92.6	93.6	86.6	98.2	98.4	98.3	98.3

3.3.7 Study of mouse embryo for microglia morphologies

Microglia are the brain resident macrophages and play vital roles in disease, development, and homeostasis. One notable characteristic of microglia is their ability to change their morphologies depending on the brain physiology and environment. For instance, in a resting state, microglia have ramified shapes, constantly surveilling the central nervous system. However, when under insults like brain damage, disease, or infection, microglia transform into amoeboid shapes and undergo changes in their gene expression profiles. Therefore, examining the morphological aspects of microglia is crucial for understanding the mechanisms underlying diseases and restoring balance in the brain.

Interestingly, microglia also exhibit gradual shift in morphologies during development as they migrate from the yolk sac to the brain parenchyma[89]. In the early stages, microglia display amoeboid shapes, which gradually shift into ramified morphologies around birth. This transition in morphological characteristics has not been fully explained yet. Consequently, there is a need for a comprehensive atlas to observe and quantify microglia in mouse embryos, allowing us to better grasp the developmental process and gain insights into the roles of microglia in shaping the brain environment.

To conduct an unbiased and comprehensive study of embryos, we slightly modified the EPIC-SHIELD pipeline, considering the variations in size and mechanical properties. The workflow for processing mouse embryos and embryonic brains includes EPIC-SHIELD treatment, delipidation, photobleaching, labeling, refractive index (RI) matching, and lightsheet imaging (**Figure 3-6 a**). In order to determine the optimal conditions for preserving proteomic data, we quantified the average signal intensities of polyclonal antibody signals on mouse brain tissues

treated with varying concentrations of SHIELD. The results showed that low concentrations of SHIELD (1-4%) exhibited no statistically significant differences compared to the PFA control sample (**Figure 3-6 b**). Following the EPIC-SHIELD treatment, we optimized delipidation and antibody staining. One of the primary objectives of this study is to provide the scientific community with quantified data regarding ramified and amoeboid microglia, and border associated macrophages (BAMs) at different regions during each developmental stage. To achieve this, the preservation of structural integrity of the tissues is crucial as the images needed to be aligned and registered with the reference atlas provided by the Allen Brain Atlas. We discovered that SDS-mediated delipidation caused significant tissue distortion, whereas sodium cholate (NaC)-based delipidation showed superior preservation of structural integrity (**Figure 3-6 c**)[90]. After heuristically testing various antibodies for green fluorescent protein (GFP) and CD206, we successfully conducted volumetric staining and imaging of intact mouse embryos and brains (**Figure 3-6 c**). The acquired volumetric data will be processed using our machine learning based cell detection and classification pipeline, MorPheT, to detect, quantify, and categorize microglia based on their morphologies and regions (**Figure 3-6 d**).

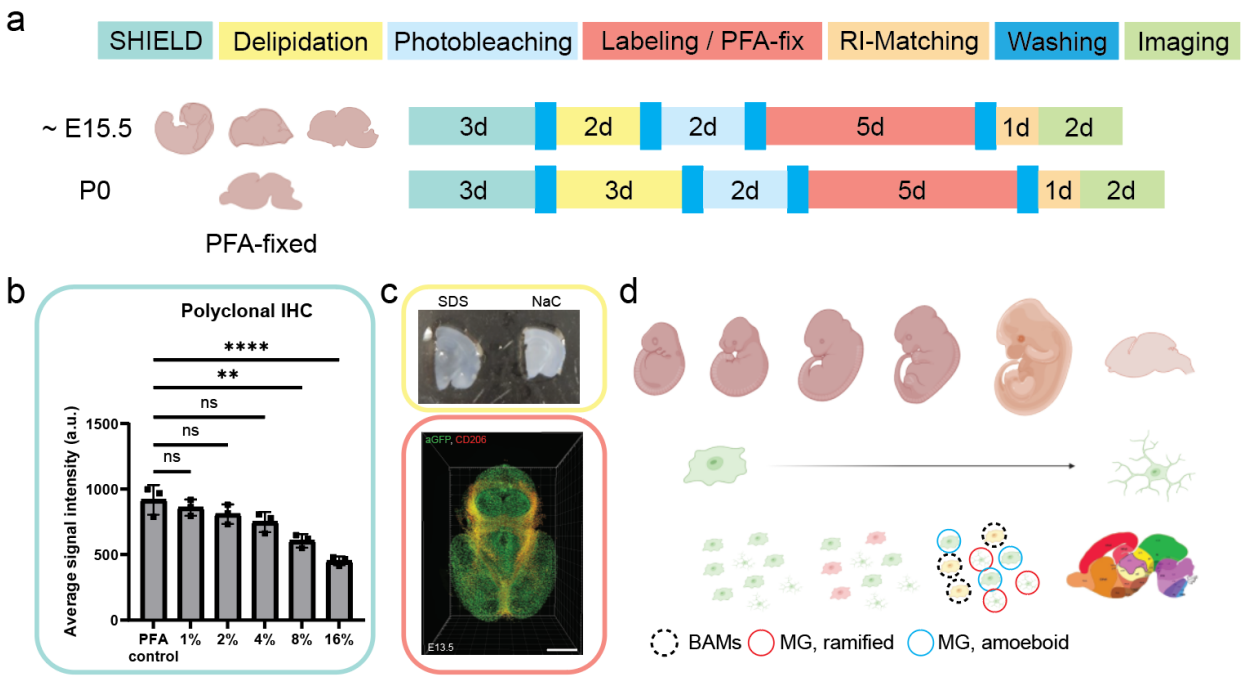

Figure 3-6. Overview of mouse embryo/embryonic brain processing for microglia study

(**a**) Schematic representation of mouse embryo processing pipeline[iii]. (**b**) Average signal intensity of polyclonal antibody signals on mouse brain tissues after applying varying SHIELD concentrations. n=3 tissue samples. Mean ± s.e.m. for all bar graphs. One-way ANOVA, Tukey's multiple comparison test, **P≤0.01, ****P≤0.0001, ns P>0.05. (**c**) Brightfield images of mouse brain slices treated with SDS and NaC (top) and volumetric visualization of E13.5 mouse brain stained with anti-GFP and CD206 (bottom). Scale bar, 500 µm (bottom). (**d**) Schematic representation of downstream analysis tool (MorPheT) for microglial analysis[3,iv].

[iii] The illustrations were generated using biorender.com
[iv] https://atlas.brain-map.org/

3.4 Conclusion

The mouse brain model is a vital tool for examining diverse biological processes in both healthy and diseased states. Consequently, integrating this mouse model with EPIC-SHIELD provides a more adaptable and scalable approach to comprehensively characterize the mouse brain. In this chapter, we introduced a pipeline that can interrogate mouse brain tissues with high scalability and multiplexity. Combined with EPIC-SHIELD treatment, we utilized high-speed lightsheet imaging to enable scalable data acquisition and nuclei-based co-registration for the integration of various biomolecular profiles. As a result, we were able to demonstrate multi-omic visualization, and the imaging of 23 different mRNA markers in thick mouse brain tissues. Additionally, we conducted holistic and unbiased interrogation of intact mouse embryos and embryonic brains, which allowed us to explore microglial development in the early stages of brain development. By studying both transcriptomic and proteomic profiles within mouse brains, combined with connectomic and morphological analysis, we envision that EPIC-SHIELD will enable an unbiased study of mouse brains at an unprecedented scale.

Chapter 4 – Multi-omic characterization of postmortem human brain tissues

The materials from this chapter are adapted from:

Seo Woo Choi†, Webster Guan†, Kwanghun Chung. Basic principles of hydrogel-based tissue transformation technologies and their applications. *Cell*, 2021; 184(16): 4115-4136.

Seo Woo Choi†, Chuanxi Zhao, Xinyi Gu, Jose Vargas-Asencio, Juhyuk Park, Yuxuan Tian, Lee Kamentsky, Nicholas B. Evans, Minyoung E. Kim, Kit-Yi Yam, Nicholas Townsend Haas, Clover Su-Arcaro, Caitlin S. Latimer, Aimee M. Schantz, C. Dirk Keene, and Kwanghun Chung, Effective preservation of biomolecules in large-scale non-perfusable tissues for spatial multi-omic analysis. *Submitted*, 2023.

†Indicates first authorship

4.1 Introduction

Although there are various models to study the brain (animal models, hiPSC-derived 2D monolayer cell culture, and 3D organoids), the direct study of human brain is the key to obtain accurate information for understanding human brain physiology behind disease and health. However, the limited availability and inconsistent quality of postmortem brain samples have hindered our ability to conduct well-defined studies on the human brain. To enable comprehensive and flexible interrogation of primary human brain tissues, we need to effectively preserve biomolecules while retaining their spatial information. With our EPIC-SHIELD protocol, which enables multi-omic preservation, we expect to be able to visualize diverse molecular profiles within the human brain. In this chapter, I will discuss my research on characterizing the human brain including a comparative study on Alzheimer's Disease (AD).

4.2 Experimental Methods

4.2.1 Human brain processing

4-mm-thick fresh frozen human brain slabs were obtained from the University of Washington BioRepository and Integrated Neuropathology (BRaIN) lab. Tissues were obtained with appropriate informed consent from the donor where appropriate and the legal next of kin. One elderly donor with dementia, and one young, cognitively intact control were utilized for testing. The donor with dementia was a 91-year-old female diagnosed with clinical Alzheimer's dementia who died naturally with a postmortem interval (PMI) to brain donation and freezing of 5.4 hours, CSF pH of 6.8, brain tissue RNA quality (RIN) of 7.9, and neuropathologically-confirmed high Alzheimer's disease neuropathologic change (ADNC), including Thal Aβ plaque distribution phase 5/5, Braak neurofibrillary tangle distribution stage VI/VI, and frequent CERAD cortical neuritic plaque density (REFERENCE PMID: 22265587; 22101365). The control donor was a 30-year-old male who died by suicide with PMI to brain donation and freezing of 7.5 hours, CSF pH of 6.6, brain tissue RNA quality (RIN) measurement of 9.6, and no diagnostic neuropathological abnormalities. Both donor brains were rapidly sliced into uniform 4-mm-thick coronal slabs, frozen in supercooled isopentane, and stored in vacuum-sealed bags until needed. Fresh frozen human brain tissues (temporal lobe) were dissected at -80°C and then immersion-fixed in 4% (w/v) PFA at pH 10 for 24 hours at 4°C. The tissues were washed with PBSN overnight at 4°C. PFA-fixed human brain tissues were sectioned into slices using vibratome, followed by EPIC-SHIELD treatment.

4.2.2 Photobleaching

After washing, tissues were placed in RI-matching media and left at room temperature to equilibrate. The tissues were photobleached for 48 hours at 4°C using a custom-built photobleacher[9].

4.2.3 Immunohistochemistry (IHC)

For IHC, primary antibodies were added in 0.1% PBSTN and the samples were incubated for 48 hours at room temperature. After primary antibody staining, the samples were washed overnight with 0.1% PBSTN. For the secondary antibody staining, antibodies and DAPI were added in 1% PBST (1xPBS + 1% (v/v) Triton-X), followed by 24-hour incubation. The samples were washed overnight with 1% PBST. Antibodies used: beta Amyloid (1-42) Monoclonal Antibody (GT622) (MA5-36246, Invitrogen), Phospho-Tau (Thr212) Polyclonal Antibody (44-740G, Invitrogen). Anti-GAD67 Antibody, clone 1G10.2 (MAB5406, Millipore Sigma), Anti-GAD2 (D5G2) (5843s, Cell Signaling Technology), Recombinant Anti-VGluT1 antibody (ab227805, Abcam), Anti-VGLUT2 antibody (135 403, SYSY).

4.2.4 Human cortex layer segmentation

Human cortical layers were manually segmented by distinguishing regional variabilities in cytoarchitecture, including differences in cell density, shape, and size of the cells observed through nuclei staining using DAPI. The boundaries of Layer I to Layer VI and white matter (WM) were manually identified and delineated using the NeuroGlancer 2.0 point annotation tool. Subsequently, a customized script was employed to generate the volumes of these regions.

4.2.5 Cell counting and co-positivity analysis

For co-registered multi-round datasets, the visualization and cell spot counting were performed using Imaris 9.0.1 software (Bitplane). For each marker, Imaris software's spot function was used to generate coordinates of positive signals. For the human tissue, a built-in function from Imaris software, Spots Colocalize, was used to count *GAD1*+pTau+ and *VGLUT1*+pTau+ cells. The cortical layer segmentation was performed manually by assessing DAPI and *VGLUT1* signal densities. The cell density calculation by layer was performed after replotting exported coordinates of FISH signals to layer segmentation masks using NeuroGlancer. The accuracy for human tissue cell detection was calculated manually (**Table 4**).

4.3 Results and Discussion

4.3.1 Human brain preservation

The human brain can be preserved through two primary methods. The first method involves immersing the entire human hemisphere into a formaldehyde solution. This approach is straightforward and easy to implement; yet it has crucial disadvantages. Notably, immersion fixation of bulk human tissues results in a gradient of fixation due to the large size of the human hemisphere[91]. Despite fast diffusion, it takes several weeks for formaldehyde to fully penetrate the innermost regions of the brain due to the quadratic dependence of diffusion time scale to the characteristic length of a tissue (**Supplementary Note 3**). The extended period of time during which biomolecules remain unfixed results in the degradation of vulnerable biomolecules, particularly mRNA transcripts, through both physical and enzymatic processes[91]. This approach preserves relatively stable and abundantly expressed molecules like proteins, which have been successfully characterized by various technologies[7,9]. In contrast, transcriptomic analysis of the human brain has primarily relied on fresh-frozen tissues. These tissues are snap frozen using alcohol, without the use of chemical fixatives like formaldehyde. This method is much quicker than formaldehyde immersion fixation and has been widely adopted for RNA sequencing as the integrity of the mRNA is relatively well-preserved. However, achieving volumetric spatial visualization of transcripts has been challenging due to the lack of an effective method for thawing the tissues while preserving transcriptomic information. Uneven thawing can lead to varying degrees of preservation, particularly when alcohol is used for snap-freezing, as alcohol permeabilizes the tissue without fixation. An example illustrates the differential preservation of mRNA in the same sample (**Figure 4-1 a**).

To address these challenges, we developed EPIC-SHIELD (discussed in Chapter 2), which combines rapid fixation with an optimized SHIELD protocol to effectively preserve transcripts in volumetric samples. With EPIC-SHIELD, we were able to successfully visualize both excitatory and inhibitory neuronal cells in thick human tissue sections (**Figure 4-1 b**).

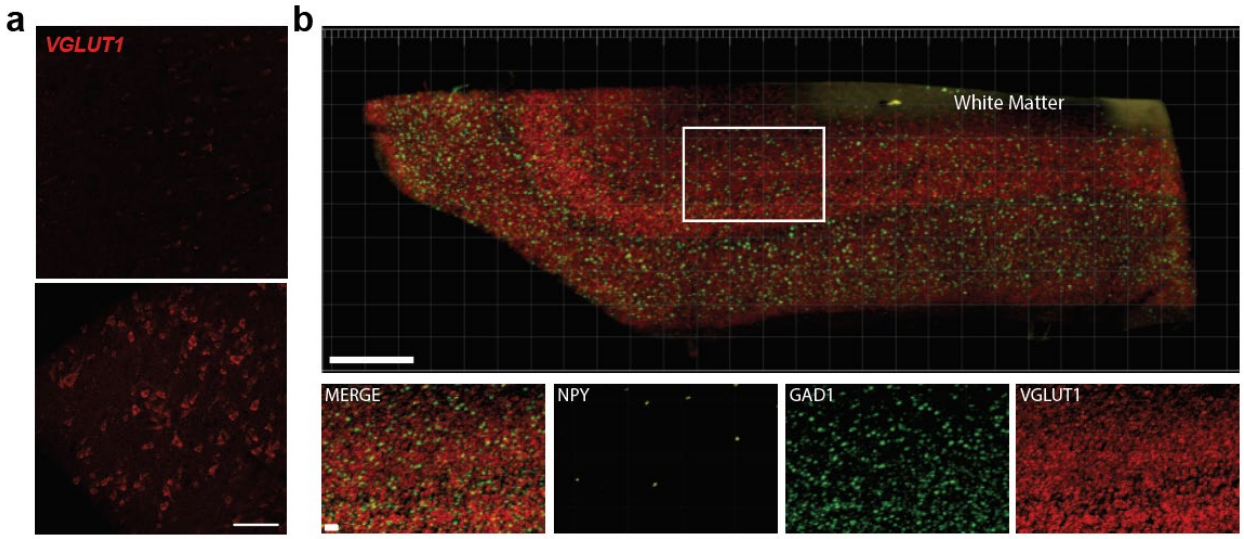

Figure 4-1. Volumetric FISH on human brain tissues

(**a**) Gradient in preservation in the same frozen human tissue after improper thawing process. Scale bar, 100 µm. (**b**) Volumetric FISH performed on 500-µm-thick human brain after EPIC-SHIELD treatment. Scale bars, 500 µm (Merge), 50 µm (Merge).

4.3.2 Autofluorescence removal

One of the main challenges when investigating the human brain is the presence of autofluorescence caused by lipofuscin, a pigment that accumulates within neural cells that are formed by various materials including metals, lipids, and proteins[92]. Lipofuscin significantly limits the use of light microscopy-based techniques as the autofluorescence signals span the entire wavelength rendering the identification of true signals extremely challenging (**Figure 4-2 a**). There are two main approaches to address this issue. The first method involves the use of Sudan Black B (SBB)[93]. When SBB dissolved in 70% (v/v) ethanol was applied to human brain tissue, there was a noticeable reduction in autofluorescence within just 20 minutes of treatment (**Figure 4-2 a**). However, the main drawback of SBB method is that it imparts a dark black color to the tissues, which obstructs the acquisition of volumetric data using a lightsheet microscope (**Figure 4-2 b**). Additionally, SBB treatment can lead to the loss of mRNA, as the use of alcohol further permeabilizes the tissues (**Figure 4-2 c**). The second method for lipofuscin removal involves photobleaching, which employs high-intensity LED light to bleach out the autofluorescence[9]. While photobleaching requires a longer processing time when compared to the SBB method (48 hours as opposed to 20 minutes), it is a gentler approach in that it does not lead to the loss of biomolecules, and the tissue retains its original color (**Figure 4-2 a**).

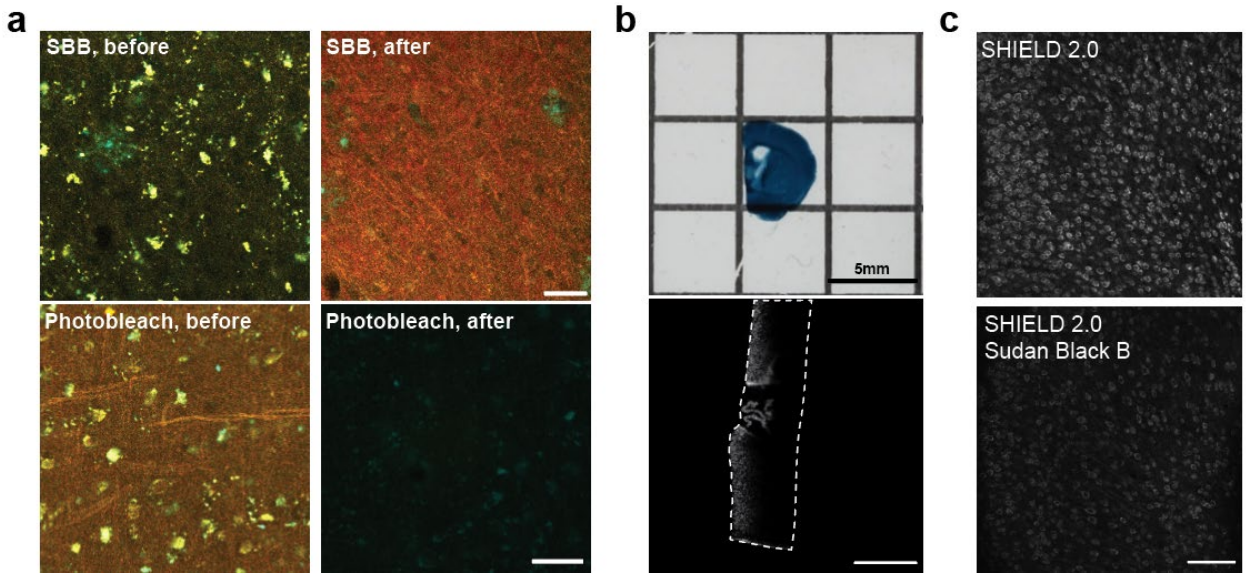

Figure 4-2. Removal of autofluorescence in human brain tissue

(**a**) Before and after images of SBB treatment and photobleaching method. Scale bar, 50μm. (**b**) Tissue stained after SBB treatment. Scale bars, 5mm (top), 500μm (bottom). (**c**) Reduction in FISH signals after SBB treatment. Scale bar, 100μm.

4.3.3 Thick human brain tissue preservation and characterization

Next, we applied EPIC-SHIELD to thick human brain tissue, which presents unique challenges towards preservation and collection of multi-omic information using light microscopy. Its non-perfusable nature and extended postmortem interval (PMI) necessitate rapid fixation to minimize physical loss of mRNAs. The existence of auto-fluorescent materials and high degree of myelination in the human brain samples require additional tissue processing steps, such as photobleaching and lipid removal, both of which can cause substantial loss of mRNAs. EPIC-SHIELD, however, can readily address these human-tissue specific challenges.

Freshly dissected and frozen human temporal lobe tissues derived from an adult control donor were EPIC-SHIELD treated, sliced into 1-mm-thick slabs, and volumetric FISH was conducted against mRNA for *NPY*, *GAD1*, and *VGLUT1* (**Figure 4-3 a**). Robust FISH signals were obtained for all three markers (**Figure 4-3 a insets**). Furthermore, effective RNA preservation in bulk human brain tissues was confirmed by optically slicing the cross-section of the tissue, where consistent and uniform FISH signal for all markers was observed throughout the depth (**Figure 4-3 b**).

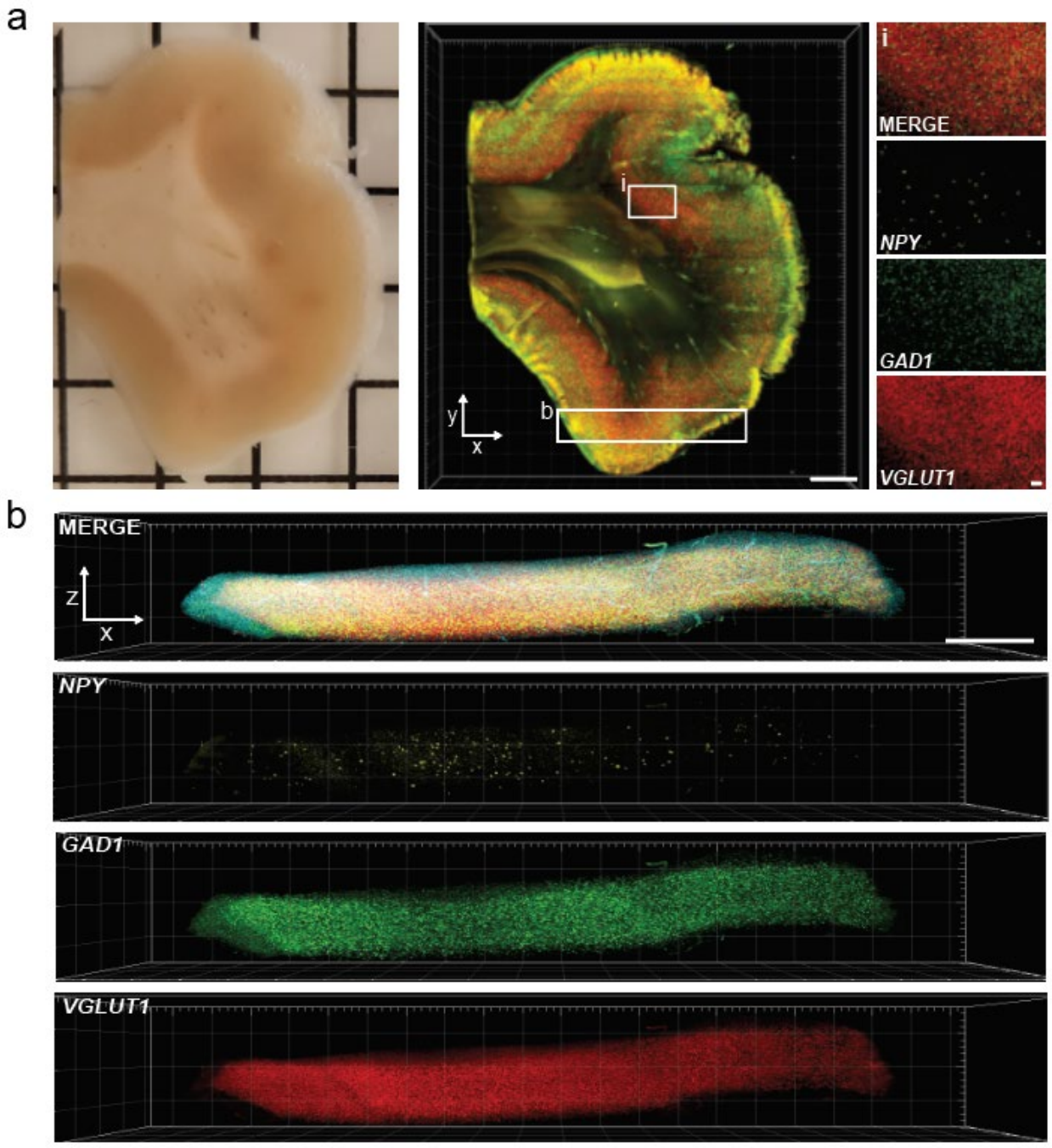

Figure 4-3. Volumetric FISH staining of 1-mm-thick human brain tissue

(**a**) A brightfield image (left) and an IASLSFM image (right) of FISH-stained *NPY*, *GAD1*, and *VGLUT1* transcripts in an EPIC-SHIELD-treated 1 mm human brain slice. Scale bars, 2 mm (middle) and 100 μm (inset). (**b**) Cross-sectional views of *NPY*, *GAD1*, and *VGLUT1* FISH signals from image in (a). Scale bar, 1 mm.

4.3.4 Multi-omic characterization of human brain: AD vs CTRL

To demonstrate the potential for multi-omic characterization of thick tissues to reveal insights into neuropathological processes, we evaluated Alzheimer's Disease (AD)-induced accumulation of beta amyloid (Aβ, 1-42) and phosphorylated tau (pTau, Thr212) pathologic peptides, and the associated impact on neuronal subpopulations across cortical layers. We performed FISH-based detection of transcripts from *GAD1* and *VGLUT1,* followed by immunofluorescence-based visualization of Aβ and pTau proteins on EPIC-SHIELD treated 500-μm-thick coronal slabs from both control and AD brain tissues (**Figure 4-4 a**, **Table 4**).

Initially, we focused on addressing the challenge of identifying excitatory and inhibitory neurons in the human brain. Immunostaining of GAD1 and VGLUT1 proteins produced dispersed profiles (**Figure 4-4 b**), impeding accurate cell-level identification and segmentation. Whereas mRNA FISH signals were predominantly localized to the cell soma, enabling accurate assignment of neurons into excitatory and inhibitory categories with high resolution (**Figure 4-4 b**). Building on the FISH-based characterization of excitatory and inhibitory neurons, we identified and segmented the cortical layers (**Figure 4-4 a**), and measured the intensity profiles of both Aβ and pTau proteins (**Figure 4-4 c**). Using this strategy, we observed a bias in Aβ protein accumulation towards layers I-III, while pTau appeared to be more abundant in layer V. Leveraging FISH-based neuronal subtyping and pTau protein signal quantification, we observed that excitatory neurons exhibited 60 times higher frequency of co-localization with pTau compared to inhibitory neurons (**Figure 4-4 d**), confirming classical literature highlighting the loss of functional excitatory neurons in association with neurofibrillary (tau) degeneration[94]. 61.2% of pTau+ cells sampled in AD brain did not express *GAD1* nor *VGLUT1*. Notably, no pTau+ cells were detected in the control brain (**Figure 4-5 a**, **b**).

Next, we quantified the cell density of excitatory and inhibitory neurons across cortical layers in both control and AD brain tissues. Cell density reduction was evident across all layers for both neuronal types in AD tissues compared to control (**Figure 4-4 e**) consistent with previous reports[94,95]. The most severe impact (82.4% relative loss for *GAD1*$^+$, 83.9% for *VGLUT1*$^+$) was observed in layers I and II, coinciding with the highest density of Aβ plaque (**Figure 4-4** c-**e**). The volumetric scalability of our technology enabled the detection of sparsely distributed *GAD1*$^+$/pTau$^+$ cells (**Figure 4-4 d**). Among the 351,216 cells characterized in this tissue volume, we found only 11 *GAD1*$^+$/pTau$^+$ cells. Most of them (7 of 11) were located in layer III. At 0.003% for *GAD1*$^+$/pTau$^+$ cells observed here, these events are unlikely to be captured in thin sections as explained previously (**Figure 3-5 b, d**). In fact, when we examined 50 virtual 10-µm-thick sections from the same tissue volume, only 10 sections showed on average 1.1 *GAD1*$^+$/pTau$^+$ cells. Together, these data demonstrate that EPIC-SHIELD enables integrated, multi-omic, volumetric evaluation of thick human tissues with unprecedented scalability and robustness.

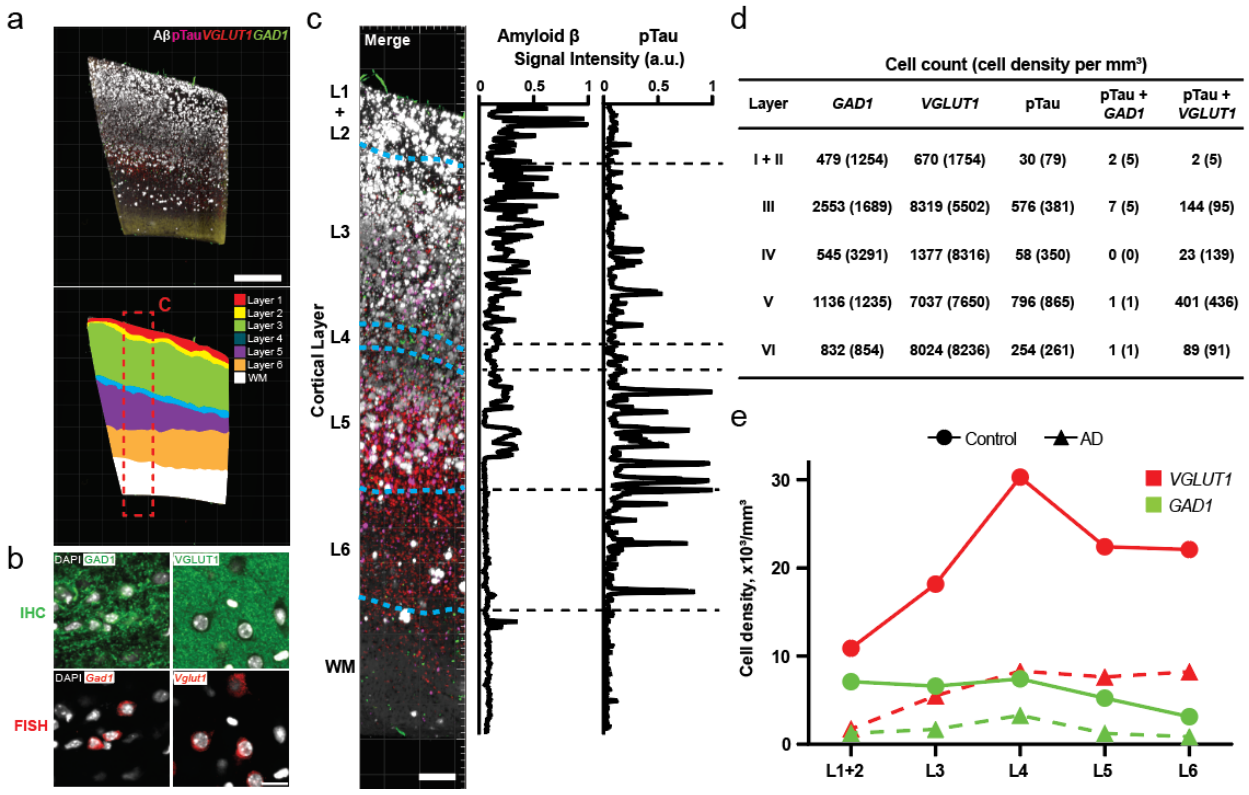

Figure 4-4. Human AD brain multiplexed imaging and analysis

(**a**) Maximum projection composite of IASLSFM image of EPIC-SHIELD-treated 500-µm-thick human AD tissue (top) and corresponding cortical layer segmentation (bottom). Scale bar, 1 mm. (**b**) Confocal microscopy images of IHC (top) and FISH (bottom) signals for the products of common inhibitory (*Gad1*) and excitatory (*Vglut1*) genes in mouse brain tissue. Scale bar, 20 µm. (**c**) Signal intensity profiles for amyloid beta and pTau protein on an annotated subsection of the image in (a). Scale bar, 200 µm. (**d**) Count and density values per cortical layer of cells expressing *VGLUT1*, *GAD1*, pTau, and their co-occurrence. (**e**) *VGLUT1*$^{+}$ and *GAD1*$^{+}$ neuronal cell densities for control and AD human brain tissues in each cortical layer.

Table 4. Multi-round FISH on 500-um-thick human brain slice

	488	**561**	**642**
Round 1	-	*GAD1*	*VGLUT1*
Round 2	Abeta	-	pTau

a

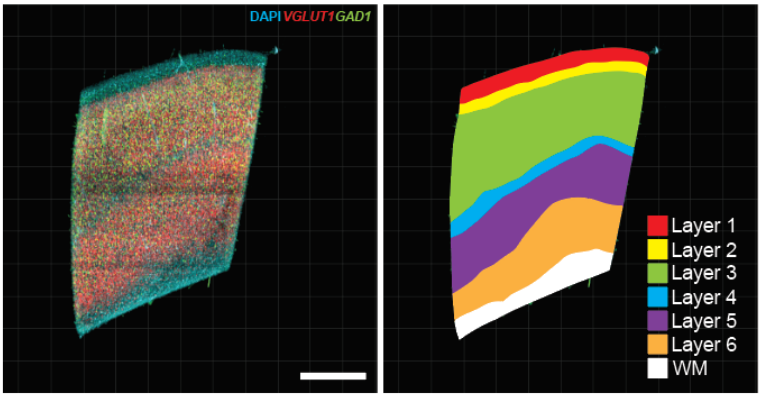

b

Cell count (cell density per mm³)

Layer	*GAD1*	*VGLUT1*
I + II	3851 (7114)	5901 (10901)
III	10891 (6599)	29991 (18172)
IV	2130 (7463)	8684 (30317)
V	5395 (5228)	23119 (22404)
VI	2851 (3133)	20094 (22082)

Figure 4-5. Human control brain multiplexed imaging and analysis

(**a**) Maximum projection composite of IASLSFM image of EPIC-SHIELD-treated 500-µm-thick human control tissue (left) and corresponding cortical layer segmentation (right). Scale bar, 1 mm. (**b**) Count and density values per cortical layer of cells expressing *VGLUT1* and *GAD1*.

4.4 Conclusion

In this chapter, we present a protocol for the effective preservation of human brain samples. Through this method, we have successfully preserved multi-omic information and achieved volumetric visualization of millimeter-thick fresh-frozen human brain sections in combination with EPIC-SHIELD treatment. Our approach involves a series of optimized steps including thawing, fixation, and removal of autofluorescence, which led to robust multi-omic characterization capabilities demonstrated by a comparative study on 500-μm-thick fresh-frozen human brain sections from both control and AD affected brains. With the help of EPIC-SHIELD, we were able to identify inhibitory and excitatory neurons through mRNA characterization and detect pTau and AB aggregates using antibodies. This method has the potential to uncover and explore mechanisms related to neurodegeneration and, more broadly, brain aging, injuries, and diseases.

Chapter 5 – Development of human brain model using human induced pluripotent stem cells

The materials from this chapter are adapted from:

Seo Woo Choi†, Kwanghun Chung, Extended microglia survival in microglia-organoid co-culture. *In Preparation*.

†Indicates first authorship

5.1 Introduction

Historically, mouse models have been the one of the standard choices for studying brain functions and disease mechanisms. However, there are significant interspecies differences that hinder the direct translation of findings from mice to humans. Recently, the development of human induced pluripotent stem cells (hiPSCs) has provided a new opportunity for generating human cells for research purposes. Nevertheless, working with monolayer cells cannot fully capture the intricate interactions that occur in three-dimensional tissue settings. In 2013, Lancaster and colleagues introduced a method for producing cerebral organoids using hiPSCs[4]. These forebrain cerebral organoids can mimic some aspects of the developmental and disease characteristics of the human brain forebrain cortex, offering a promising alternative. However, one limitation of this approach is that the cerebral organoids do not fully recapitulate the human brain environment. For example, cerebral organoids primarily consist of cells from the neuroectodermal lineage, which exclude many critical cell types such as those found in the brain parenchyma and vasculature. Among these excluded cell types, microglia play a significant role in both normal and diseased states by regulating brain homeostasis and responding to damage. In this section, I will outline my

strategy for generating human brain organoids that are co-cultured with microglia to address this limitation.

5.2 Experimental Methods

5.2.1 Generation of human brain organoids

The organoids were generated using the original Qian et al. (2018) protocol with some minor modifications[5,96]. First, the hiPSCs (ATCC, Cat. No. ACS-1019) were maintained in a feeder-free condition to reach >80% confluency. Then, the iPSCs were dissociated into single cells by treating with ethylenediaminetetraacetic acid (EDTA, ThermoFisher, Cat. No. AM9261) and accutase (Corning, Cat. No. 25-058-CI). The cells were re-suspended in an ultra-low attachment 96-well round plate (45,000 cells per well, Corning, Cat. No. 7007) to promote self-assembly into a 3D structure, called embryoid bodies (EBs). After 8 days of self-aggregation, multiple EBs were embedded in Matrigel as a single cookie-shape in an ultra-low attachment 6-well plate (Corning, Cat. No. 3471). The organoids were kept in the Matrigel (Corning, Cat. No. 354234) cookie for 7 days during which ventricular zones formed. After this period, the organoids were broken out of the Matrigel cookie, to remove premature neuronal differentiation and to selectively leave the progenitor cells. These organoids were cultured in an ultra-low attachment 6-well plate with applied shaking to enhance the exchange of nutrients and O_2/CO_2.

5.2.2 Generation and characterization of human microglia-like cells

The MG-like cells (referred as microglia from now on) were generated using the original McQuade et al. (2018) protocol with some minor modifications[97]. First, STEMdiff™ Hematopoietic Kit (STEMCELL™ Technologies, Cat. No. 05310) was used to generate hematopoietic progenitor cells (HPCs) for 12 days. After generation of HPCs, further differentiation of progenitor cells into microglial lineage was directed by the addition of cytokines

including macrophage colony stimulating factor (M-CSF, 25 ng/mL, Peprotech, Cat. No. 300-25-50UG), interleukin-34 (IL-34, 100 ng/mL, Cat. No. 200-34-50UG), and transforming growth factor β (TGFβ, 50 ng/mL, Cat. No. 100-21-50UG). After a month of differentiation, the media was supplemented with CD200 (100 ng/mL, R&D Systems, Cat. No. 10032-CD-050) and a chemokine ligand CX3CL1 (100 ng/mL, Cat. No. 300-31-100UG). In this way, microglia can be derived within two months.

5.2.3 Immunocytochemistry and RT-PCR

After the generation of microglia, the cells were in suspension culture. To adhere these cells, square glass cover glasses (VWR, Cat. No. 16004-308) was washed with 70% (v/v) Ethanol. After sterilization, square cover glasses were coated with fibronectin (1 $\mu g/mL^2$, Millipore Sigma, Cat. No. 10838039001). The attached microglia were fixed with PBS-buffered 4% (w/v) PFA for 30 minutes at room temperature, followed by permeabilization using 1% PBST for 20 minutes. These permeabilized cells were stained with antibodies in 6-well-plate, and were imaged using Leica confocal microscope. For RT-PCR, RNA was extracted from microglia and hiPSC-control using RNeasy Kits (Qiagen, Cat. No. 74004). For the primer design, NCBI Primer-BLAST (https://www.ncbi.nlm.nih.gov/tools/primer-blast/index.cgi) was used. The primers were designed to have minimum product size of 500 bp. For cDNA generation, RNA was mixed with Oligo(dT) primers (Invitrogen, Cat. No. 18418012), dNTP mix (New England BioLabs, Cat. No. N0447S), SuperScript™ IV Reverse Transcriptase (Invitrogen, Cat. No. 18090010), and RNaseOUT (Invitrogen, Cat. No. 10777017). After the generation of cDNA, PCR was performed, by mixing cDNA with primers and running the reaction for 20-30 cycles. The product of PCR was analyzed using agarose gel electrophoresis.

5.2.4 Incorporation of microglia in human brain organoids

After separate generation of cerebral organoids and microglia from hiPSCs, suspended microglia were added into the wells containing organoids for co-culture, at 10,000 microglia cells per organoid. Briefly, cerebral organoids at day 30-35 were transferred to ultra-low attachment 24-well plate (Corning, Cat. No. 3473) using wide bore transfer pipettes (VWR, Cat. No. 76285-362). Four organoids were transferred to each well. Then, the microglia were harvested from the differentiation well plates, using pipettes to gently detach the cells from the well plates. Suspended microglia were collected in a 15-mL conical tube, and were centrifuged down at 300g for 5 minutes to form a pellet. The microglia pellet was resuspended in 2 mL organoid media (Forebrain third medium)[96], and the cell numbers were counted. Next, the microglia cells numbers were diluted to have 20,000 cells per mL, and the final volume of microglia-suspended media was supplemented by M-CSF (25 ng/mL) and IL-34 (100 ng/mL). After aspirating out the old media from 24 well plate, organoids were suspended in 2 mL of microglia-suspended culture media. The microglia were left to settle down on the organoids for 24 hours without any shaking. After 24 hours, partial media change (1 mL of Forebrain third medium, without any M-CSF or IL-34) was performed and an additional stationary culture was performed for 24 hours. After 48 hours of co-culture, the organoids were transferred back to ultra-low attachment 6-well plates and gentle shaking was applied.

5.3 Results and Discussion

5.3.1 Organoid and microglia characterization

After the generation of forebrain organoids, we were able to confirm the identity by staining the organoid slices with various forebrain markers (**Figure 5-1 a**). To demonstrate that the cells we derived from this protocol were human microglia, we performed characterization using immunocytochemistry (ICC) and polymerase chain reaction (PCR). For ICC, we were able to adhere floating microglia on the glass through fibronectin coating. These adhered microglial cells were stained using antibodies for various microglia-related markers (Iba1, P2RY12, PU.1, TMEM119, CX3CR1) and all results indicated that the cells we derived expressed microglia-related genes (**Figure 5-1 b**). Next, we generated primers targeting microglia-related genes (*Iba1*, *Cx3Cr1*, *Pu.1*, and *Csf1r*). Then, we extracted RNA from the hiPSCs (negative control) and microglia, reverse transcribed into cDNA, and performed PCR. The gel electrophoresis results show that the cells from the differentiation protocol expressed microglial genes, while iPSCs did not (**Figure 5-1 c**). After the co-culture, we treated organoids with EPIC-SHIELD protocol, sliced, and stained with DAPI and Iba1 (microglia marker). The microglia were well incorporated into the organoids, and showed elongated morphologies characteristic of immature microglia (**Figure 5-2**).

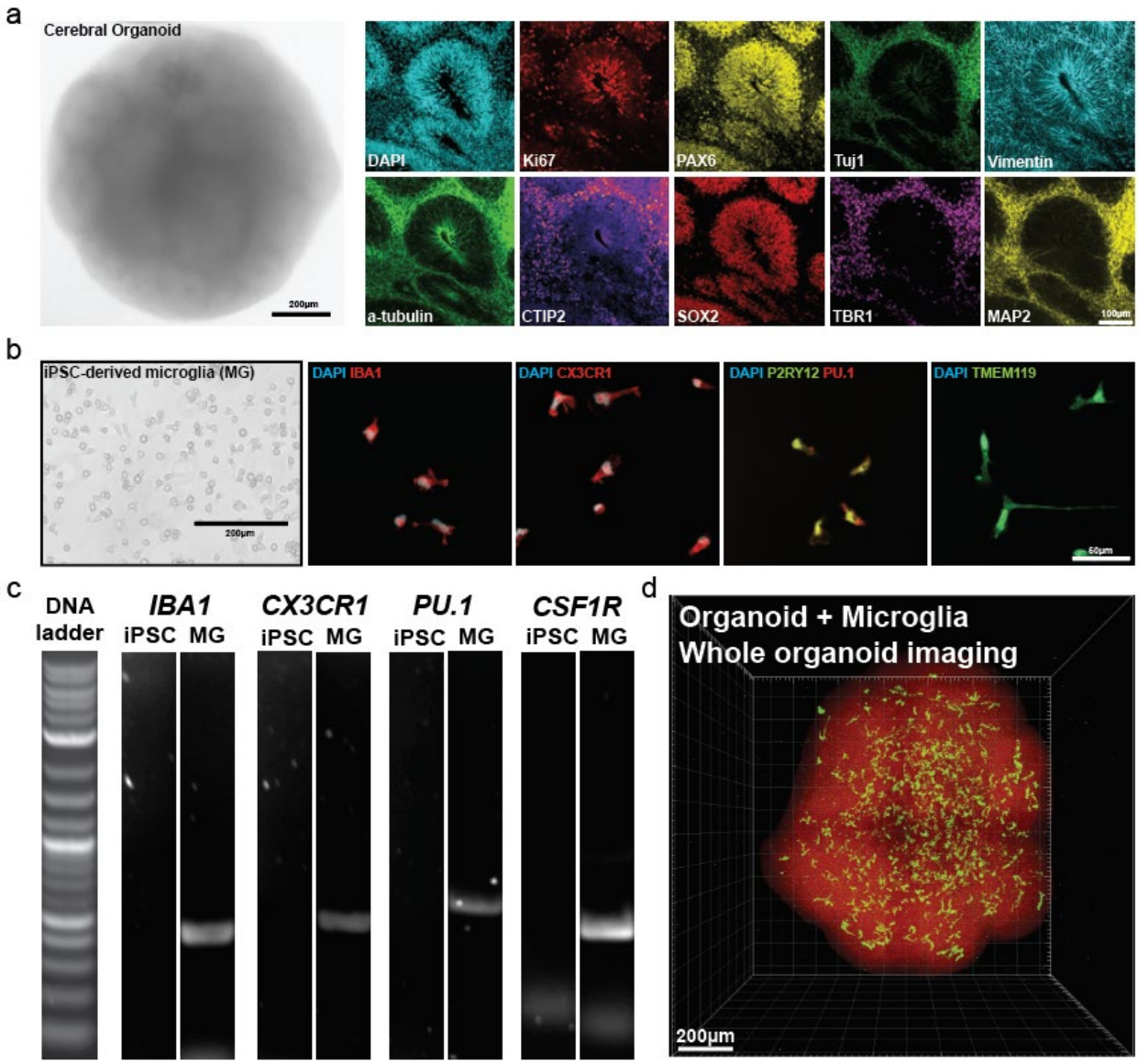

Figure 5-1. hiPSC-derived organoid and microglia characterization

(**a**) Bright field image of a cerebral organoid, and EPIC-SHIELD-enabled IHC characterization of the same slice. Scale bars, 200 μm (bright field image), 100 μm (IHC). (**b**) Immunocytochemistry on iPSC-derived microglia. Scale bar, 50 μm. (**c**) RT-PCR of iPSC-derived microglia. (**d**) Whole organoid imaging enabled by EPIC-SHIELD. Scale bar, 200 μm.

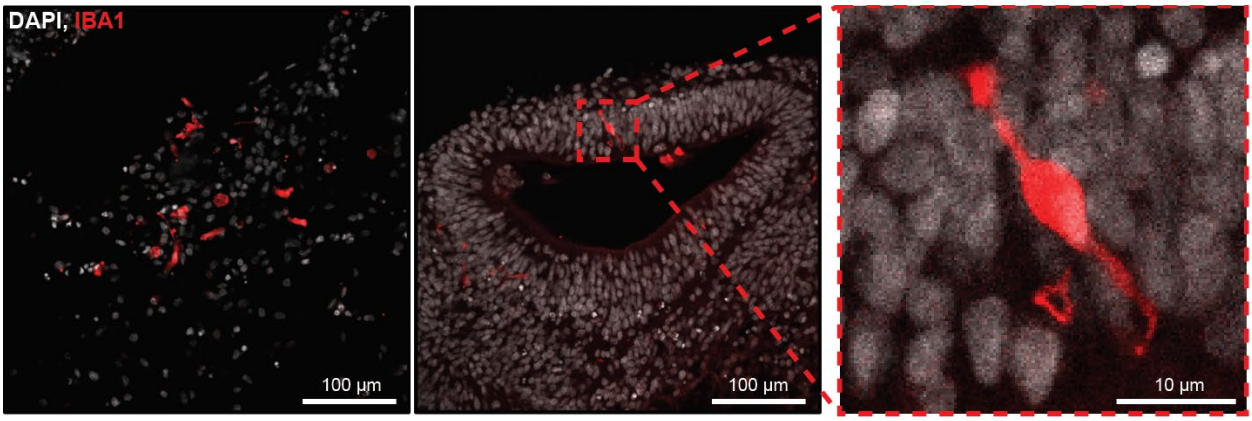

Figure 5-2. Microglia co-cultured with cerebral organoids

5.3.2 EPIC-SHIELD on whole organoid for volumetric staining and characterization

One of the main challenges in studying organoids is the need for a comprehensive view of the entire organoid, rather than relying solely on sliced sections. Cerebral organoids lack organized anatomical structures, which can mislead the analysis and assessment of co-culture efficiency when based on just a single or a few slices. Therefore, we treated intact cerebral organoids with our EPIC-SHIELD protocol for volumetric and unbiased study. To confirm the successful application of the EPIC-SHIELD protocol to organoid systems, we sliced and stained the organoid slices for mRNAs and protein detection (**Figure 2-8**, **Figure 2-9**). Additionally, we conducted three rounds of immunohistochemistry (IHC) on a 200-μm-thick organoid slice, which was prepared after EPIC-SHIELD treatment and full delipidation. The results demonstrated that EPIC-SHIELD effectively preserves biomolecules within cerebral organoids, allowing the tissues to withstand harsh elution conditions (70-80°C, 200 mM SDS, 1 hour, **Figure 5-1 a**).

While EPIC-SHIELD successfully preserves biomolecules within whole organoids, labeling the entire organoid presents another challenge. Antibodies are relatively large proteins (~150 kDa) that have limited penetration into the tissue. Various technologies have attempted to address this issue by either quenching the reaction or applying external forces to expedite antibody delivery[32,47,65,98]. These methods allow the rate of diffusion to increase relative to the rate of reaction, allowing full penetration of molecular probes across the tissue volume without depletion. For instance, stochastic electrotransport introduced electric field to rapidly deliver antibodies[98], while SWITCH quenched the binding reaction and enabled antibodies to diffuse into the tissue[32]. More recently, eFLASH used affinity modulation to gradually change the antibody binding affinity while using an electric field to expedite the delivery[65]. Among these technologies, we adopted the SWITCH technology because it does not require specialized equipment and can facilitate high-

throughput processing. Consequently, we successfully stained the entire organoid evenly using our SWITCH technology (**Figure 5-1 d**).

5.3.3 Co-culturing of human microglia in neuronal environment at lower temperature

Next, we conducted experiments to determine if we could establish long-term cultures of microglia. In a conventional culture environment at 37°C, we observed a gradual decrease in the microglia population, leading to their complete disappearance within approximately two months after co-culture initiation (**Figure 5-3 a**). However, when we cultured microglia-organoid co-culture at a lower temperature, we managed to achieve the survival of these microglial cells (**Figure 5-3 b, c**). Notably, the morphology of microglia exhibited extended ramification, indicating their maturation and adaptation to the neuronal environment (**Figure 5-3 d**). Furthermore, we extended the co-culture period up to 105 days and we were still able to observe the survival of microglia within the organoids. This suggests that lower temperature culture can facilitate the long-term co-culture of microglia with organoids, potentially leading to the development of a more robust model for studying the human brain (**Figure 5-3 e**).

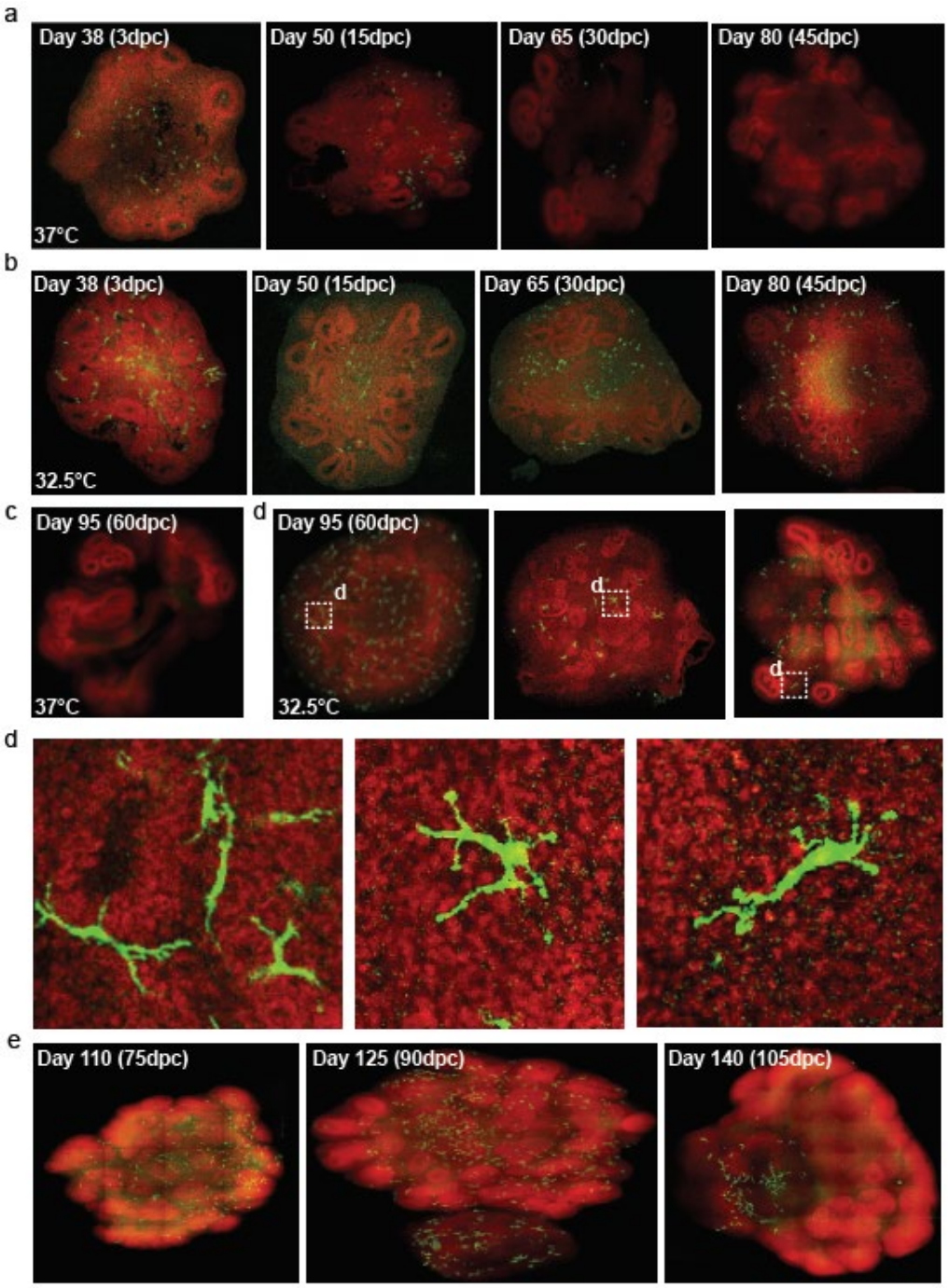

Figure 5-3. Organoid-microglia co-culture at different temperature

(**a**) Gradual reduction of co-cultured microglia in cerebral organoids at 37°C. (**b**) Survival of co-cultured microglia in cerebral organoids at 32.5°C. (**c**) Microglia in cerebral organoids at 37°C and 32.5°C, after 60 days of co-culture. (**d**) Ramification of microglia in prolonged, 32.5°C co-culture in cerebral organoids. (**e**) Prolonged microglia survival in organoids at 32.5°C co-culture condition, up to 100+ days.

5.4 Conclusion

Human induced pluripotent stem cell (hiPSC)-derived organoids hold immense potential for advancing our understanding of human brain physiology. Therefore, it is crucial to create a model that closely resembles the actual human brain to obtain precise insights into the mechanisms governing its functions and dysfunctions. In the future, we plan to conduct IHC to confirm which markers are expressed by microglia in the organoids cultured at lower temperatures. Additionally, single-cell RNA sequencing (scRNA-seq) can be carried out to identify genes that are differentially regulated in microglia at various temperatures. Moreover, we are intrigued by the need to investigate the factors contributing to the prolonged survival of microglia. This could potentially stem from the direct impact of temperature on microglia-like cells, or it may result from the effects of the neuronal microenvironment being influenced by temperature variations.

Chapter 6 – Conclusion

The materials from this chapter are adapted from:

Seo Woo Choi†, Chuanxi Zhao, Xinyi Gu, Jose Vargas-Asencio, Juhyuk Park, Yuxuan Tian, Lee Kamentsky, Nicholas B. Evans, Minyoung E. Kim, Kit-Yi Yam, Nicholas Townsend Haas, Clover Su-Arcaro, Caitlin S. Latimer, Aimee M. Schantz, C. Dirk Keene, and Kwanghun Chung, Effective preservation of biomolecules in large-scale non-perfusable tissues for spatial multi-omic analysis. *Submitted*, 2023.

†Indicates first authorship

6.1 Conclusion

Comprehending biological tissues is essential for revealing the processes that drive both normal and abnormal functions. The intricate and interlinked nature of brain tissues presents significant obstacles when it comes to studying and characterizing them. In this thesis, I have developed EPIC-SHIELD, a universally applicable tissue preservation technique for the effective long-term preservation of multi-omic information in thick perfusable and non-perfusable tissues. Motivated by developments in spatial omics technologies, we set out to address the limitations associated with expanding these techniques to thick biological tissues to enable unbiased studies at a larger scale. Depending on the source of the tissue, and collection and storage methodologies, the integrity of biological samples can vary greatly. In addition, chemical treatment steps required to process think tissues further contribute to decay of the sample quality. These factors have significantly limited the scale in which omics evaluation can be performed.

Revisiting the chemical principles dictating the mechanism of PFA-mediated fixation and leveraging computational modeling, we proposed optimized conditions for rapid stabilization of tissues. Using perfusable mouse and non-perfusable human brain samples as model systems, we demonstrated how accelerated PFA-fixation through pH modulation initially prevents biomolecular loss and degradation commonly associated with tissue acquisition and processing. Effective preservation of biomolecules resulted in stronger, more robust FISH signals in all cases. Higher quality signals have significant implications in terms of enhanced reproducibility and improved dynamic range of capture, opening the door for the study of less abundant molecules.

Having established the conditions for rapid initial capture of biomolecules, a complementary fixation step was implemented to provide long-term stability and robustness for downstream processing, including multi-round and multi-omic imaging of thick tissues. To this purpose, we employed a polyepoxy-based secondary fixation optimized for mRNA preservation. Using mouse and human brain as models, we demonstrated how the combination of accelerated PFA, and mRNA-optimized polyepoxy fixation, termed EPIC-SHIELD, enables robust and long-term stabilization of mRNA transcripts and proteins. The tissue-gel hybrid produced by sequential fixation preserves the biomolecules in place, even when subjected to extended storage periods or harsh conditions required for multi-omic imaging of thick tissues such as delipidation and probe destaining. Leveraging these features, we demonstrate volumetric capture of transcriptomic information in 1-mm-thick human brain slabs, a qualitative improvement compared to other spatial transcriptomic techniques that tend to work in the 10-20 μm range[6,71,99]. The biomolecular stability by EPIC-SHIELD enables maximal information retrieval from biological tissues, a critical aspect when dealing with rare or precious samples, such as the human brain tissues.

EPIC-SHIELD greatly improves the capacity to explore cellular composition and architecture within thick tissues. Combined with rapid image acquisition through light-sheet microscopy and data integration through nuclei-based co-registration, volumetric techniques improve the extent of biomolecular information that can be extracted from samples, reduce sectioning biases, and enhance sensitivity to rare or unevenly distributed cell types, allowing a comprehensive examination of cells and their connections[20,47]. The linear relationship between the number of captured cells and the tissue thickness serves as evidence for potential jump in data richness. Parallel to the gains in the number of cells captured, the dimensionality of the data is further improved by multiplexed data collection.

As proof of concept, a preliminary view of the cellular architecture in mouse cortex was presented. Notably, FISH staining resulted in much clearer cellular level identification and quantification of glutamatergic and GABAergic neurons, traditionally difficult using antibodies due to the localization of their characteristic transporter proteins across the cell body, axons terminals, and synaptic vesicles[100,101]. The addition of volumetric mRNA detection to the cell typing toolbox greatly enhances the capacity to study cellular composition and architecture in tissues with higher confidence and less biases. Detection of inhibitory long-range projecting neurons (*Vglut1*$^{-}$, *Gad1/2*$^{+}$, *Nos1*$^{+}$, *Npy*$^{+}$, *Sst*$^{+}$) in mouse brains, present at 8 cells out of total 28,670 cells, constitutes pressing evidence. In addition, application of EPIC-SHIELD pipeline to mouse embryos and embryonic brains allowed the study of microglial migration and maturation during the early brain development.

The universal applicability of EPIC-SHIELD is best demonstrated in the characterization of postmortem human brain tissues. We successfully preserved and visualized mRNA signals up to 1-mm-thick human brain tissues, an unprecedented scale to our knowledge. Furthermore, owing

to the multi-omic capability of EPIC-SHIELD, we performed a comparative study of the association of protein aggregates (pTau and Aβ) to FISH-defined neuronal subtypes in control and AD tissue. In this study, rare *GAD1*$^{+}$/pTau^{+} cells were detected in human AD brains, which were present at 11 cells out of total 351,216 cells. Using this unique feature, potentially novel observations for the mechanism of AD pathology were obtained.

Lastly, an *in vitro* model to study human brain was presented using hiPSC-derived cerebral organoids. The main challenge in establishing an *in vitro* model for the human brain was that current cerebral organoid models had limited cell type diversity due to the primed stem cell differentiation path towards neuroectodermal cells, omitting important non-neuronal cells like microglia. To address this challenge, I have generated a co-culture model, embedding hiPSC-derived microglia from the neuro-mesodermal lineage into the cerebral organoids. Another significant challenge with current approach was that the number of co-cultured microglia naturally decreased over time. To extend microglial survival, microglia-organoid co-culture model was cultured at a lower temperature (32.5°C). This approach not only extended microglial survival up to 100+ days (compared to <45 days in conventional culture conditions), but also allowed higher degree of ramification of microglia indicating favorable co-culture conditions. The assessment of co-culture and microglia morphologies were made possible by the implementation of EPIC-SHIELD, which allowed unbiased interrogation of whole organoids without the need of thin sectioning.

6.2 Future Work

This thesis mainly focused on the technological and methodological development that opened up various potential directions in the field of biology and neuroscience. However, there are still numerous challenges that need to be addressed:

1. Additional optimization of EPIC-SHIELD conditions for thicker and larger tissues such as entire 4-mm-thick human brain slabs, whole macaque/marmoset brains, and other mammalian organs.
2. Optimization of delipidation technology to minimize the damages on biomolecules, especially the low-abundant transcripts and surface proteins.
3. Automation of multi-round staining and imaging.
4. Full characterization of microglia-organoid system and compare with primary human tissues.

Though EPIC-SHIELD demonstrated its wide and general applicability, there are still rooms for improvement when broadening the use towards other mammalian organs. For example, non-human primates are highly useful models as they are genetically similar to humans than are the mouse models, possess similar complexity in the brain structures, and show higher cognitive abilities[102,103]. To successfully connect *in vivo* studies from marmoset or macaque to biomolecular expression, EPIC-SHIELD could be an essential bridge. In addition, fresh frozen human tissues are prepared as 4-mm-thick slabs, which are carefully recorded and banked. If EPIC-SHIELD can extend the volumetric capability towards these intact slabs, the synergy would expedite the molecular visualization of entire human brain with minimal loss of connectivity information.

Another improvement we can aim to achieve is the optimization of delipidation technology. Currently, delipidation is a useful and indispensable step to expose biomolecules to molecular probes, and to allow tissue homogenization for optical clearing and deep tissue imaging. However, the removal of this compartmentalization inevitably leads to the biomolecular loss and damage, especially for the low-abundant transcripts and surface proteins. Thus, by optimizing delipidation step, either by altering the chemicals or by efficiently scaling up, we can expect to apply EPIC-SHIELD to intact human and other mammalian organs.

Another challenge lies on the automation of EPIC-SHIELD pipeline. Currently, the entire pipeline was demonstrated on a single slab, involving numerous manual steps such as chemical treatment, labeling, imaging, and de-labeling. However, these repeated imaging, tissue retrieval, and chemical equilibration steps inevitably lead to the tissue damage and varying imaging qualities. Errors caused by such interruptions can affect the downstream steps such as nuclei-based co-registration, quantification, and analysis. Therefore, an automation approach, in which the tissues are placed on a fixed chamber and the solution change is performed automatically, is crucial to improve the scalability of EPIC-SHIELD pipeline.

Lastly, several future goals have been suggested for the *in vitro* model of the human brain: microglia-organoid co-culture system. Currently, we have achieved extended survival of microglia at a lower temperature culture condition. However, the underlying mechanism, as well as the molecular profiles of microglia was not explored in this thesis. In the future, the microglia-organoid co-culture systems that are maintained for extended period (3+ months after co-culture) can be digested to yield single cells. Then, either fluorescence assisted cell sorting (FACS) or magnetic assisted cell sorting (MACS) can be used to enrich microglia population, which can be submitted for single-cell RNA-sequencing to obtain expression profiles. The gene expression from

co-cultured microglia can be compared to the existing gene expression data for primary microglia[104] to find whether the lower temperature condition allows the maturation of microglia towards the primary human microglia.

In summary, due to its outstanding features and universal applicability, we anticipate that the implementation of EPIC-SHIELD will significantly improve the depth, sensitivity, and reproducibility of spatial biomolecular characterization studies in the future. When integrated with other orthogonal technologies, such as RNA-sequencing, genetic modification, and viral labeling technologies, EPIC-SHIELD can become a powerful tool for mapping neural circuits and elucidating mammalian organ structures. Furthermore, the simpleness of our perfusion-based/non-perfusion-based protocols allows us to extend the utility towards other human organs, non-human primate organs, human clinical samples such as tumors and biopsies, stem cell derived organoids[105], and monolayer cell culture systems. Harnessing the versatility and effectiveness of our technology, we envision that EPIC-SHIELD can unveil unexplored territories of biological functions and dysfunctions.

Appendix

Supplemental Information

Supplementary Note 1.
Estimation of deprotonated amine at different pH

$$pH = pKa + \log\left(\frac{[A^-]}{[HA]}\right)$$

Lysine pKa = 10.53

At pH7.4

$$7.4 = 10.53 + \log\left(\frac{[NH_2]}{[NH_3^+]}\right)$$

$$\frac{[NH_2]}{[NH_3^+]} = 10^{-3.13} = 0.000741310241$$

$$[NH_2] = 7.41 \times 10^{-4}[NH_3^+]$$

$$\%[NH_2] = \frac{[NH_2]}{[NH_3^+] + [NH_2]} \times 100\% = \frac{7.41 \times 10^{-4}}{1 + 7.41 \times 10^{-4}} \times 100\% = 0.0741\%$$

At pH10

$$10 = 10.53 + \log\left(\frac{[NH_2]}{[NH_3^+]}\right)$$

$$\frac{[NH_2]}{[NH_3^+]} = 10^{-0.53} = 0.295120923$$

$$[NH_2] = 2.95 \times 10^{-1}[NH_3^+]$$

$$\%[NH_2] = \frac{[NH_2]}{[NH_3^+] + [NH_2]} \times 100\% = \frac{2.95 \times 10^{-1}}{1 + 2.95 \times 10^{-1}} \times 100\% = 22.787\%$$

pH7.4 vs pH10

$$\frac{\%[NH_2]_{pH10}}{\%[NH_2]_{pH7.4}} = \frac{22.787}{0.0741} = 307.5\ fold\ increase$$

Supplementary Note 2.
Protocols for processing a wide range of sample types and species (mouse, rat, marmoset, macaque, human)

Our EPIC-SHIELD is applicable to any tissue types from various species including, but not limited to, mouse, rat, marmoset, macaque, and human organs.

Mouse/Rat whole organ perfusion-based fixation protocol: The perfusion of mouse/rat needs to be performed with ice-cold 1xPBS, followed by ice-cold EPIC-SHIELD perfusion solution (4% (w/v) PFA + 1% SHIELD at pH 10). The harvested organs are post-fixed in EPIC-SHIELD perfusion solution at 4°C for 24 hours with gentle shaking. After 24 hours, the excess PFA can be washed using pre-cooled 1% SHIELD buffer at pH 10 at 4°C (SHIELD-OFF) for at least 6 hours. SHIELD-OFF buffers need to be changed frequently to remove excess PFA. For the ON step, the organs will be moved to room temperature (RT) with fresh 1% SHIELD buffer at pH 10 (SHIELD-ON) solution and the crosslinking reaction will take place for 24 hours with gentle shaking. After the ON step, the excess SHIELD solution is washed overnight with PBSN with frequent buffer changes.

Macaque/marmoset whole organ perfusion-based fixation protocol: The size of the monkey brain is roughly 1/12 of that of the human brain (~100 cm^3)[106], which allows rapid diffusion of formaldehyde throughout the entire tissue. Thus, combined with perfusion, the fixation with 4% (w/v) PFA at pH 10 is not diffusion-limited. For the SHIELD OFF/ON part, we need to consider that the P3PE molecule in the SHIELD solution having higher molecular weight (520 Da), whose effective diffusion coefficient is lower than that of formaldehyde molecules[73]. However, we found that the SHIELD epoxy molecule reaction at 4°C is minimal and exhibits reaction-limited system at room temperature (data not shown).

Combining these, the perfusion of macaque/marmoset needs to be performed with ice-cold 1xPBS, followed by ice-cold EPIC-SHIELD perfusion solution. The harvested monkey organs are post-fixed in EPIC-SHIELD perfusion solution at 4°C for 24 hours with gentle shaking. To wash off excess PFA, the organs are washed with pre-cooled SHIELD-OFF solution at 4°C, with frequent buffer changes for the first 6 hours, then every 6 hours up to total 24 hours. For the ON step, the organs are moved to room temperature after switching to fresh SHIELD-ON buffer, with the incubation time of 24 hours with gentle shaking. After the ON step, the excess SHIELD solution is washed overnight with PBSN with frequent buffer changes.

Human fresh slab (4 mm) immersion-fixation protocol: In this protocol, we are dealing with fresh human brain slab, sliced at 4-mm-thickness. As the smallest dimension is in millimeter scale, the processing of fresh human slab is carried out through immersion in EPIC-SHIELD perfusion solution at 4°C with gentle shaking. After 24 hours, the excess 4% pH 10 PFA is washed using pre-cooled SHIELD-OFF solution at 4°C for at least 6 hours. The buffers need to be changed frequently to remove excess formaldehyde. For the ON step, the slab will be moved to room temperature and the crosslinking reaction will take place for 24 hours with gentle shaking. After the ON step, the excess SHIELD solution is washed overnight with PBSN with frequent buffer changes.

Human frozen slab immersion-fixation protocol: The protocol for frozen brain slab (4-mm-thick) is performed similar to the fresh brain slab, with a single modification: the frozen slabs are directly immersed and thawed in EPIC-SHIELD perfusion solution at 4°C with gentle shaking, for 24 hours.

The table below summarizes the suggested protocol for various biological samples.

<table>
<tr><th>Step</th><th>Solution</th><th>Condition</th><th>Mouse/ Rat</th><th>Macaque/ Marmoset</th><th>Human, Fresh</th><th>Human, Frozen</th></tr>
<tr><td rowspan="2">EPIC-SHIELD perfusion/ immersion</td><td rowspan="2">4% PFA + 1% SHIELD</td><td rowspan="2">pH 10, 4°C</td><td colspan="4">24 hours</td></tr>
<tr><td colspan="2">Perfusion</td><td colspan="2">Immersion</td></tr>
<tr><td rowspan="2">Washing</td><td rowspan="2">1% SHIELD</td><td rowspan="2">pH 10, 4°C (pre-cooled)</td><td>6 hours</td><td>24 hours</td><td colspan="2">6 hours</td></tr>
<tr><td colspan="4">4x buffer change</td></tr>
<tr><td>SHIELD-OFF</td><td>1% SHIELD</td><td>pH 10, 4°C (pre-cooled)</td><td>-</td><td>24 hours</td><td colspan="2">-</td></tr>
<tr><td>SHIELD-ON</td><td>1% SHIELD</td><td>pH 10, RT</td><td colspan="4">24 hours</td></tr>
<tr><td>Washing</td><td>PBSN</td><td>pH 7.4, RT</td><td colspan="4">Overnight with 4x buffer change</td></tr>
</table>

Supplementary Note 3.
DERIVATION OF DIFFUSION TIME SCALE

Starting from a chemical conservation equation for a control volume:

$$\frac{\partial C}{\partial \mathrm{t}} = \mathrm{D}_{eff}\nabla^2 C$$

C denotes the concentration of any chemicals, and D_{eff} is the effective diffusivity. After perfoming scaling analysis, the equation is simplified to:

$$\frac{C_0}{t_d} \sim \frac{\mathrm{D}_{eff} C_0}{L^2}$$

C_0 is the initial concentration of chemicals, t_d is the diffusion time scale, and L is the characteristic length. Rearranging the equations, we have an expression for the diffusion time scale:

$$t_d \sim \frac{L^2}{\mathrm{D}_{eff}}$$

References

1. Molyneaux, B. J., Arlotta, P., Menezes, J. R. L. & Macklis, J. D. Neuronal subtype specification in the cerebral cortex. *Nat. Rev. Neurosci.* **8**, 427–437 (2007).
2. Kelava, I. & Lancaster, M. A. Stem Cell Models of Human Brain Development. *Cell Stem Cell* **18**, 736–748 (2016).
3. Leung, C. & Jia, Z. Mouse Genetic Models of Human Brain Disorders . *Frontiers in Genetics* vol. 7 40 (2016).
4. Lancaster, M. A. *et al.* Cerebral organoids model human brain development and microcephaly. *Nature* **501**, 373–379 (2013).
5. Qian, X. *et al.* Brain-Region-Specific Organoids Using Mini-bioreactors for Modeling ZIKV Exposure. *Cell* **165**, 1238–1254 (2016).
6. Langseth, C. M. *et al.* Comprehensive in situ mapping of human cortical transcriptomic cell types. *Commun. Biol.* **4**, 1–7 (2021).
7. Zhao, S. *et al.* Cellular and Molecular Probing of Intact Human Organs. *Cell* **180**, 796-812.e19 (2020).
8. Lai, H. M. *et al.* Next generation histology methods for three-dimensional imaging of fresh and archival human brain tissues. *Nat. Commun.* **9**, (2018).
9. Park, J. *et al.* Integrated platform for multi-scale molecular imaging and phenotyping of the human brain. *bioRxiv* 2022.03.13.484171 (2022).
10. Darmanis, S. *et al.* A survey of human brain transcriptome diversity at the single cell level. *Proc. Natl. Acad. Sci. U. S. A.* **112**, 7285–7290 (2015).
11. Frei, A. P. *et al.* Highly multiplexed simultaneous detection of RNAs and proteins in single cells. *Nat. Methods* **13**, 269–275 (2016).
12. Zeisel, A. *et al.* Cell types in the mouse cortex and hippocampus revealed by single-cell RNA-seq. *Science (80-.).* **347**, 1138–1141 (2015).
13. Corsortium, H. The human body at cellular resolution: the NIH Human Biomolecular Atlas Program. *Nature* **574**, 187–192 (2019).
14. Insel, T. R., Landis, S. C. & Collins, F. S. The NIH BRAIN Initiative. *Science (80-.).* **340**, 687–688 (2013).
15. Regev, A. *et al.* Science Forum: The Human Cell Atlas. *Science (80-.).* **340**, 687–688 (2013).
16. Micheva, K. D. & Smith, S. J. Array Tomography: A New Tool for Imaging the Molecular Architecture and Ultrastructure of Neural Circuits. *Neuron* **55**, 25–36 (2007).
17. Ueda, H. R. *et al.* Tissue clearing and its applications in neuroscience. *Nat. Rev. Neurosci.* (2020) doi:10.1038/s41583-019-0250-1.

18. Spalteholz, W. Über das Durchsichtigmachen von Über das Durchsichtigmachen von menschlichen und tierischen Präparaten (Leipzig: S. Hierzel). (1914).

19. Chiang, A. S. *et al.* Three-dimensional mapping of brain neuropils in the cockroach, Diploptera punctata. *J. Comp. Neurol.* **440**, 1–11 (2001).

20. Chung, K. *et al.* Structural and molecular interrogation of intact biological systems. *Nature* **497**, 332–337 (2013).

21. Dodt, H. U. *et al.* Ultramicroscopy: Three-dimensional visualization of neuronal networks in the whole mouse brain. *Nat. Methods* **4**, 331–336 (2007).

22. Ertürk, A. *et al.* Three-dimensional imaging of solvent-cleared organs using 3DISCO. *Nat. Protoc.* **7**, 1983–1995 (2012).

23. Ertürk, A. *et al.* Three-dimensional imaging of the unsectioned adult spinal cord to assess axon regeneration and glial responses after injury. *Nat. Med.* **18**, 166–171 (2012).

24. Hama, H. *et al.* Scale: A chemical approach for fluorescence imaging and reconstruction of transparent mouse brain. *Nat. Neurosci.* **14**, 1481–1488 (2011).

25. Ke, M. T., Fujimoto, S. & Imai, T. SeeDB: A simple and morphology-preserving optical clearing agent for neuronal circuit reconstruction. *Nat. Neurosci.* **16**, 1154–1161 (2013).

26. Kuwajima, T. *et al.* ClearT: A detergent- and solvent-free clearing method for neuronal and non-neuronal tissue. *Dev.* **140**, 1364–1368 (2013).

27. Palmer, W. M. *et al.* PEA-CLARITY: 3D molecular imaging of whole plant organs. *Sci. Rep.* **5**, 1–6 (2015).

28. Schwarz, M. K. *et al.* Fluorescent-protein stabilization and high-resolution imaging of cleared, intact mouse brains. *PLoS One* **10**, 1–26 (2015).

29. Susaki, E. A. *et al.* Whole-brain imaging with single-cell resolution using chemical cocktails and computational analysis. *Cell* **157**, 726–739 (2014).

30. Yang, B. *et al.* Single-cell phenotyping within transparent intact tissue through whole-body clearing. *Cell* **158**, 945–958 (2014).

31. Belle, M. *et al.* Tridimensional Visualization and Analysis of Early Human Development. *Cell* **169**, 161-173.e12 (2017).

32. Murray, E. *et al.* Simple, Scalable Proteomic Imaging for High-Dimensional Profiling of Intact Systems. *Cell* **163**, 1500–1514 (2015).

33. Park, Y. *et al.* Protection of tissue physicochemical properties using polyfunctional. (2018) doi:10.1038/nbt.4281.

34. Renier, N. *et al.* IDISCO: A simple, rapid method to immunolabel large tissue samples for volume imaging. *Cell* **159**, 896–910 (2014).

35. Ku, T. *et al.* Multiplexed and scalable super-resolution imaging of three-dimensional protein localization in size-adjustable tissues. *Nat. Biotechnol.* **34**, 973–981 (2016).

36. Chen, F., Tillberg, P. W. & Boyden, E. S. Expansion Microscopy. *Science (80-.).* **347**, 543–548 (2015).

37. Park, H. E. *et al.* Scalable and Isotropic Expansion of Tissues with Simply Tunable Expansion Ratio. *Adv. Sci.* **6**, (2019).

38. Ku, T. *et al.* Elasticizing tissues for reversible shape transformation and accelerated molecular labeling. *Nat. Methods* (2020) doi:10.1038/s41592-020-0823-y.

39. Chang, J. B. *et al.* Iterative expansion microscopy. *Nat. Methods* **14**, 593–599 (2017).

40. Chozinski, T. J. *et al.* Expansion microscopy with conventional antibodies and fluorescent proteins. *Nat. Methods* 1–7 (2016) doi:10.1038/nmeth.3833.

41. Sylwestrak, E. L., Rajasethupathy, P., Wright, M. A., Jaffe, A. & Deisseroth, K. Multiplexed Intact-Tissue Transcriptional Analysis at Cellular Resolution. *Cell* **164**, 792–804 (2016).

42. Tillberg, P. W. *et al.* Protein-retention expansion microscopy of cells and tissues labeled using standard fluorescent proteins and antibodies. *Nat. Biotechnol.* **34**, 987–992 (2016).

43. Wang, G., Moffitt, J. R. & Zhuang, X. Multiplexed imaging of high-density libraries of RNAs with MERFISH and expansion microscopy. *Sci. Rep.* **8**, 1–13 (2018).

44. Ramos-Vara, J. A. Technical Aspects of Immunohistochemistry. *Vet. Pathol.* **42**, 405–426 (2005).

45. Usher, P. A. *et al.* Sensitive and Specific In Situ Hybridization for Early Drug Discovery BT - In Situ Hybridization Protocols. in (ed. Nielsen, B. S.) 103–123 (Springer New York, 2014). doi:10.1007/978-1-4939-1459-3_10.

46. Choi, H. M. T., Beck, V. A. & Pierce, N. A. Next-generation in situ hybridization chain reaction: Higher gain, lower cost, greater durability. *ACS Nano* **8**, 4284–4294 (2014).

47. Choi, S. W., Guan, W. & Chung, K. Basic principles of hydrogel-based tissue transformation technologies and their applications. *Cell* **184**, 4115–4136 (2021).

48. Chen, K. H., Boettiger, A. N., Moffitt, J. R., Wang, S. & Zhuang, X. Spatially resolved, highly multiplexed RNA profiling in single cells. *Science (80-.).* **348**, 1360–1363 (2015).

49. Femino, A. M., Fay, F. S., Fogarty, K. & Singer, R. H. Visualization of single RNA transcripts in situ. *Science (80-.).* **280**, 585–590 (1998).

50. Codeluppi, S. *et al.* Spatial organization of the somatosensory cortex revealed by osmFISH. *Nat. Methods* **15**, 932–935 (2018).

51. Lubeck, E. & Cai, L. Single-cell systems biology by super-resolution imaging and combinatorial labeling. *Nat. Methods* **9**, 743–748 (2012).

52. Lubeck, E., Coskun, A. F., Zhiyentayev, T., Ahmad, M. & Cai, L. Single-cell in situ RNA profiling by sequential hybridization. *Nat. Methods* **11**, 360–361 (2014).

53. Moffitt, J. R. *et al.* Molecular, spatial, and functional single-cell profiling of the hypothalamic preoptic region. *Science (80-.).* **362**, (2018).

54. Chen, F. *et al.* Nanoscale imaging of RNA with expansion microscopy. *Nat. Methods* **13**, 679–684 (2016).

55. Shah, S. *et al.* Single-molecule RNA detection at depth by hybridization chain reaction and tissue hydrogel embedding and clearing. *Development* **143**, 2862–2867 (2016).

56. DePas, W. H. *et al.* Exposing the Three-Dimensional Biogeography and Metabolic States of Pathogens in Cystic Fibrosis Sputum via Hydrogel Embedding , Clearing , and rRNA Labeling. *Am. Soc. Microbiol.* **7**, 1–11 (2016).

57. Moffitt, J. R. *et al.* High-performance multiplexed fluorescence in situ hybridization in culture and tissue with matrix imprinting and clearing. *Proc. Natl. Acad. Sci. U. S. A.* **113**, 14456–14461 (2016).

58. Eng, C. H. L. *et al.* Transcriptome-scale super-resolved imaging in tissues by RNA seqFISH+. *Nature* (2019) doi:10.1038/s41586-019-1049-y.

59. Ke, R. *et al.* In situ sequencing for RNA analysis in preserved tissue and cells. *Nat. Methods* **10**, 857–860 (2013).

60. Lee, J. H. *et al.* Highly Multiplexed Subcellular RNA Sequencing in Situ. *Science (80-.).* **343**, 1360–1364 (2014).

61. Wang, X. *et al.* Three-dimensional intact-tissue sequencing of single-cell transcriptional states. *Science (80-.).* **361**, 1–18 (2018).

62. Aloisi, F. Immune function of microglia. *Glia* **36**, 165–179 (2001).

63. Salter, M. W. & Stevens, B. Microglia emerge as central players in brain disease. *Nat. Med.* **23**, 1018–1027 (2017).

64. Ormel, P., Vieira de Sa, R., Hol, E. & Pasterkamp, R. J. Microglia innately develop within cerebral organoids. *Manuscr. Submitt. Publ.* (2018) doi:10.1038/s41467-018-06684-2.

65. Yun, D. H. *et al.* Ultrafast immunostaining of organ-scale tissues for scalable proteomic phenotyping. *Biorxiv* (2019).

66. Schwanhüusser, B. *et al.* Global quantification of mammalian gene expression control. *Nature* **473**, 337–342 (2011).

67. Stark, R., Grzelak, M. & Hadfield, J. RNA sequencing: the teenage years. *Nat. Rev. Genet.* **20**, 631–656 (2019).

68. Alon, S. *et al.* Expansion sequencing: Spatially precise in situ transcriptomics in intact biological systems. *Science (80-.).* **371**, (2021).

69. Achim, K. *et al.* High-throughput spatial mapping of single-cell RNA-seq data to tissue of origin. *Nat. Biotechnol.* **33**, 503–509 (2015).

70. Satija, R., Farrell, J. A., Gennert, D., Schier, A. F. & Regev, A. Spatial reconstruction of single-cell gene expression data. *Nat. Biotechnol.* **33**, 495–502 (2015).

71. Kleshchevnikov, V. *et al.* Cell2location maps fine-grained cell types in spatial transcriptomics. *Nat. Biotechnol.* **40**, 661–671 (2022).

72. Kennedy-Darling, J. & Smith, L. M. Measuring the formaldehyde protein-DNA cross-link reversal rate. *Anal. Chem.* **86**, 5678–5681 (2014).

73. Syková, E. & Nicholson, C. Diffusion in brain extracellular space. *Physiol. Rev.* **88**, 1277–1340 (2008).

74. Fox, C. H., Johnson, F. B., Whiting, J. & Roller, P. P. Formaldehyde fixation. *J. Histochem. Cytochem.* **33**, 845–853 (1985).

75. McGhee, J. D. & von Hippel, P. H. Formaldehyde as a Probe of DNA Structure. 4. Mechanism of the Initial Reaction of Formaldehyde with DNA. *Biochemistry* **16**, 3276–3293 (1977).

76. Winkelman, J. G. M., Voorwinde, O. K., Ottens, M., Beenackers, A. A. C. M. & Janssen, L. P. B. M. Kinetics and chemical equilibrium of the hydration of formaldehyde. *Chem. Eng. Sci.* **57**, 4067–4076 (2002).

77. Kishi, J. Y. *et al.* SABER amplifies FISH: enhanced multiplexed imaging of RNA and DNA in cells and tissues. *Nat. Methods* **16**, 533–544 (2019).

78. Beliveau, B. J. *et al.* OligoMiner provides a rapid, flexible environment for the design of genome-scale oligonucleotide in situ hybridization probes. *Proc. Natl. Acad. Sci. U. S. A.* **115**, E2183–E2192 (2018).

79. Melan, M. A. Overview of Cell Fixation and Permeabilization BT - Immunocytochemical Methods and Protocols. in (ed. Javois, L. C.) 55–66 (Humana Press, 1995). doi:10.1385/0-89603285-X:55.

80. McGhee, J. D. & Von Hippel, P. H. Formaldehyde as a probe of DNA structure. I. Reaction with exocyclic amino groups of DNA bases. *Biochemistry* **14**, 1281–1296 (1975).

81. Paananen, H. & Pakkanen, T. T. Kraft lignin reaction with paraformaldehyde. *Holzforschung* **74**, 663–672 (2020).

82. Wang, Y. *et al.* EASI-FISH for thick tissue defines lateral hypothalamus spatio-molecular organization. *Cell* **184**, 6361-6377.e24 (2021).

83. Goltsev, Y. *et al.* Deep Profiling of Mouse Splenic Architecture with CODEX Multiplexed Imaging. *Cell* **174**, 968-981.e15 (2018).

84. Saka, S. K. *et al.* Immuno-SABER enables highly multiplexed and amplified protein imaging in tissues. *Nat. Biotechnol.* **37**, 1080–1090 (2019).

85. Zhang, M. *et al.* Spatially resolved cell atlas of the mouse primary motor cortex by MERFISH. *Nature* **598**, 137–143 (2021).

86. Huang, Z. J. & Paul, A. The diversity of GABAergic neurons and neural communication elements. *Nat. Rev. Neurosci.* **20**, 563–572 (2019).

87. Galiano, M. R. *et al.* Myelin basic protein functions as a microtubule stabilizing protein in differentiated oligodendrocytes. *J. Neurosci. Res.* **84**, 534–541 (2006).

88. Perrenoud, Q. *et al.* Characterisation of type I and type II nNOS-expressing interneurons in the barrel cortex of mouse. *Front. Neural Circuits* **6**, 1–31 (2012).

89. Li, Q. & Barres, B. A. Microglia and macrophages in brain homeostasis and disease. *Nat. Rev. Immunol.* **18**, 225–242 (2018).

90. Na, M. *et al.* Sodium Cholate-Based Active Delipidation for Rapid and Efficient Clearing and Immunostaining of Deep Biological Samples. *Small Methods* **6**, (2022).

91. McFadden, W. C. *et al.* Perfusion fixation in brain banking: a systematic review. *Acta Neuropathol. Commun.* **7**, 146 (2019).

92. Moreno-García, A., Kun, A., Calero, O., Medina, M. & Calero, M. An overview of the role of lipofuscin in age-related neurodegeneration. *Front. Neurosci.* **12**, 1–13 (2018).

93. Oliveira, V. C. *et al.* Sudan Black B treatment reduces autofluorescence and improves resolution of in situhybridization specific fluorescent signals of brain sections. *Histol. Histopathol.* **25**, 1017–1024 (2010).

94. Fu, H. *et al.* Tau Pathology Induces Excitatory Neuron Loss, Grid Cell Dysfunction, and Spatial Memory Deficits Reminiscent of Early Alzheimer's Disease. *Neuron* **93**, 533-541.e5 (2017).

95. Kurucu, H. *et al.* Inhibitory synapse loss and accumulation of amyloid beta in inhibitory presynaptic terminals in Alzheimer's disease. *Eur. J. Neurol.* **29**, 1311–1323 (2022).

96. Qian, X. *et al.* Generation of human brain region–specific organoids using a miniaturized spinning bioreactor. *Nat. Protoc.* **13**, 565–580 (2018).

97. McQuade, A. *et al.* Development and validation of a simplified method to generate human microglia from pluripotent stem cells. *Mol. Neurodegener.* **13**, 1–13 (2018).

98. Kim, S. Y. *et al.* Stochastic electrotransport selectively enhances the transport of highly electromobile molecules. *Proc. Natl. Acad. Sci. U. S. A.* **112**, E6274–E6283 (2015).

99. Borm, L. E. *et al.* Scalable in situ single-cell profiling by electrophoretic capture of mRNA using EEL FISH. *Nat. Biotechnol.* (2022) doi:10.1038/s41587-022-01455-3.

100. Behar, K. L. GABA Synthesis and Metabolism. in *Encyclopedia of Neuroscience* (ed. Squire, L. R. B. T.-E. of N.) 433–439 (Academic Press, 2009). doi:10.1016/B978-008045046-9.01240-7.

101. Lachamp, P., Crest, M. & Kessler, J.-P. Vesicular glutamate transporters type 1 and 2 expression in axon terminals of the rat nucleus of the solitary tract. *Neuroscience* **137**, 73–81 (2006).

102. Samandra, R., Haque, Z. Z., Rosa, M. G. P. & Mansouri, F. A. The marmoset as a model for investigating the neural basis of social cognition in health and disease. *Neurosci. Biobehav. Rev.* **138**, 104692 (2022).

103. Perez-Cruz, C. & Rodriguez-Callejas, J. de D. The common marmoset as a model of neurodegeneration. *Trends Neurosci.* **46**, 394–409 (2023).

104. Svoboda, D. S. *et al.* Human iPSC-derived microglia assume a primary microglia-like state after transplantation into the neonatal mouse brain. *Proc. Natl. Acad. Sci.* **116**, 25293–25303 (2019).

105. Albanese, A. *et al.* Multiscale 3D phenotyping of human cerebral organoids. *Sci. Rep.* **10**, 1–17 (2020).

106. Croxson, P. L., Forkel, S. J., Cerliani, L. & Thiebaut De Schotten, M. Structural Variability Across the Primate Brain: A Cross-Species Comparison. *Cereb. Cortex* **28**, 3829–3841 (2018).